



**A CIRCUMFERENTIAL STRETCH BIOREACTOR FOR
MECHANICAL CONDITIONING OF SMOOTH MUSCLE RINGS**

A Thesis

Submitted to the Faculty of the

WORCESTER POLYTECHNIC INSTITUTE

In partial fulfillment of the requirements for the

Degree of Master of Science
In Biomedical Engineering

May 1, 2014

By

Jennifer Lee Cooper

Approved

Glenn R. Gaudette, Ph.D.
Associate Professor
Department of Biomedical Engineering
Worcester Polytechnic Institute
Committee Member

Karen L. Troy, Ph.D.
Assistant Professor
Department of Biomedical Engineering
Worcester Polytechnic Institute
Committee Member

Marsha W. Rolle, Ph.D.
Associate Professor
Department of Biomedical Engineering
Worcester Polytechnic Institute
Thesis Advisor

Table of Contents

Table of Figures	5
Table of Tables	7
Acknowledgements.....	8
Abstract.....	9
Abbreviations.....	10
Chapter 1: Overview and Objectives.....	11
Chapter 2: Background.....	13
2.1 Clinical Need for Vascular Grafts.....	13
2.2 Blood Vessel Physiology	14
2.3 Developing Tissue-Engineered Blood Vessels.....	15
2.3.1 Scaffold Approaches	15
2.3.2 Cell-Derived Approaches	18
2.4 Influencing Structure and Function with Mechanical Conditioning.....	19
2.4.1 Effect of Mechanical Stimulation on TEBVs.....	19
2.4.2 Bioreactors for Mechanical Stimulation of TEBVs	22
Chapter 3: Development and Characterization of a Cyclic Stretch Bioreactor	26
3.1 Introduction.....	26
3.1.1 Principal Mechanism for Tissue Stretching	26
3.1.2 Overview of Original Prototype and System Challenges.....	27
3.2 Methods and Materials.....	29
3.2.1 Manufacture.....	30
3.2.2 System Characterization and Validation	30
3.2.3 Determining Statistical Significance	34
3.3 Results.....	34

3.3.1	Bioreactor Components and Design Modifications	35
3.3.2	Tubing and Cam Validation	41
3.3.3	Regional Tubing Distension.....	46
3.4	Summary and Discussion.....	46
Chapter 4:	Analysis of Dynamically-Cultured SMC Rings	50
4.1	Introduction.....	50
4.2	Methods and Materials.....	50
4.2.1	Cell Culture and Ring Fabrication.....	50
4.2.2	Analyzing Ring Distension using HDM	51
4.2.3	Preparing and Setting up the Bioreactor for Experimentation	52
4.2.4	Dynamic Culture Experiments	53
4.2.5	Calculating Ring Thickness.....	54
4.2.6	Histological Analysis of ECM Composition.....	54
4.2.7	Immunohistochemical Analysis of Contractile Proteins and Proliferating Cells.....	55
4.2.8	Calculating Ring Cell Density.....	56
4.2.9	Calculating Nuclear Alignment.....	57
4.2.10	Uniaxial Tensile Testing	60
4.2.11	Determining Statistical Significance	61
4.3	Results.....	62
4.3.1	Tissue Ring Distension during Dynamic Culture.....	62
4.3.2	Effect of Low Stretch on SMC Rings	64
4.3.3	Effect of High Stretch on SMC Rings.....	66
4.3.4	Additional Analyses of SMC Rings Dynamically Cultured at 0-15% Stretch..	69
4.4	Summary and Discussion.....	78

Chapter 5: Conclusions and Future Work	86
References.....	90
Appendix A: Bill of Materials	95
Appendix B: CAD Drawings	97

Table of Figures

Figure 1 – Schematic of Stretch Effects on SMC Ring	12
Figure 2 – Cellular Orientation in Response to Stretch	20
Figure 3 – Vascular Bioreactor Configurations	22
Figure 4 – Principal Stretching Mechanism.....	27
Figure 5 – Cyclic Stretch Bioreactor Prototype	28
Figure 6 – DVT® Setup for Cam Validation.....	32
Figure 7 – Motor-Shaft System.....	35
Figure 8 – Motor Enclosure	36
Figure 9 – Tissue Culture Chamber	37
Figure 10 – Syringe Support.....	38
Figure 11 – Tissue Culture Chamber Lid	39
Figure 12 – Final Bioreactor Assembly	40
Figure 13 – Tubing Distension vs. Syringe Plunger Depression	42
Figure 14 – Distension Characterization of Four Cams.....	43
Figure 15 – Example of Tubing Image during HDM Analysis	44
Figure 16 – Strain vs. Frame Number for 10% Cam using HDM	45
Figure 17 – Dynamic Tubing Distension at Four Stretch Magnitudes	45
Figure 18 – Regional Tubing Distension at 10% Stretch	46
Figure 19 – Self-Assembly Ring Schematic.....	51
Figure 20 – Preparing SMC Rings for Dynamic Culture	53
Figure 21 – Calculating Cell Density.....	57
Figure 22 – Calculating Nuclear Alignment: Preparing the Image	58
Figure 23 – Calculating Nuclear Alignment: Determining Angles	60
Figure 24 – Uniaxial Mechanical Testing Setup.....	61
Figure 25 – SMC Ring Distension Analysis using HDM.....	62
Figure 26 – SMC Ring Distension vs. Culture Time at Four Stretch Magnitudes	63
Figure 27 – Picosirius Red/Fast Green Staining of SMC Rings Cultured at Low Stretch Magnitudes.....	65

Figure 28 – DVT [®] Image and Average Thickness of SMC Rings Cultured at Low Stretch Magnitudes.....	65
Figure 29 – Picrosirius Red/Fast Green Staining of SMC Rings Cultured at High Stretch Magnitudes.....	66
Figure 30 – Alcian Blue Staining of SMC Rings Cultured at High Stretch Magnitudes	67
Figure 31 – DVT [®] Images and Average Thickness of SMC Rings Cultured at High Stretch Magnitudes.....	68
Figure 32 – Mechanical Testing Analysis of SMC Rings Cultured at High Stretch Magnitudes	69
Figure 33 – Picrosirius Red/Fast Green Staining of Dynamically Cultured SMC Rings.....	70
Figure 34 – Alcian Blue Staining of Dynamically Cultured SMC Rings.....	71
Figure 35 – Stretched SMC Ring Morphology as a Function of Tubing Position.	71
Figure 36 – Average Thickness of Dynamically Cultured SMC Rings.....	72
Figure 37 – Average Cell Density of Dynamically Cultured SMC Rings.....	73
Figure 38 – Nuclear Alignment Analysis	74
Figure 39 – Average Angle of Alignment per Stretch Magnitude.....	75
Figure 40 – Stress vs. Strain Curve of Dynamically Cultured SMC Rings.....	76
Figure 41 – Mechanical Testing Analysis of Dynamically Cultured SMC Rings.....	77
Figure 42 – Alignment Analysis of Native Vessel Control.	80
Figure 43 – Comparing Mechanical Testing Results between Experiments	83
Figure 44 – Cam Profiles.	89

Table of Tables

Table 1 – Bioreactors Utilized for Mechanical Conditioning of Vascular Grafts	24
Table 2 – SMC Ring Stretch Normalized to Tubing Stretch	63

Acknowledgements

I would like to first and foremost thank my advisor, Marsha Rolle, for her endless optimism, support, and guidance these past few years.

I would also like to thank my committee members, Professors Glenn Gaudette and Karen Troy, for their quality feedback and discussions throughout this project.

I would like to thank the graduate students and undergraduate volunteers in the Rolle lab, with special thanks to Zoë Reidinger and Hannah Strobel for their words of wisdom and words of laughter.

I am grateful for the assistance of John Favreau and Katrina Hansen in collecting and analyzing data from the high density mapping experiments; Kevin Arruda and the WPI machine shops in manufacturing the bioreactor; and Jason Forte and Yuan (Benny) Yin, who acted as unofficial mentors and answered my unending list of questions.

Finally, I would like to thank my family and friends for their endless support and patience, and for listening to me rant about science!

Abstract

Vascular grafts are used to repair, replace, or bypass diseased arteries, and there is a growing need for tissue-engineered blood vessels (TEBVs) as replacement grafts. Three-dimensional, self-assembled smooth muscle cell (SMC) rings can be fabricated and fused to create SMC tissue tubes with a structure similar to native vessels; however, this approach is limited by the underdeveloped mechanical integrity of the tissue. Thus, the goal of this research is to design, manufacture, and validate a cyclic circumferential stretch bioreactor to mechanically stimulate SMC tissue rings, with the goal of developing rings that can withstand the physiological forces of the *in vivo* environment. The bioreactor consists of a closed cam-syringe-tubing system that forces fluid into the tubing with each rotation of the cam, thereby distending and relaxing the tubing. Various sized cams were implemented to modify the distension of the tubing (5%, 7.5%, 10%, and 15% stretch magnitudes). Tissue rings are placed on the tubing, which is housed in a custom culture chamber. The tubing was validated using DVT[®] imaging technology to distend approximately 5, 7.5, 10, and 15% under static conditions. High density mapping was used to analyze the dynamic distension of the tubing and tissue rings. During bioreactor operation, the tubing distends 1-2% less than expected for the fabricated cams (5, 7.5, 10, 15%), and the tissue ring distends 31-56% less than the tubing on which it is located. To assess the effects of cyclic distension, 7-day-old SMC rings were cultured dynamically for 7 days and exposed to 0%, 5%, 7.5%, 10%, or 15% cyclic stretch (1 Hz, 100% duty cycle). Histology and immunohistochemistry indicate that both stretched and non-stretched rings synthesized collagen and glycosaminoglycans, but the contractile proteins α -smooth muscle actin and calponin were not synthesized. A decrease in cell density was observed as the magnitude of stretch increased, and the 5-15% stretched samples demonstrated more cellular alignment than the 0% stretch control samples. Mechanical testing analysis concluded that the stretched rings exhibited a reduction in ultimate tensile strength, maximum tangent modulus, maximum strain, and maximum load compared to unstretched control samples. It is anticipated that future work, including modifications of the culture medium and mechanical stimulation parameters (eg. reduced duty cycle, reduced frequency), has the potential to achieve the expected outcome of this research – a strong, aligned, contractile vascular smooth muscle cell tissue ring through dynamic culture using a cyclic circumferential stretch bioreactor.

Abbreviations

ANOVA	analysis of variance
CD	cyclic distension
ECM	extracellular matrix
GAG	glycosaminoglycan
HDM	high density mapping
ICD	incremental cyclic distension
ID	inner diameter
MTM	maximum tangent modulus
OD	outer diameter
PBS	phosphate buffered saline
PDMS	polydimethylsiloxane
PR	picosirius red
PR/FG	picosirius red/fast green
ROI	region of interest
SM	smooth muscle
SMC	smooth muscle cell
TEBV	tissue-engineered blood vessel
UHMWPE	ultra-high molecular weight polyethylene
UTS	ultimate tensile stress
VSCM	vascular smooth muscle cell

Chapter 1: Overview and Objectives

The overall goal of this project is to create a cyclic stretch bioreactor to provide mechanical stimulation of tissue-engineered blood vessels (TEBVs) derived from human smooth muscle cell self-assembly.^[1] A prototype bioreactor was previously developed,^[2] but the system is limited by its functionality, consistency, and reliability, including motor stoppage, media leakage, syringe malfunctions, spring inconsistencies, and component stability. The objective of this thesis project was to incorporate the main stretching mechanism of the prototype into a newly designed and manufactured system. Once fabricated, the bioreactor assembly and operation were validated using static digital imaging analysis and high density mapping.^[3] Finally, we measured the effects of the dynamic culture on smooth muscle cell tissue ring extracellular matrix (ECM) composition, tensile strength, and cellular alignment. In order to achieve the overall goal of the research, we accomplished two project objectives – manufacture of the bioreactor and analysis of the effects of the bioreactor (dynamic culture) on tissue structure.

Objective 1: Bioreactor Evaluation, Design, Construction, and Validation

The first objective encompasses all relevant tasks prior to tissue culture within the bioreactor, such as testing during operation, prototype component decomposition, and system evaluation. Sub-objectives of this objective include (1) analyze the characteristics of the prototype design; (2) implement design modifications as necessary; (3) manufacture the new bioreactor in its entirety; and (4) validate the new bioreactor system. The main deliverable of this aim was a functional system for the dynamic culture of smooth muscle cell tissue rings.

Objective 2: Analysis of Mechanical Conditioning on Tissue Rings

The second objective of the project was to analyze the effect of mechanical stimulation on tissue ring extracellular matrix composition and structure, cellular orientation, and tensile strength. We hypothesized that cyclic stretching during ring culture would i) increase collagen synthesis and deposition; ii) align the cells circumferentially relative to the lumen; and iii) increase the ultimate tensile strength of the rings (see Figure 1). The ultimate goal of this objective was to fabricate tissue rings that resembled the structural and physical characteristics of native vessels (eg. collagen deposition, SMC contractile protein expression, ultimate tensile strength ~ 2 MPa^[4-6]).

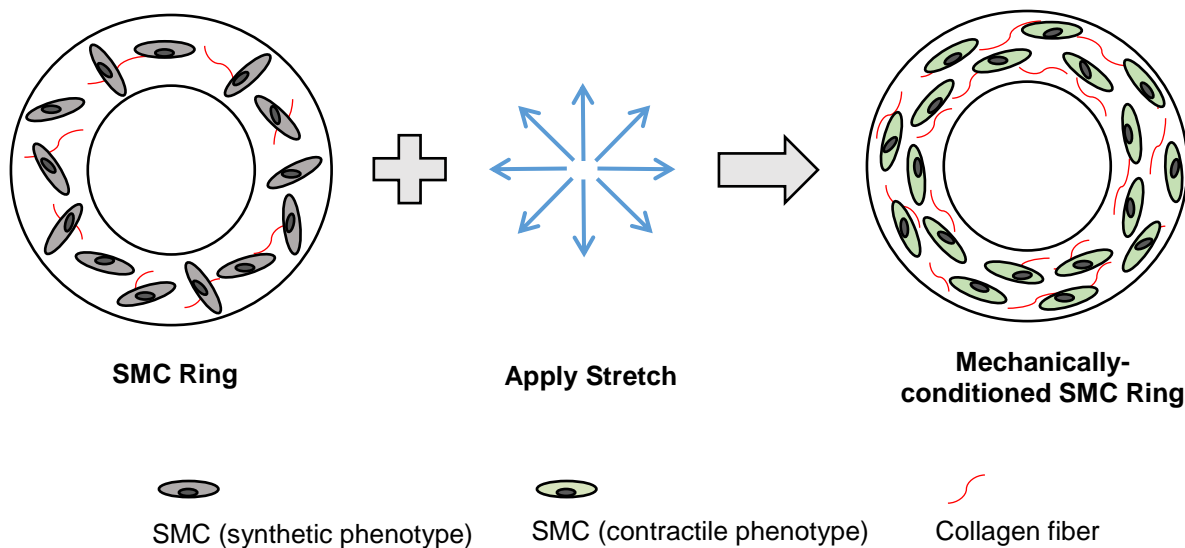


Figure 1 – Schematic of Stretch Effects on SMC Ring. Expected results of stretching SMC rings include increased matrix synthesis, circumferential alignment of cells, and cell maturation to a contractile phenotype.

In order to achieve the overall goal of developing strong, aligned, smooth muscle cell rings for the development of TEBVs, a thorough understanding of current challenges and approaches to designing and fabricating TEBVs is required. The following chapter is a brief review of the need for vascular grafts, the structure of blood vessels, advancements in developing TEBVs, and mechanical stimulation as an influence for the structure and function of TEBVs. Chapter Three discusses experiments relevant to the first objective, including details such as limitations with the prototype bioreactor, design modifications and implementations on the new bioreactor, and validation testing. The new bioreactor features the prototype’s concept for distension, which is driven by a cam-syringe-tubing subsystem. A syringe and tubing are filled with fluid and the system is closed with a pinch clamp. As the bioreactor operates, fluid is forced into the tubing with each cam rotation, thereby distending and relaxing the tubing and rings. Revisions over the prototype include higher-quality syringes, a single motor-shaft system, and an enclosed motor, as well as other minor modifications. The effects of the dynamic conditioning on the tissue rings is described and discussed in Chapter Four. Analyses of stretched SMC rings included histology, immunohistochemistry, cell density, nuclear alignment, and uniaxial tensile testing. Finally, Chapter Five presents a summary of this project and future work.

Chapter 2: Background

The significance of developing tissue-engineered blood vessels (TEBVs) stems from the overwhelming population suffering from heart disease. In 2009, cardiovascular disease (CVD) accounted for 32.3% of all deaths, claiming a life every 40 seconds (on average).^[7] Of the estimated 83.6 million Americans with CVD, 15.4 million suffer from coronary heart disease (CHD), which causes approximately 1 of every 6 deaths in the US.^[7]

2.1 Clinical Need for Vascular Grafts

Coronary heart disease (CHD) is a general term that includes individuals who suffer from acute myocardial infarction, angina pectoris, or most commonly, atherosclerosis, which is the hardening of the arteries.^[7] Elevated levels of cholesterol, high blood pressure, and smoking are possible causes of arterial wall damage, which over time, leads to the buildup and compaction of fats, cholesterol, platelets, and other cellular debris within the arterial lumen.^[8, 9] As this buildup (plaque) thickens, the artery becomes narrow and hard (atherosclerotic), thereby slowing blood flow through the artery. The reduced flow creates additional strain on the heart and can weaken the heart wall. Other complications can arise if a piece of the plaque breaks off or if a blood clot forms. Both of these obstacles are capable of blocking off blood flow within the arterial system and ultimately, inducing a myocardial infarction (heart attack) or stroke.^[10] When medication and lifestyle changes are insufficient treatment for atherosclerosis, a bypass procedure may be required to install an additional vessel to bypass the blocked vasculature and restore blood flow.^[11]

With almost 400,000 procedures a year,^[12] coronary artery bypass graft (CABG) is commonly used to treat CHD with blockages in the coronary arteries of the heart. During a CABG procedure, a substitute vessel, such as the internal mammary artery or saphenous vein, is harvested and relocated to the region of the heart where the blood flow has been blocked. The vessel is surgically placed such that the blockage is bypassed and blood flow is restored throughout the heart.^[13] However, blood vessels throughout the body are not analogous. Their composition and structure varies based on their location and function in the body. For example, arteries have a larger amount of smooth muscle tissue than veins to resist the high pressure of the

blood flowing from the heart.^[14] Consequently, unless a closely-matched vessel is harvested, the “gold standard” autologous grafts may ultimately be a less-than-ideal replacement.^[15] Furthermore, in individuals with highly atherosclerotic vasculature, the individual may not have healthy, unobstructed blood vessels or may not have any available vessels to transplant if a CABG has previously been performed. With over one million surgical procedures annually to treat diseased blood vessels,^[16] there is a substantial need for small-diameter (less than 4 mm) replacement vessels in order to fulfill the high demand.

2.2 Blood Vessel Physiology

Vasculature, the organized arrangement of blood vessels, plays a crucial role within the cardiovascular system. It is responsible for the dispersion of blood from the heart to the body through arteries and arterioles; the exchange of gases and nutrients through capillaries; and the return of blood to the heart through venules and veins.^[17] *In vivo*, blood vessels experience oscillatory (circumferential) stretch of ~5-15% during the cardiac cycle,^[18, 19] and the actual strain value is dependent on the vessel’s location within the cardiovascular system. The walls of all blood vessels, except capillaries, have three distinct layers (tunicas), and the composition and morphology of each vessel type is reflective of its specific function and location in the body. By studying native vasculature, we can achieve a more complete understanding of how to design a construct for use as a vascular graft.

The tunica intima is the innermost layer of a blood vessel (the only layer in the capillaries) and is a barrier between the vessel wall and the flowing blood in the lumen. It consists of a single layer of endothelial cells that are oriented longitudinally with blood flow and is anchored to a filamentous basement membrane.^[20] The endothelial lining functions to prevent blood clots and secrete extracellular matrix proteins, including collagen and laminin,^[21] and contributes little to the tension in the vessel wall.^[14] Bundled around the tunica intima is the internal elastic lamina, an elastic membrane that is more prominent in muscular arteries and separates the tunica intima from the tunica media.^[21]

The tunica media is the central layer of the vessel wall, in between the tunica intima and the tunica adventitia. In the arteries, the media is the thickest layer and is distinguished by large

amounts of circularly-oriented smooth muscle cells (SMCs) (more predominate in smaller distributing arteries) and fenestrated elastin sheets.^[20, 21] This composition supports the muscular layer's responsibility of retaining active tension in the vessel wall through contraction and relaxation in order to control and disperse the pulsing, high-pressure blood flowing from the aorta.^[14, 22] Primary proteins responsible for this contractility include α -smooth muscle actin, smooth muscle-myosin heavy chain, and calponin.^[23, 24] The tunica media in veins is typically thin and contains less elastin and smooth muscle than arteries^[14] and are subjected to lower pressures.^[17]

The outermost layer of a blood vessel is the tunica adventitia, which is predominately a layer of connective tissue and fibroblasts and is distinguished by highly-collagenous extracellular matrix (ECM).^[20, 21] In arteries, the thickness of the adventitia is minor compared to the media, but this layer provides stability and rupture resistance from the high pressures.^[20]

From the physiological understanding of the structure and function of blood vessels, we can better apply engineering principles to cells and tissues in order to fabricate a blood vessel replacement that will resist rupture *in vivo* and successfully incorporate into the surrounding tissue. Several techniques for developing TEBVs have been explored, and the past and present approaches and challenges to creating a TEBV are described in the following section.

2.3 Developing Tissue-Engineered Blood Vessels

In an effort to create a suitable replacement vessel for vascular grafting, both synthetic grafts and tissue-engineered prostheses have been developed. Ideally, the alternative vessel should mimic native physiology as much as possible in order to retain vessel patency and achieve successful integration into the surrounding tissues. When developing a successful graft, the following characteristics should be considered: biocompatibility, strength, compliance, immunogenicity, and thromogenicity.^[25] The successful incorporation of these properties will positively influence how the body responds to the implant and how well the implant meets the needs of the body.

2.3.1 Scaffold Approaches

Early studies explored synthetic vascular grafts, using a scaffold of polyethylene terephthalate (PET, Dacron[®]) or expanded polytetrafluoroethylene (ePTFE, Gore-tex[®]). Today, these synthetic

grafts are quite successful as large diameter (7-9 mm) replacements;^[26] but in smaller vessels, the nonexistent endothelial lining of these synthetic materials permits luminal platelet adhesion and ultimately thrombus formation.^[26, 27] Furthermore, in small-diameter applications, long-term success is unattainable due to poor patency from low-flow conditions and compliance mismatch between the native vasculature and the synthetic conduit.^[25] Efforts to overcome the completely synthetic nature of the Dacron[®] and Gore-tex[®] grafts were made by pre-coating the ePTFE with fibrin glue to promote the formation of an endothelial cell monolayer on the luminal surface of the graft,^[28] as well as *in vitro* seeding of the glue-coated ePTFE graft with autologous endothelial cells before implantation.^[29] The latter protocol demonstrated an intact endothelialized luminal surface after three and a half years and a patency rate comparable to autologous vein grafting (~70% for above-knee grafting and ~80% for below-knee grafting).^[29] However, long-term adaptation is hindered by the inability of vascular cells to remodel the synthetic graft and the nonexistent vasoactivity of the graft, due to its synthetic nature.^[15]

An alternative to a permanent synthetic graft is a synthetic *biodegradable* or *bioabsorbable* scaffold, typically formed from polyesters such as polylactic acid (PLA) and polyglycolic acid (PGA), which is degraded at controlled rates as new tissue is synthesized. These grafts are often pre-seeded with cells for growth potential and provide a support structure for the inward migration of host cells and subsequent remodeling and repair of the implant site.^[30, 31] Shum-Tim *et al.*^[32] seeded autologous lamb endothelial, smooth muscle, and fibroblast cells onto a biodegradable PGA-polyhydroxyalkanoate (PHA) scaffold 7 days before implantation for use as an aortic graft in lambs. After five months, the tissue-engineered “biological” scaffolds remained patent and aneurysm-free, whereas the acellular polymer tube controls were occluded at day 1 and each subsequent time point. Additional promising results were observed in a clinical study by Shin’oka *et al.*,^[33] who seeded autologous bone marrow cells onto a degradable L-lactide and E-caprolactone scaffold for 2-4 hours before implanting the construct in 23 human patients as an extracardiac total vascapulmonary connection graft. Follow up evaluations (median 16.7 months after surgery) discovered no complications, including rupture, aneurysm formation, or calcification, and patency in all grafts.

To address the challenges presented by synthetic materials, the use of natural scaffolds (eg. biological tissues) has been explored. These scaffolds are derived from human or animal tissues

and are decellularized, typically with enzymatic or detergent treatments, to remove the host cells, preventing immunoreactions after transplantation. The resulting graft is an ECM scaffold, complete with native structure, biocompatibility, and intrinsic biological factors (eg. proteins, receptors, etc.) for improved cellular infiltration and tissue growth.^[26] Robotin-Johnson *et al.*^[34] used porcine acellular small intestinal submucosa (SIS) as a superior vena cava graft, demonstrating patency after five years, the development of an endothelial lining, and the overall positive influence of the collagenous matrix of the SIS as a framework for vascular remodeling and new tissue formation. Although natural scaffold grafts show promise, they are an imperfect solution as the harsh decellularization protocols often strip the tissue the desirable native elements in the matrix (eg. proteoglycans), thereby resulting in decreased strength and tissue size.^[30]

Similar to the natural scaffold is the biopolymer scaffold approach, pioneered by Weinberg and Bell,^[35] the first to develop a completely biological tissue-engineered blood vessel (TEBV). The graft consisted of a collagen gel and bovine smooth muscle cell foundation that supported an inner confluent layer of bovine endothelial cells and outer layer of bovine fibroblasts, grossly mimicking native arterial physiology. Although the biological materials present in this approach favor cellular attachment and signaling and tissue restructuring, the graft delivered minimal resistance to bursting under pressure. A mesh Dacron[®] sleeve was positioned around the gel to provide additional mechanical support, but the model was still mechanically underdeveloped for *in vivo* grafting. Consequently, studies have instead substituted fibrin for the collagen, aiming to improve the strength and stiffness of the scaffold.^[30, 36] Grassl *et al.*^[36] cultured fibrin constructs representing the medial layer of blood vessels with rat neonatal SMCs for 3 weeks and achieved an ultimate tensile stress (UTS) twice that of similar constructs fabricated from collagen (4.76×10^{-5} Pa vs. 1.87×10^{-5} Pa). The fibrin constructs also demonstrated morphological and structural characteristics similar to the collagen alternative, including circumferential alignment of the SMCs. Although promising, these specific fibrin-based TEBVs only demonstrated an UTS of 14×10^{-5} Pa, compared to 21×10^{-5} Pa for the rat abdominal aorta.

2.3.2 Cell-Derived Approaches

An alternative to the scaffold techniques for developing TEBVs is the cell-derived approach, in which grafts are fabricated without a pre-made scaffolding infrastructure. This approach harnesses the cell's ability to synthesize its own supporting matrix and signal and interact with other biological substances, all while maintaining biocompatibility. Permitting cells to self-assemble and drive their own tissue formation has the potential to develop a vascular graft with a structural morphology, composition, and function similar to native vasculature.^[37-39]

The “sheet-based” tissue engineering approach developed by L'Heureux *et al.*^[37, 40] demonstrated that the fabrication of a completely biological vessel capable of withstanding *in vivo* hemodynamics was possible. This model uses human SMCs and fibroblasts independently cultured in ascorbic acid-supplemented media to induce ECM synthesis and the formation of cellular sheets. The SMC sheet is then wrapped around a mandrel to achieve a tubular structure and the fibroblast sheet is wrapped over the SMC sheet. Once the sheets formed a cohesive vessel, the mandrel support was removed and the construct was seeded with endothelial cells, thereby creating a structure with an adventitia-like, media-like, and intima-like layer. This method achieves a vessel with natural structural characteristics, ECM proteins, and mechanical integrity. However, the total culture time of 13 weeks is highly limiting in terms of manufacturing and the turn-around time for clinical applications (eg. bypass grafting). Despite fabrication challenges, however, L'Heureux's technique has shown promise in clinical studies using a similar model consisting of a living fibroblast (autologous) adventitia, a decellularized internal membrane, and an endothelium from autologous endothelial cells.^[31, 40, 41]

In contrast, Gwyther *et al.*^[1] created a “ring-based” tissue engineering model as a means to quickly fabricate cell-derived vascular grafts. Rat aortic smooth muscle cells were seeded into annular agarose molds and allowed to self-assemble around a central post. The molds were designed with 2 mm, 4 mm, or 6 mm central posts to vary the inner diameter of the ring. After 8 days of culture, the rings were mechanically robust, with UTS values of 169, 339, and 503 kPa for the 2, 4, and 6 mm rings, respectively. Histology revealed glycosaminoglycans (GAGs) as the primary ECM constituent, but collagen had also been deposited throughout the rings. Furthermore, the ring-shaped tissues were then adjacently stacked on a mandrel and cultured,

allowing the individual rings to fuse into a cohesive tubular structure, which was then harvested as a single unit. The tubes remained intact after removal from the mandrel, but the fusion points between the rings were still visible. Although this approach lacks the multilayer structural organization of other TEBVs, it achieves a completely biological conduit fabricated in only two weeks.

Although a well-defined protocol or technique is required to fabricate a vascular construct, another crucial aspect of TEBV development is the appropriate external stimuli. By controlling chemical, electrical, and mechanical stimuli, the cells and tissues can be influenced and guided towards a specific activity, expression, or lineage. One of the ways to direct the structure and function of a TEBV is through subjection to mechanical conditioning, as described in the next section.

2.4 Influencing Structure and Function with Mechanical Conditioning

A key component to successful tissue-engineering is the ability to externally replicate the *in vivo* environment, thereby introducing the engineered tissue to stimuli present in the body *before* implantation. Simply, *ex vivo* pre-conditioning via a bioreactor physiologically prepares the tissue for *in vivo* adaptation. Bioreactors provide a means for applying chemical, electrical, or mechanical stimulation in order to direct or induce cellular activity, while providing controlled and repeatable culture conditions.^[42, 43] A common challenge in the development of functional TEBVs is achieving a mechanically-robust graft that is physically capable of withstanding native hemodynamic forces and pressures; as such, bioreactors are frequently employed as mechanical stimulators to condition the grafts during culture.

2.4.1 Effect of Mechanical Stimulation on TEBVs

Understanding the biomechanical cues that cells experience is crucial when developing a TEBV. Primary forces experienced by native vessels include radial and circumferential cyclic stresses, as applied by the pulsing blood flowing through the vessels.^[15, 44] The signals cells receive from these environmental cues enable the cells to actively monitor the hemodynamic environment and ultimately, direct cell-mediated vascular remodeling of the blood vessel walls as necessary to maintain appropriate environmental conditions.^[45] Similar results are observed *in vitro* when

TEBVs are subjected to mechanical stimulation. Primary effects of mechanical stimulation on vascular smooth muscle cells (VSMCs) include circumferential cellular orientation, an increase in synthesis of ECM components, improvement in mechanical integrity, and modulation in cell phenotype.

2.4.1.1 Cellular Alignment

It is well known^[44, 46-48] that mechanical stimulation in the form of stretch induces cells, including endothelial cells, smooth muscle cells, and fibroblasts, to align perpendicular to the stretch direction in 2D culture (see Figure 2). Cells grown on cyclically stretched substrates will align in the direction of minimum strain, in what has been described as an “avoidance reaction.”^[49] In 3D, through *in vitro* radial stretching of vascular constructs, vascular smooth muscle cells align circumferentially around the lumen, as observed in native vessels.^[50, 51] Cells nearer the graft lumen are exposed to higher stretch magnitudes and demonstrate more complete alignment, whereas cells near the central region of the graft are subjected less stretching and are consequently less highly aligned.^[52] The extent of alignment varies with stretch magnitude, frequency, and duration, is controlled through various signaling systems.^[44, 52, 53]

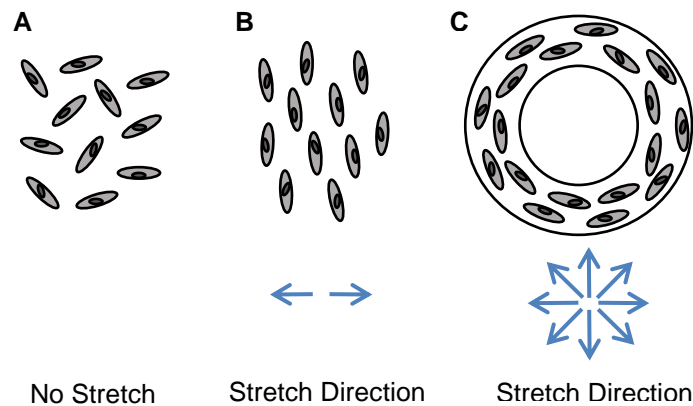


Figure 2 – Cellular Orientation in Response to Stretch. (A) Cells are randomly oriented in static (2D) culture; (B) cells align perpendicular to stretch direction in 2D when subjected to cyclic stretching; and (C) cells align perpendicular to stretch direction in a circumferential manner when subjected to cyclic stretching in 3D constructs or *in vivo*.

2.4.1.2 Increased Synthesis of ECM Components

Furthermore, mechanical conditioning via cyclic strain stimulates the up-regulation and synthesis of extracellular matrix elements, predominately collagen and glycosaminoglycans (GAGs).^[54]

Compared to stationary controls, stretching SMCs *in vitro* dictates a 2-4 fold increase of collagen I/III, elastin, hyaluronan, and chondroitin 6-sulfate synthesis without any significant change in DNA synthesis, suggesting an increase in cellular ECM synthesis and not a correlation with an increase in cell number.^[45, 54, 55] Other studies confirm significance in collagen and elastin synthesis in stretched samples over control samples at comparable culture conditions.^[45, 55, 56]

2.4.1.3 Improved Mechanical Strength

In conjunction with an increase in ECM synthesis and cellular alignment, ultimate tensile stress (UTS) is also increased in constructs subjected to dynamic conditioning. Cyclic strain stimulates tissue remodeling and reorganization of the matrix structure via matrix metalloproteinase 2 (MMP-2), ultimately influencing the tensile properties of the construct.^[45, 57] Several studies have demonstrated that stretching a collagen-based SMC construct significantly increases UTS, ranging from 7-22 kPa (4 day constructs at 1 Hz and 10% stretch) with controls failing at less than 5 kPa.^[45, 50] Using a fibrin-based tubular construct with porcine valve interstitial cells, Syedien *et al.* achieved a 191% increase in UTS with incremental steps of stretching magnitude (7.5% - 10% - 12.5% - 15%) for three weeks.^[56]

2.4.1.4 Phenotypic Modulation

Vascular smooth muscle cells (VSMCs) have been shown to modulate between phenotypes, allowing them to appropriately respond to the environmental cues imposed upon them. *In vivo*, SMCs reside in the “contractile” phase where the primary function is ensuring and maintaining the contraction and relaxation of blood vessel walls. In this state, contraction proteins, including α -smooth muscle actin, smooth muscle-myosin heavy chain, and calponin are heavily expressed. During pathological conditions or when removed from their native environment, however, SMCs can shift to a “synthetic” phase, primarily migrating, proliferating, and synthesizing proteins (ECM).^[24, 58-61]

By imparting physiological strains on TEBVs through stretching, various signaling pathways are influenced and are consequently able to direct the phenotype of the VSMCs.^[24] By subjecting VSMCs on a poly-(lactide-co-caprolactone) (PLCL) scaffold to 5% radial distention at 1 Hz for 8 weeks, Jeong *et al.* observed a 2.5-fold increase in α -smooth muscle actin over control samples.^[62] Similar results were achieved by Qu *et al.* with a Flexercell strain unit at 1 Hz and

10% elongation for 24 hours.^[61] The latter study showed not only significant expression of α -smooth muscle actin, but also mRNA expression of smooth muscle (SM) 1/2 myosin heavy chain and calponin.

2.4.2 Bioreactors for Mechanical Stimulation of TEBVs

In order to replicate the *in vivo* environment that so heavily dictates cellular function and physiology, vascular bioreactors are used to provide mechanical stimulation during culture to induce native anatomy into the tissue-engineered substrates. Primarily, vascular bioreactor configurations consist of either a perfusion system or a stretching mechanism (see Figure 3).

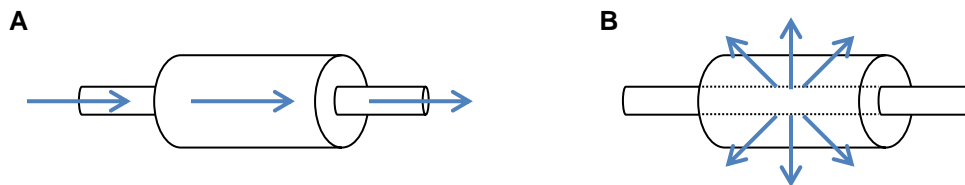


Figure 3 – Vascular Bioreactor Configurations. Bioreactor configurations for conditioning TEBVs include: (A) perfusion systems that flow media through the lumen of the construct; and (B) stretching systems that use regulated air or fluid flow to distend and relax the tubing, around which the construct is placed.

The perfusion systems often generate either continuous or pulsatile flow through the lumen of the TEBV and are typically controlled via compressed air or a peristaltic pump. These systems act on the engineered constructs through shear stress and are intended to mimic *in vivo* hemodynamics by replicating physiological flow and pressure profiles.^[63] Perfusion bioreactors are largely advantageous because they allow for controlled nutrient delivery to the luminal surface, instead of relying on diffusion from the exterior surface.^[64, 65] With this system, pressure, frequency, and flow rate can be manipulated, with various systems ranging from 25-180 mmHg, 1-1.5 Hz, and 40-130 mL/min, respectively.^[62, 64, 66] These values have been reported for studies evaluating TEBVs constructed from PGA scaffolds,^[64] polyethylene glycol (PEG)-based hydrogels,^[66] and PLCL scaffolds.^[62]

In current stretching methods, the TEBV is placed around a mandrel, which is then inflated using pressurized air or fluid to create circumferential distension.^[50, 56] These cyclic distension (CD) bioreactors stimulate via pulsatile distension, since VSMCs are not directly subjected to shear stress *in vivo*, but rather synchronized stretching during contraction and relaxation.^[30] Similar to

the perfusion bioreactors, the stretching configurations also allow for variable culture parameters and are typically operated at 1-1.5 Hz^[44, 50, 55, 57] and 7-15% circumferential strain.^[50, 55-57, 66]

Several CD bioreactors have been developed, but current studies have been limited to dynamic conditioning of TEBVs constructed from synthetic polymers or natural scaffold materials, including cell-seeded collagen gel constructs/sponges,^[50, 55] cell-seeded fibrin-based constructs,^[56] and fibronectin-coated PGA constructs.^[55] There has been report of mechanical stimulation on cell-derived, engineered tissue sheets,^[67] however, minimal data for conditioning 3D cell-derived TEBVs or engineered tissue rings is available. Furthermore, these systems typically use complex components, including pressure regulators, distributors, and solenoid valves to pneumatically control the tubing distension. Also, there have been no details reported about independent control over each culture chamber, indicating that all the chambers must be cultured at the same parameters (eg. frequency, pressure, duty cycle). A brief summary of bioreactors used for mechanical conditioning of vascular grafts is provided in Table 1.

Table 1 – Bioreactors for Mechanical Conditioning of Vascular Grafts. Brief summary of example bioreactors used to culture tissue-engineered blood vessels.

Investigator	Construct	Bioreactor Type	Culture Parameters
Engbers-Buijtenhuijs, <i>et al.</i> ^[68]	Human umbilical SMCs in porous collagen/elastin tubular scaffold	Pulsatile flow	120 beats/min 9.6 mL/min Up to 14 days
Syedain, <i>et al.</i> ^[56]	Porcine valve interstitial cells in tubular fibrin gel	Cyclic circumferential stretch	2.5% to 20% radial strain Constant and incremental strains 0.5 Hz with 12.5% duty cycle 3 weeks
Kim, <i>et al.</i> ^[55]	Rat SMCs in collagen sponges	Cyclic longitudinal stretch	7% uniaxial strain 1 Hz 5 weeks or 20 weeks
Seliktar, <i>et al.</i> ^[50]	Rat aortic SMCs in tubular collagen gel	Cyclic circumferential stretch	10% radial strain 1 Hz 4 and 8 days
Jeong, <i>et al.</i> ^[62]	Rabbit aortic SMCs in PLCL tubular scaffold	Pulsatile flow	130 mL/min 25 mmHg 1 Hz 5% radial distension 8 weeks
Narita, <i>et al.</i> ^[63]	Canine aortic SMC in PLA tubular scaffold	Pulsatile flow	120 beats/min 500 mL/min 40 mmHg systolic pressure
Williams and Wick ^[64]	Bovine aortic SMCs and bovine ECs in tubular porous PGA scaffold	Pulsatile flow	40 mL/min 1.5 Hz Up to 25 days
Niklason, <i>et al.</i> ^[69]	Bovine aortic SMCs in tubular PGA scaffold	Pulsatile flow	165 beats/min 5% radial distension 5 and 8 weeks
Gauvin, <i>et al.</i> ^[67]	Cell-derived human DF sheet	Cyclic longitudinal strain	10% uniaxial strain 1 Hz 3 days

In conclusion, this literature review provides a basic overview of the structure and function of blood vessels in order to better utilize engineering and design techniques to develop a small-diameter tubular construct for vascular grafting. The primary methods to fabricate a TEBV are through the use of (1) scaffolds or (2) cell-derived tissues. Common synthetic and natural scaffolding materials include PET or ePTFE, PLA or PGA, decellularized tissues, and collagen or fibrin gels. Cell-derived approaches, on the other hand, are solely cell-based and are supported by the ECM synthesized by the cells. “Sheet-based” and “ring-based” tissue engineering are examples of this approach. Aside from selecting the best technique to develop a TEBV, external stimuli in the form of mechanical conditioning can be implemented to influence the morphology

and mechanical integrity of the construct. Vascular bioreactors are typically used to dynamically culture the constructs through either pulsatile flow or cyclic stretching. With this knowledge and the documented culture parameters from various studies, we can begin to design a custom bioreactor for the purpose of mechanically conditioning engineered vascular tissues.

The goal of this project was to design a bioreactor to impart cyclic circumferential stretch on self-assembled smooth muscle cell rings generated as described by Gwyther *et al.*^[1] We expected that by subjecting the SMC rings to dynamic culture, we could increase ECM deposition, cellular alignment, and tissue strength; and these results would assist in the development of an ideal blood vessel replacement graft. The following chapter describes in detail the manufacture and validation of the cyclic stretch bioreactor designed to impart mechanical stimulation on the engineered tissues through stretching of silicone tubing, which cyclically distends and relaxes via fluid pressurized by a motor-cam system.

Chapter 3: Development and Characterization of a Cyclic Stretch Bioreactor

3.1 Introduction

The details provided in the previous discussion of bioreactors for culturing TEBVs were considered when designing a bioreactor system for the culture of tissue rings.^[1] The fundamental concept designed for stretching the rings, described in the following section, was developed as a part of a Major Qualifying Project at WPI by a team of three students, Kenneth Adams, Keith Bishop, and Elizabeth Casey.^[2] The team was able to manufacture a prototype, but several features required improvement to maintain functionality, consistency, and reliability of the device. The main problem areas on the prototype included the motor subsystem, syringe subsystem, and the chamber subsystem. Based on these findings, new components were designed to ensure that the bioreactor is able to consistently stretch tissue rings at specified stretch magnitudes for at least several days in the incubator, without incurring any mechanical or user difficulties. The new parts were then manufactured and assembled, and the final system was validated using DVT[®], a digital imaging analysis system, and high density mapping (HDM), a phase correlation algorithm for determining subpixel displacement. The focus of this chapter is the design, manufacture, and validation of the custom cyclic stretch bioreactor, as described in Objective 1.

3.1.1 Principal Mechanism for Tissue Stretching

One of the advantages of this bioreactor design is the simplicity of the principal mechanism for stretching the tissue rings. Distension within the bioreactor is driven by a cam-syringe-tubing subsystem (see Figure 4). The syringe and tubing are filled with fluid (dH_2O) and the system is closed with a pinch clamp. With each cam rotation, the plunger is depressed, forcing fluid from the syringe into the tubing, thereby distending the tubing. As the cam rotates to its minimum section, the spring concentric with the plunger uncoils, driving the plunger back to its initial position, subsequently relaxing the tubing.

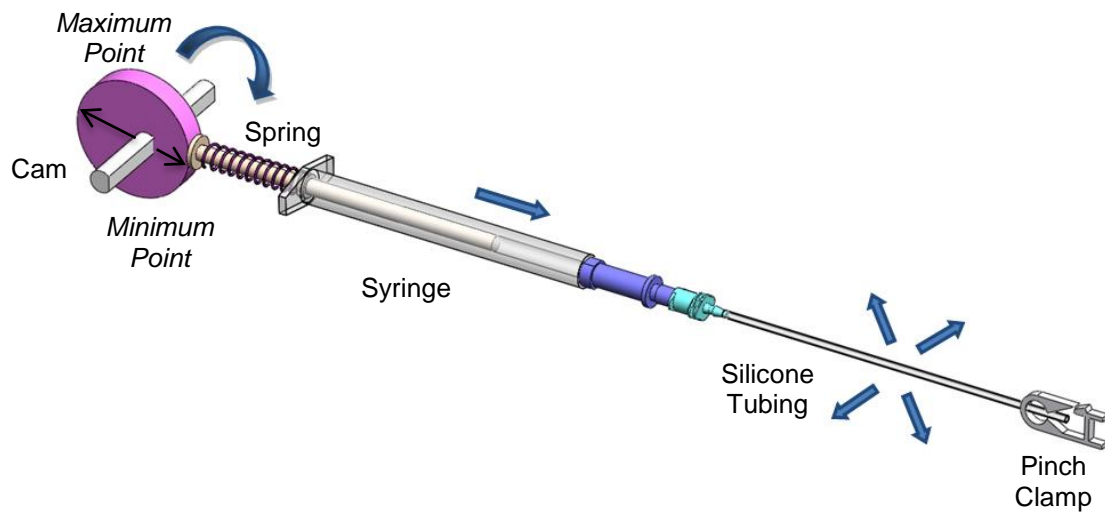


Figure 4 – Principal Stretching Mechanism. The cam-syringe-tubing assembly drives the stretching of the tissue ring. The syringe and tubing are filled with fluid and the system is closed with a pinch clamp. Fluid is forced further into the tubing with each rotation of the cam, thereby distending and relaxing the tubing, around which the rings are placed.

This fundamental concept from the prototype was carried over into the new design; however, the majority of the components on the prototype were replaced with newly designed and machined parts. An overview of the prototype and the design modifications are detailed in the following section.

3.1.2 Overview of Original Prototype and System Challenges

The prototype (see Figure 5) consisted of a motor-cam assembly that interfaced with a syringe-tubing subsystem, as previously described. The base was constructed of polycarbonate and supported all the components. The system consisted of five motor-syringe-tubing-chamber systems. The motors were vertically anchored through the base, such that the output shaft was pointing upward above the base. An acrylic cam with a D-profile cut to match that of the output shaft was concentrically placed on the motor shaft. A shaft collar was placed concentrically on top of the cam to prevent vertical motion of the cam on the shaft. The cam interfaced with a plastic flange extender connected to the plunger flange to increase the contact area of the cam against the plunger. Located around the plunger was the spring to return the plunger to its initial position with each cam rotation. The syringe barrel was pressed into the female end of a luer fitting threaded through the culture chamber. Each barrel was supported by a finger clamp, which

was pressed into a plastic block that was screwed into the base. The chambers were positioned in a tray milled from polycarbonate, which was secured to the base with polydimethylsiloxane (PDMS) supports. The chambers were held in place within the tray using finger screws. Lids for the chambers were constructed from Lexan[®] polycarbonate. A ~2 mm (OD) silicone tube, residing inside the chamber, was connected to the male end of a barbed luer fitting using heat shrink wrap. The female end of this fitting was pressed into the male end of the threaded luer. The end of the tubing distal to the syringe was closed with a pinch clamp, which was anchored in place with a dowel pin pressed into the base of the chamber.

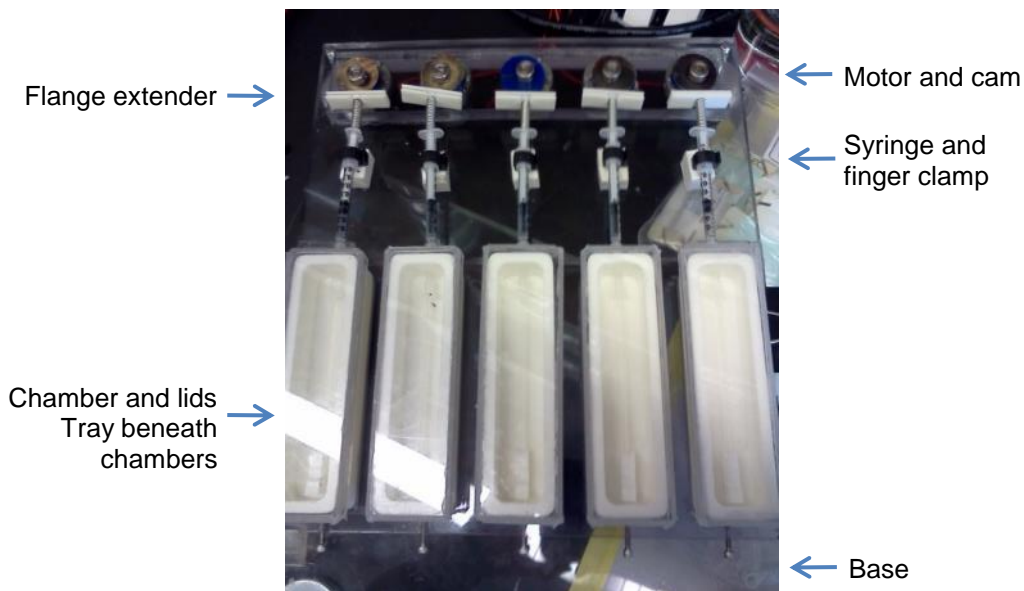


Figure 5 – Cyclic Stretch Bioreactor Prototype. The prototype foundation was a polycarbonate base. Five chambers constructed of high-temperature UHMWPE were fit into a tray that was positioned on top of the base. Each chamber was connected to a 1 mL disposable syringe that was supported with finger clamps. The lids were fabricated from thin polycarbonate sheets. A spring was placed around each plunger, and the end of the plunger interfaced with a plastic flange extender that contacted the cam on the motor. Each chamber-syringe system was driven with its own motor.

Inspection of the motor system revealed that the front half of the motors were exposed, subjecting the internal gears and lubrication to the warm, moist incubator environment. With repeated exposure to these conditions, the lubrication inside the motors became too viscous and prohibited the gears from properly rotating. Each chamber of the bioreactor was connected to its own (identical) motor, but consistency between the motors could not be established, creating a challenge when trying to control all possible variables. Furthermore, the electrical wiring of the motors had been disrupted and select motors would shut off when others were turned on.

In the syringe system, not all of the syringes were aligned to their corresponding cam/motor assembly, creating a nonlinear application of force on the plunger. The syringes used were a 1 mL Monoject luer-slip (LS) syringe and had a flexible plunger, which was easily deformed in the horizontal direction when depressed by the cam. Extended testing with the system running over two days revealed a major flaw in the syringe design. The repeated back-and-forth motion of the plunger created enough friction to cause the rubber tip on the plunger to become stuck in place and cease all distending motion. Also, the springs on the syringe plunger had a spring constant of 6.78 lbs/in, requiring an unnecessarily large amount of force from the bioreactor system, and thereby adding unnecessary stress on the motor. The clamps used to secure the syringes in place were difficult to manipulate and interfered with the tray when moving the chambers.

Within the chamber system, there was leaking at the threaded luer fitting, allowing media to drip out of the chamber, onto the tray exposed to the incubator environment. The chambers experienced shrinkage during sterilization, and finger screws were used to secure the chambers in place. The screws, however, were difficult to turn and created indents in the chambers. The tray was designed to sit on top of the base and PDMS edges were attached to the base to hold the tray edges in place. However, the tray was not sufficiently stabilized and had to be secured to the base with large binder clips. Furthermore, the seams on the lids were poorly joined and did not suitably fit the chamber.

3.2 Methods and Materials

After a thorough analysis of the prototype and documentation of the features that needed improvement, new components were designed and manufactured. The bioreactor was then

characterized and validated using digital imaging analysis and high density mapping to ensure functionality. The following sections detail the methods and materials used to complete the fabrication and validation of the bioreactor.

3.2.1 Manufacture

The majority of non-commercial components were manufactured in the Higgins Laboratory machine shop at Worcester Polytechnic Institute (WPI), but the cams were created via a laser cutter at the Washburn Shops at WPI. Equipment used at the machine shop included a manual mill, a computer numerical control (CNC) machine, and a drill press. Materials were selected based on machinability, operating temperature, and corrosion resistance to ensure that all parts could not only be manufactured, but also steam-sterilized and operable in the humid incubator conditions. The only machined components requiring sterilization via autoclave were the tissue chambers and the tissue chamber lids. The tissue chambers were constructed from high-temperature ultra-high molecular weight polyethylene (UHMWPE) (McMaster-Carr), which has a maximum temperature of 275°F. The chamber lids were constructed of Lexan[®] polycarbonate (GE) and 5052-H32 aluminum (OnlineMetals, Inc.), which has very good corrosion resistance. The cams are acrylic (PLASTiCare, LLC) and all other custom components were machined from impact-resistant slippery UHMWPE (McMaster-Carr) or aluminum. All commercial components are either aluminum or stainless steel. A complete list of all materials can be found in Appendix A: Bill of Materials.

3.2.2 System Characterization and Validation

Following assembly, the bioreactor was validated through a variety of functionality and reliability tests. The system was run outside the incubator to verify that 1) the cam-syringe-tubing subsystem functioned as designed; 2) the motor was able to effectively transmit sufficient torque to the cams to simultaneously depress the four syringe plungers; and 3) the tubing distended to the correct stretch magnitude for each cam size. The bioreactor was then allowed to run inside the incubator for seven days to confirm that the motor was sufficiently enclosed and that the humid incubator environment was not affecting the electrical system.

3.2.2.1 *Static Tubing and Cam Validation via DVT[®]*

Manual, static testing of the syringe-tubing system was conducted to characterize the amount of fluid required to distend the tubing to various magnitudes and to ensure that the various-sized cams were distending the tubing to the appropriate value. During the tubing characterization testing, the syringe was filled with water and connected to the luer fitting on the tubing. The plunger was slowly depressed to force fluid through the tubing, and the system was closed with a pinch clamp once the tubing was uniformly filled. The diameter of the tubing at this initial point was captured with a DVT[®] Series 600 SmartImage Sensor (Cognex, Model 630) and calculated based on position sensors using DVT[®] Framework 2.2 software (Cognex). The plunger was then incrementally depressed to various positions and an image was captured at each position. For each depression position, the outer diameter of the tubing was then measured at five points along the length of the tubing using the captured image. The five measurements were then averaged and the percent change (distension) was calculated using the average of the five measurements from the initial position.

A similar protocol was used to verify that the tubing diameter with each cam rotation correctly corresponded to the appropriate-sized cam. Before testing, four syringes were placed on the bioreactor and each cam on the bioreactor was a different size, corresponding to four different distension values (5%, 7.5%, 10%, and 15%), which were selected based on physiological stretch values observed throughout the cardiovascular system.^[18, 19] The shaft was rotated such that the minimum point on the bioreactor, where the syringe plunger is at a maximum volume, was labeled with a marker. Then, the shaft was rotated such that the maximum point on each cam was now interfacing with the syringe, and these points were marked on each syringe. One at a time, the syringes were positioned in a syringe pump, such that the tubing was located beneath the DVT[®] camera (see Figure 6). Images were captured at the initial point and then at the second marked line. Using the position sensors, tubing diameter measurements were recorded at five positions along the length of the tubing for each image. The five measurements were then averaged and the percent distension for that tubing sample of the specific cam size was calculated.

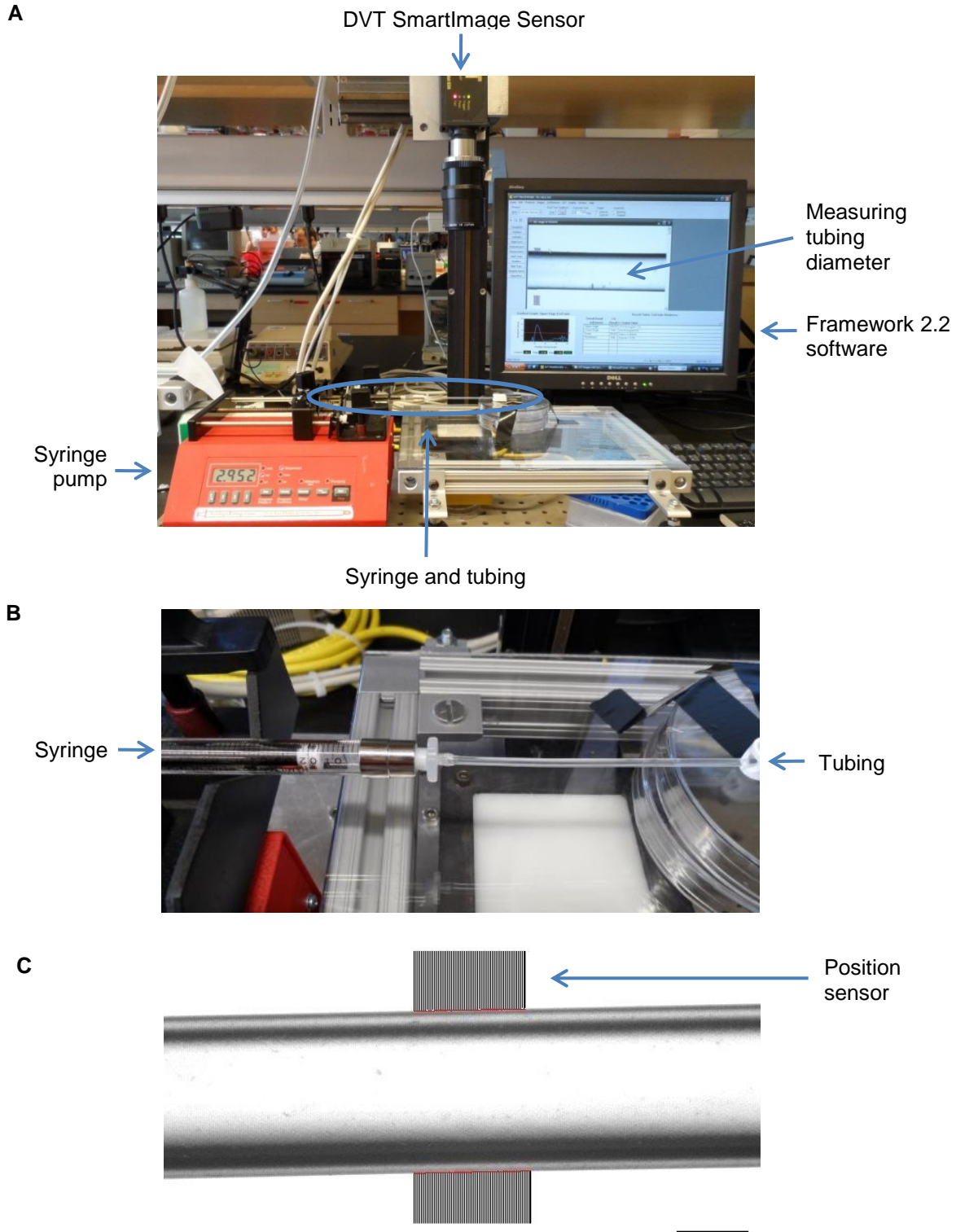


Figure 6 – DVT® Setup for Cam Validation. Using DVT® to calculate the diameter of the tubing based on known syringe volumes to verify the tubing distension with each cam size. (A) Setup for DVT® analysis; (B) syringe and tubing during DVT® analysis; (c) example captured tubing image and position sensors used to determine tubing edge to calculate tubing diameter; scale=750 μ m.

3.2.2.2 *Dynamic Tubing Validation via HDM*

High density mapping (HDM),^[3] developed by the Gaudette Lab at WPI, was utilized to analyze the dynamic distension of the tubing during bioreactor operation. Similar to previous testing, the syringe was filled with water and connected to the luer fitting threaded through the chamber. The female end of the luer fitting on the tubing was then connected to the male end of the threaded fitting. The plunger was slowly depressed to the starting volume that corresponds to the cam size (2.0 mL), ensuring that the tubing was uniformly filled with fluid and free of bubbles. The pinch clamp was immediately closed. The syringe-chamber system was placed on the bioreactor with the 5% cam. The middle region of the tubing was coated with mixture of silicon carbide particles (Alfa Aesar silicon carbide 400 grinding compound, 39800) and retroreflective beads (3M Scotchlite 8017 reflective ink part B, 75-0500-2359-9) to create a “speckle” pattern. The bioreactor was switched on and video of the operation was recorded (20 seconds) using a high speed camera (Photron FASTCAM 1280 PCI and Nikon AF Micro-Nikkor 105 mm lens; 1280x1024 resolution). Following video capture, the syringe-chamber system was moved to the 7.5%, 10%, and 15% cams (in this order) and the process was repeated for each stretch size. The same tubing sample was used for each test.

A second HDM study was performed to validate the distension of the tubing along the entire length of the tubing to determine if regional distension differences exist. The syringe-tubing system was setup as described, but the entire length of the tubing was coated in speckle and only the 10% cam was used. A ruler was used to create a scale (0 cm to 8 cm) on the bottom of the chamber to identify regions on the tubing. The 0 cm mark was located at the interface between the tubing and the luer-to-barb fitting. One centimeter increments up to eight centimeters were marked on the chamber. The final mark (8 cm, furthest point from cam) was located near the pinch clamp. The length of the tubing was separated into four regions (1-2.5 cm, 2.5-4 cm, 4-5.5 cm, and 5.5-7 cm), with each region name corresponding to the length of the tubing being analyzed, in regard to the distance from the 0 cm mark. The syringe and tubing was set and positioned, and the first video (1-2.5 cm) was recorded with a high speed camera (FASTEC IMAGING HighSpec 4 and Nikon AF Micro-Nikkor 105 mm lens; 1696x1710 resolution). Without adjusting the syringe and tubing, the system was repositioned to bring the next region (2.5-4 cm) into camera view, and video was recorded. This process was repeated for the

remaining two regions. The tubing was then removed and the entire process was repeated with a new tubing sample.

Following each test, the video was saved as a series of .tif images (raw data). These images were then processed through MATLAB using a custom speckle tracking program, which utilizes a subpixel phase correlation algorithm. For each tubing sample, the following protocol was completed:

1. Run HDM code → an image from the video is generated
2. Using the image, draw a rectangle on the section of tubing to be analyzed → the region of interest (ROI) is selected and the data are analyzed
3. Run strain code → average Green strain is calculated and exported into Excel
4. Create strain vs. time graph and document the minimum and maximum strain of five cycles on the curve
5. Calculate the difference between the minimum and maximum strain of the five cycles and average the values → distension value is determined

3.2.3 Determining Statistical Significance

Statistical analyses were performed using SigmaPlot 12.3 (Systat Software, Inc.). Data were tested using the Shapiro-Wilk normality test and the equal variance test. A one way analysis of variance (ANOVA) and post-hoc Tukey pairwise multiple comparison test (if applicable) were performed on all data. The one way ANOVA was used to compare the means of the samples and determine if a difference between the groups (eg. stretch magnitudes) existed. If the one way ANOVA detected that the means were not equal, the Tukey test was then performed to analyze any differences in the means of all possible two-way comparisons (eg. 5% vs. 7.5%, 5% vs. 10%, etc.). All tests utilized a p value of 0.05; a difference in means was considered statistically significant for any p value less than 0.05.

3.3 Results

Using the equipment provided by WPI and commercially-available fasteners and minor components, the bioreactor was fully manufactured and assembled. The design modifications

and final assembly are described in detail below, as well as the results of the bioreactor validation testing.

3.3.1 Bioreactor Components and Design Modifications

In response to the challenges with the previous system, new components were drafted in SolidWorks (Dassault Systèmes, SolidWorks Corp.) (see Appendix B: CAD Drawings) and a new system (see Figure 12) was built in its entirety. The new parts were selected and designed to promote system efficiency, reliability, and completeness.

3.3.1.1 Motor-Shaft System

As mentioned, the previous design consisted of five statically-mounted motors, such that the output shaft of the motor is vertically exposed. With the new design, a 1 Hz single-motor (RobotShop, Inc.) and extended shaft system (see Figure 7) replaces the five-motor system. New wiring (Turn 4 Hobbies) was soldered to the motor and connected to the electrical system. The motor is encased in an adhesive-lined flexible heat shrinking tubing (Raychem) to protect the wiring connection.

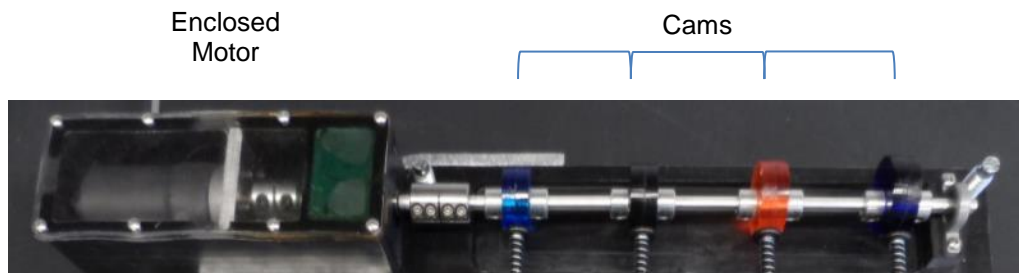


Figure 7 – Motor-Shaft System. A single motor is connected to a main shaft that supports four separate cams.

By reducing the number of motors and implementing a more powerful motor, each syringe-chamber assembly is conditioned simultaneously. This setup reduces variability in the motors and initial cam starting position and permits consistent plunger depression across the chambers. The aluminum shaft (Home Depot) has a D-profile cut and the cams have a matching D-profile cut, ensuring that there is no independent rotation of the cams on the shaft.

3.3.1.2 Motor Enclosure

A motor enclosure (see Figure 8) was designed to support the motor system and isolate the motor from the incubator environment. In the previous design, the wired end of each motor was sealed with moisture resistant shrink wrap, but the opposite end of the motor was completely exposed to the humid conditions of the incubator. Moisture from the incubator was able to penetrate through the exposed area where the output shaft interfaced with the motor and subsequently thicken the internal lubrication on the gears, ultimately reducing the functionality of the motors.

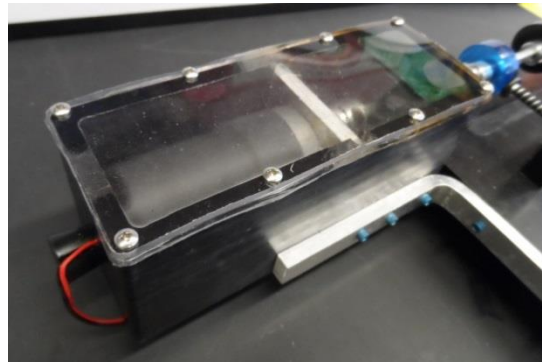


Figure 8 – Motor Enclosure. An enclosure was built to support the motor and isolate it from the humid environmental conditions in the incubator. The mount consists of two chambers, one for the motor and one for a grease box.

The mount consists of two chambers, two bearings, a shaft extender, and a double-wide shaft collar. It is attached to the base of the bioreactor with custom aluminum brackets. In the main chamber, the output shaft of the motor is connected to a round ¼” aluminum shaft extender via a double-wide shaft collar (Rutland). The shaft extender penetrates through the dividing wall between the two chambers and all the way through the second chamber. A bearing (Stock Drive Products) is located within the dividing wall, concentric to the shaft, to provide a seal to the main chamber. The second chamber is filled with grease (Lucas Oil Products, Inc.) to act as a humidity barrier. Because the humidity is entering from the front of the motor, the moisture will act on the grease in the minor chamber before it acts on the grease in the motor itself. The grease in the chamber can be removed and refilled, as necessary. The shaft extender exits the support wall, which also contains a bearing (Stock Drive Products) to help prevent the entrance of moisture. Connected to the shaft extender via a rigid coupling (Rutland) is the main shaft that supports the cams.

An aluminum plate slides into the main chamber. The face of the motor sits flush against the plate and is secured into the plate with screws. This allows for quick removal of the motor if necessary (e.g. to replace it), while ensuring that the motor is correctly aligned within the system.

The motor support has a horizontal lid that sits flush on top of the enclosure. A thin sheet of PDMS sits between the mount and the lid to provide an extra seal. On the wall closest to the rear of the motor is an exit hole for the motor wires. A rubber stopper (Alliance Express) is pressed into this hole, with the wires squeezed around the circumferential surface.

3.3.1.3 Tissue Chambers

The chambers (see Figure 9) were modified to separate the chamber wall into two different height levels to assist in preventing media from spilling onto the top surface of the chamber. The upper level is the top surface of the chamber and the lower level is approximately three-fourths the total height of the chamber. A luer fitting (Value Plastics, Inc.) is threaded through the wall facing the shaft-cam system and interlocks with the syringe. The pinch clamp that seals the tubing fits over a small dowel pin (McMaster-Carr) that extends from the bottom of the chamber in order to hold the clamp in position.

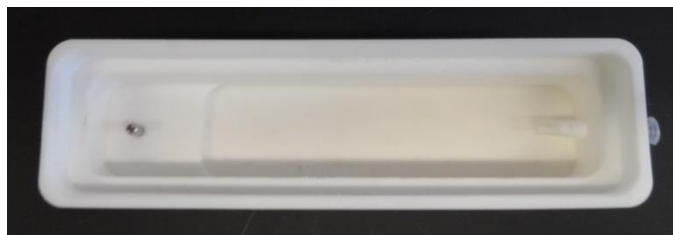


Figure 9 – Tissue Culture Chamber. The culture chamber was milled from high-temperature UHMWPE and includes a dowel pin to stabilize the pinch clamp and a threaded luer fitting through the chamber wall for connection to the syringe.

3.3.1.4 Syringe Supports

Syringe supports are utilized to prevent vertical motion of the syringes and stabilize the syringes during plunger depression. These supports were designed to allow more freedom when setting the tray on the base. Previously, one-piece U clamps (finger clamps) were attached to the base, with one clamp for each syringe. The hinged, top-portion of the clamp would interfere with the

syringes while the syringe-tray assembly was being moved on and off the base and the clamps were different to open and close.

The new supports (see Figure 10) are a two-piece system. The bottom piece extends the width of all the chambers and has semi-circle cutouts at each syringe location. Once the syringe-tray assembly is in place, the top-piece can be easily mounted onto the syringes and attached to the bottom-piece with two finger screws. This new system provides improved functionality and user-friendliness.

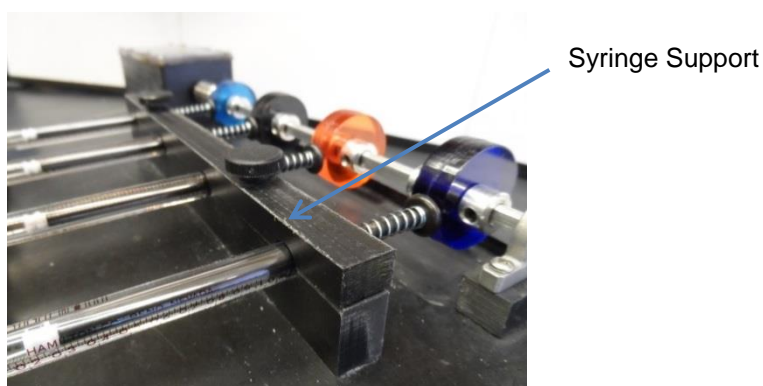


Figure 10 – Syringe Support. The syringe support is a two-piece system fabricated from UHMWPE that stabilizes the syringes during cam movement.

3.3.1.5 Tissue Chamber Lids

The original tissue chamber lids (see Figure 11) were created by joining pieces of cut Lexan[®] polycarbonate. They were poorly sealed and very fragile. The lids were re-designed in a two-piece fashion. Because the lid should be transparent to allow visibility into the chamber, using a solid piece of plastic was not a suitable option since milling the plastic would create a cloudy surface finish. Instead, a thin piece of Lexan[®] polycarbonate (GE) was attached to a thin edging created from aluminum. Aluminum (OnlineMetals.com) was selected because of its high-machinability, especially for thin-walled applications. The Lexan[®] is tightly secured to the aluminum edging with several small screws (McMaster-Carr). The lids securely fit over the chambers but still allow for gas exchange.



Figure 11 – Tissue Culture Chamber Lid. The lids for the chambers are a two-piece design constructed from Lexan[®] polycarbonate and aluminum.

3.3.1.6 Syringe

The previous single-use (disposable) 1 mL Monject luer-slip syringes were replaced with reusable 1 mL Hamilton 1001 gastight luer-lock syringes (Hamilton). The luer-lock fitting provides a more secure attachment to the threaded luer fitting seated through the chamber. The syringe consists of a borosilicate glass barrel and a polytetrafluoroethylene (PTFE) plunger tip. The rigid plunger prohibits non-linear deflection during cam interactions (over the previous plastic plunger) and the glass barrel and PTFE tip permits better continuous movement capabilities (over the previous rubber tip).

3.3.1.7 Spring

The original springs used to return the plunger to its starting position were excessively resistant to compression due to the larger-than necessary spring rate. Furthermore, the previous springs were cut to achieve the desired length, resulting in inconsistencies across each syringe-spring unit. The new springs (Century Spring Corp.) have a spring rate of 2 lbs/in., which provides much less resistance on the motor-cam system over the previous springs. Even though the new springs are more easily compressed, they still retain their function of returning the plunger to its initial position. The original length of 1.380 inches is acceptable and does not require resizing.

3.3.1.8 Final Cyclic Stretch Bioreactor Assembly

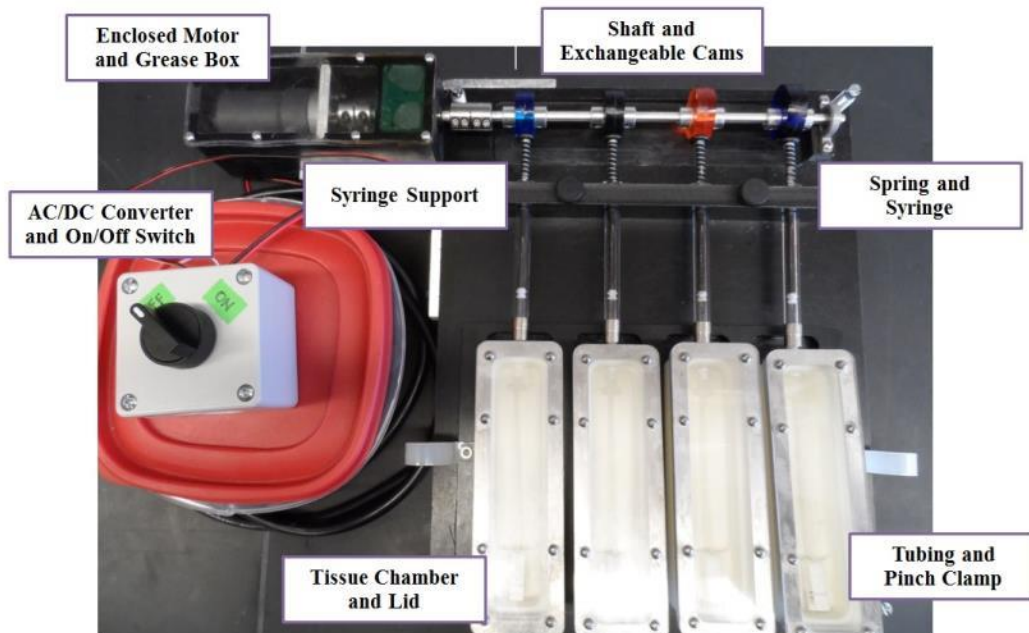


Figure 12 – Final Bioreactor Assembly. The new version of the cyclic stretch bioreactor with redesigned components and new features.

The final assembly is illustrated in Figure 12. The motor is enclosed within the motor support and is attached to a solid, circular shaft extender with a double-wide shaft collar. The shaft extender then passes into the second chamber of the motor support, which is filled with grease, and exits the motor support. Outside the motor support, the shaft extender is connected to a D-profile solid (main) shaft with a coupling. The main shaft is then supported at the far end of the bioreactor with a self-lubricating ball bearing. Each cam is held in place on the main shaft with a shaft collar (McMaster-Carr) positioned on each side of the cam. A spring is concentrically placed on each plunger between the flange of the syringe barrel and the flange of the syringe plunger. The syringes are stabilized by the syringe support and lock into the luer fittings threaded through the tissue chambers. The silicone tubing is connected to a female-to-barb luer fitting and secured in place with shrink wrap. The tubing is then slipped into place on the male end of the threaded luer fitting. The silicone tubing is closed with a pinch clamp (Z-man Corp.), which is positioned over a dowel pin set into the bottom of the tissue chamber. The lids are set on top of the chamber and are held in place by the lid walls. The on/off controller is wired to the motor within the motor support, and the hole through which the wire passes is sealed with a rubber

stopper. The AC/DC converter (Hengfu) is wired to the on/off selector switch (AutomationDirect.com) that is located in a plastic shelter. The on/off controller and AC/DC converter remain outside the incubator during experimentation. The entire system is supported by leveling mounts (feet) threaded (McMaster-Carr) through the base, allowing for a small range of height adjustment, as necessary.

No modifications or design changes were implemented for the tubing and new tubing assemblies were fabricated as described in Adams, *et al.*^[2] Briefly, 10 cm lengths of silicone tubing (0.058" ID, 0.077" OD, Specialty Manufacturing, Inc.) and 4 mm lengths of heat shrink wrap (Mouser Electronics) were cut with a no. 10 scalpel blade. One end of each piece of tubing was trimmed at a 45° angle to promote easier loading of rings onto the tubing. Gently, the non-trimmed end of the tubing was positioned over the barb of the female luer-to-barb fitting (Value Plastics, Inc.). A piece of heat shrink wrap was then slide over the tubing, starting at the trimmed end, and positioned midway over the tubing-barb junction. A heat gun (Wagner, HT1000) was then used to shrink the wrap and seal the tubing to the barb. The heat gun was turned on and allowed to warm up for 1 minute. While holding the luer fitting in one hand with forceps, the other hand gently moved the heat gun from side to side over the shrink wrap, staying approximately 6" away from the tubing. The fitting was rotated 360° over a 15 second period to ensure complete shrinkage.

Additionally, the cams were also fabricated in the same manner as for the prototype,^[2] with the exception of multiple sizes being manufactured to allow for various stretch magnitudes, representing the range of physiological stretch values. The cams were designed with an eccentric (circular with offset axis of rotation) profile to provide smooth, continuous motion and an offset D-profile cut for the shaft to pass through. The minimum offset was consistent for each cam size such that the initial position for all syringe plungers is consistent.

3.3.2 Tubing and Cam Validation

The tubing distension was (statically) characterized with the DVT[®] SmartImage Sensor digital image analysis system five separate times using five separate tubing assemblies, and the average distension of all trials was plotted against the corresponding syringe plunger depression levels (see Figure 13). A trendline was established to determine the relationship between the volume of

fluid forced into the tubing and the resulting distension (Cauchy/engineering strain) of the tubing.

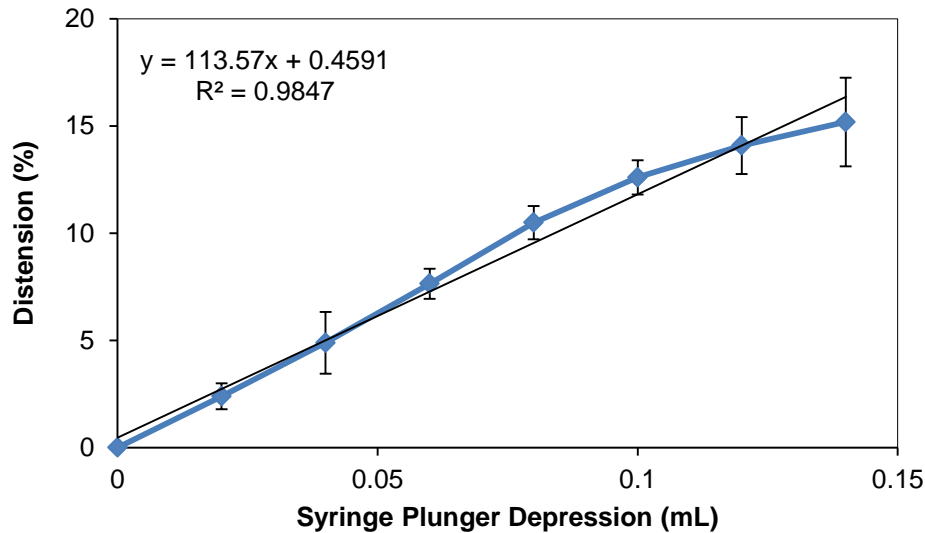


Figure 13 – Tubing Distension vs. Syringe Plunger Depression. Static testing using DVT[®] image analysis was conducted to correlate tubing distension values with (syringe) plunger movement to determine cam offsets. Data reported as mean \pm SEM, n=5.

The resulting equation ($y=113.57x+0.4591$) was used to calculate the offset requirement of the cams. Using 5, 7.5, 10, and 15% distension (y), the respective volume required (x) was calculated. This value was then converted to a linear distance using the relationship 1 mL volume change (Hamilton 1001 syringe) equals 6 mm of linear distance. The resulting distance is the offset required between the center of the shaft to the maximum point on the cam minus the center of the shaft to the minimum point on the cam.

Figure 14 compares the actual distension achieved (Cauchy/engineering strain) in the tubing against the theoretical or calculated distension based on the generated equation. The solid black line refers to the theoretical distension that should be achieved for each microliter of fluid forced into the syringe (based on $y=113.57x+0.4591$). The (grayscale) bars refer to the distension actually achieved by the manufactured cams. The labels on the bars indicate a) the cam size, b) the actual distension achieved, and c) the amount of fluid movement into the syringe to achieve the corresponding distension.

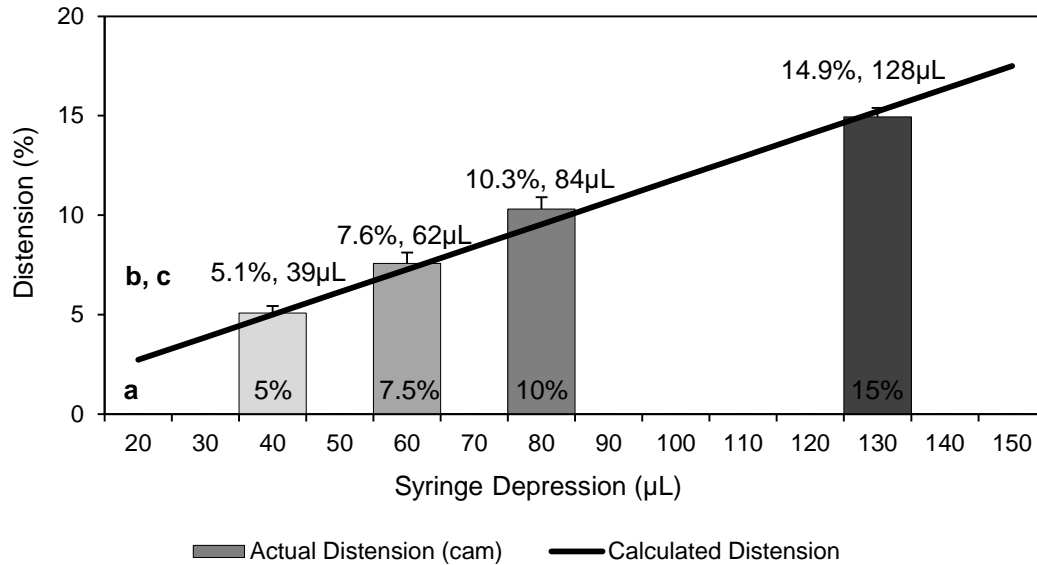


Figure 14 – Distension Characterization of Four Cams. The (theoretical) calculated distension values based on previous data ($y=113.57x + 0.4591$) is shown as the (black) line and the actual distension using the four fabricated cam sizes is shown as the (grayscale) bars. Letter “a” refers to the size (stretch magnitude) of the cam; letter “b” refers to the mean of the actual distension; and letter “c” refers to how much fluid is forced into the tubing to achieve the corresponding distension. Data reported as mean \pm SEM, n=5.

Actual distension values of 5.1, 7.6, 10.3%, and 14.9% were achieved, suggesting that the cam offsets correctly correspond to the desired stretching magnitudes during static testing. A possible cause of variance can be attributed to the tolerances during machining the cams. However, the demonstrated distension values are sufficient for the purpose of this research, and the stretch magnitudes will continue to be represented as 5, 7.5, 10, and 15%.

HDM was completed to analyze the (dynamic) distension of the tubing during bioreactor operation. After each test, the recorded video was saved as a series of images. An example of a saved image of the speckled tubing is presented in Figure 15A. Figure 15B shows the corresponding ROI that was manually selected for this sample. The area shaded in red is the region of tubing to be analyzed in the custom speckle tracking program in MATLAB. The green box in the ROI is the 32x32 pixel subimage, which was repeatedly shifted 16 pixels (blue box) throughout the ROI to determine the subpixel displacements.

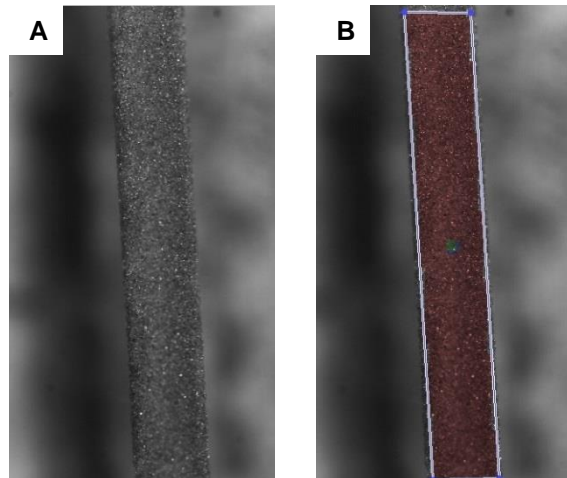


Figure 15 – Example of Tubing Image during HDM Analysis. Tubing that has been “speckled” is shown in (A) and the same image opened in MATLAB with the ROI selected is shown in (B).

After data processing, a strain curve was generated to calculate the distension values. An example of the 10% cam strain vs. frame number graph is shown in Figure 16. The data correspond to Green’s strain in the circumferential direction. Distension values were determined by first selecting five consecutive cycles on the graph, as indicated by the blue boxes. The minimum and maximum strain value for each cycle was determined and the difference between these points was calculated. This value corresponds to the distension of the tubing; the five distension values were averaged to produce the distension value for each sample of each cam size. The samples were averaged to generate the final distension value for each cam.

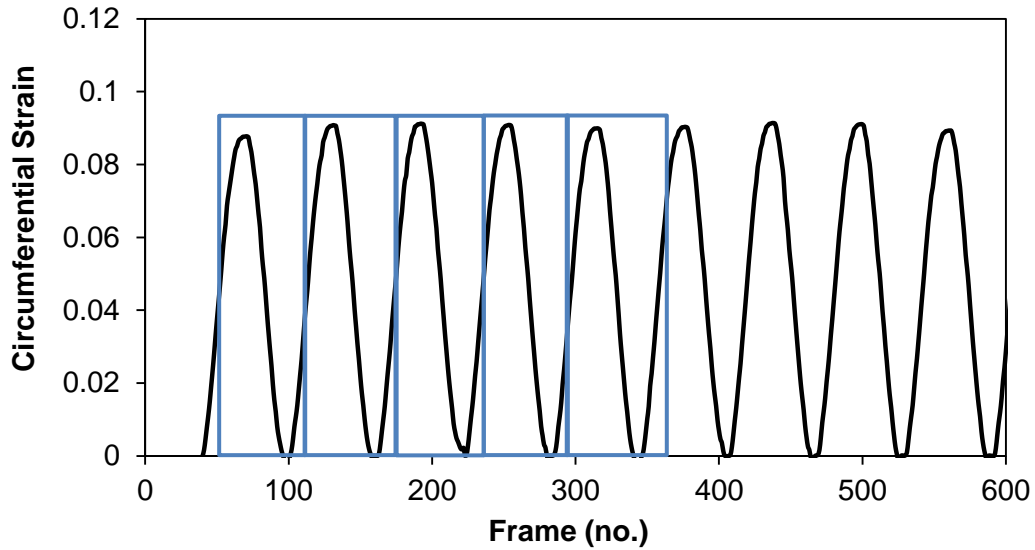


Figure 16 – Strain vs. Frame Number for 10% Cam using HDM. The raw data were processed and analyzed in MATLAB using a custom speckle tracking program to produce a curve of Green’s circumferential strain on the tubing during bioreactor operation. The difference between the minimum and maximum strain for five separate cycles (blue boxes) was calculated and these values were averaged to determine the distension for that sample.

The average dynamic distension for each cam size is described in Figure 17. The 5%, 7.5%, 10%, and 15% cams achieved distensions of 3.7%, 6.4%, 8.3%, and 12.7%, respectively (reported as mean \pm SEM, n=3).

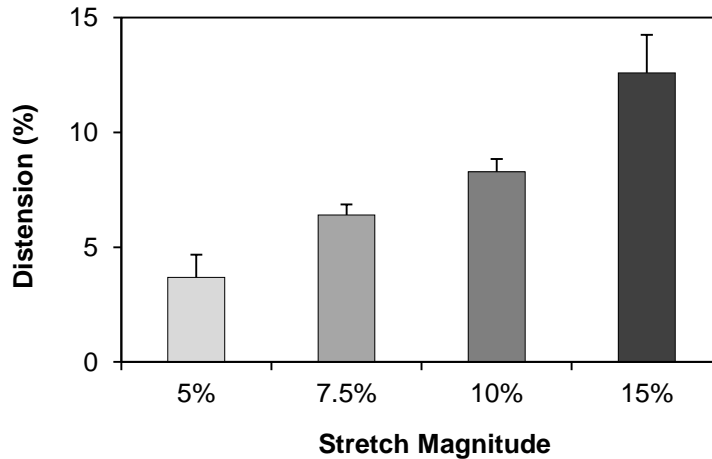


Figure 17 – Dynamic Tubing Distension at Four Stretch Magnitudes. HDM was used to determine the distension values of the tubing during bioreactor operation using four different cam sizes. Data reported as mean \pm SEM, n=3.

3.3.3 Regional Tubing Distension

Analysis of regional tubing distension at 10% stretch is presented in Figure 18. The region closest to the cam (1-2.5 cm) distended, over an average of three samples, 7.2%. Moving away from the cam, the next region (2.5-4 cm) was 7.5%, followed by 5.8% and 2.9% for the 4-5.5 cm and 5.5-7 cm regions, respectively. The data passed the Shapiro-Wilk normality test and equal variance test and a one way ANOVA was run on the data. The p value of the ANOVA test was 0.108, indicating no significance between the distension values at the various regions. However, the power of the ANOVA, with an alpha of 0.050, was 0.306, which is lower than the standard (0.800) and suggests that the data are not strong enough to determine significance if it exists. When only looking at the graph of distension vs. tubing position, there does appear to be a negative trend between distension and increased distance from the cam. An increase in sample size would improve the power of the data and possibly enable detection of significance in this trend.

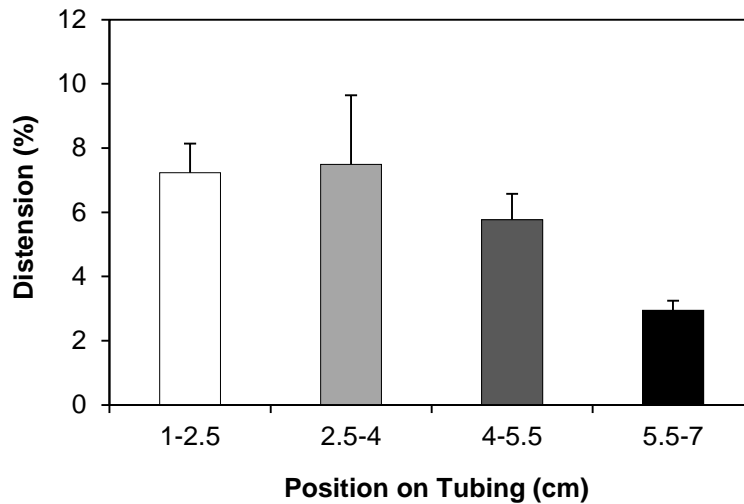


Figure 18 – Regional Tubing Distension at 10% Stretch. HDM was used to determine distension values along the length of the tubing in increasing distance away from the (10%) cam. Data reported as mean \pm SEM, n= 3.

3.4 Summary and Discussion

This chapter has discussed in detail the methods, materials, and results regarding Objective 1, the design, manufacture, and validation of a cyclic stretch bioreactor for the dynamic culture of SMC tissue rings. The prototype developed by Adams, Bishop, and Casey^[2] was reviewed and analyzed and new system components were designed to improve the functionality of the

bioreactor. A new system was completely manufactured and assembled, with design emphasis on the stability and ease of use of the device. The system uses a closed cam-syringe-tubing assembly to drive distension. A syringe and tubing are filled with fluid, and during each rotation of the cam, the syringe plunger forces more fluid into the tubing, causing the tubing to distend.

Modifications included a reduction in motors to a single motor-shaft system; new springs, syringes, chambers, and chamber lids; a motor enclosure; and a syringe support. Together, these revisions lead to the fabrication of a bioreactor that is easy to use and can consistently stretch tissue rings for an extended period of time (seven days) in normal culture conditions, while maintaining sterility. Various-sized cams were fabricated to alter the stretch magnitude of the tubing, and ultimately the tissue ring.

The bioreactor was characterized and validated using a DVT[®] SmartImage Sensor camera and corresponding Framework 2.2 software. With this digital imaging analysis system, the outer diameter of the tubing was measured in order to calculate the linear offset distance of the cams to achieve various stretch values. Dynamic distension testing was conducted using high density mapping, which uses a high speed camera to record video of the tubing speckled with silicon carbide particles and retroreflective beads. The data were then analyzed in MATLAB using a phase correlation algorithm to track the speckle throughout motion of the tubing distending. A strain curve was then created and the tubing distension values were calculated.

Static/dynamic testing of the tubing diameter demonstrated distension values of 5.1/3.7%, 7.6/6.4%, 10.3/8.3%, and 14.9/12.7% stretch for the 5, 7.5, 10, and 15% cams. These data indicate a 1-2% loss of distension during bioreactor operation. This loss may be a reflection of the inability of the tubing to completely distend while subjected to the quick 1 Hz rotation. Because of the unique cam system, however, it is feasible to manufacture new cams that compensate for this loss, if desired.

Also, there appears to be a negative trend in dynamic distension along the length of the tubing (moving further from the cam) While the cause for these results is unknown, the data suggest that the bioreactor system may not be achieving uniform stretch along the length of the tubing during operation. The device may actually more closely resemble a continuum of stretch, as

opposed to discreet stretch magnitudes. The highest distension achieved in the regional testing, 7.5%, is still 2.5% lower than the desired 10% stretch and 0.8% lower than the dynamic testing experiment (7.5% vs. 8.3%). The regional testing data, however, were acquired with a higher resolution camera and the dynamic testing data utilized the more central regions on the tubing for analysis. Both of these variables may contribute to the discrepancies in the distension values. Furthermore, the data suggest that static testing of the components (syringe, tubing) does not accurately predict dynamic bioreactor function. As mentioned, one possibility for this loss is that the tubing is incapable of completely distending to its maximum during the continuous syringe plunger movement, as opposed to the manual, steady positioning of static testing. Again, however, it is possible to fabricate new cams to compensate for the loss.

While some specifications of this system are comparable to those described in previous reports (eg. motor frequency,^[50, 59] strain %, ^[45, 50, 55, 56] and silicone tubing^[45, 50]), other components are unique to this bioreactor. The system described in this work utilized diH₂O pressurized by a mechanical system (syringe-cam-gearbox motor assembly) to distend the tubing, whereas others have used air^[56, 59] or cultured medium^[50] pressurized with solenoid valves and pressure regulators. Also, because the shaft permits the simultaneous use of multiple cams, several stretch magnitudes can be tested in parallel in the same experiment. One caveat to consider in this design, however, is that the strain rates are not consistent across the cam sizes. Each cam completes a full rotation in one second, but the strain (stretch) imparted on the tubing changes based on the cam in use (5%, 7.5%, 10%, 15%), thereby affecting the strain rate. At this time, the impact of this variable is unknown, and it may not be possible to compensate for this variable without adjusting other culture parameters. For example, each cam size could be connected to its own motor running at an appropriate frequency such that the (change in strain)/time would be equal across the stretch magnitudes, but then the frequencies would not be consistent. An additional consideration is altering the position of the cams on the shaft. Currently, the cams are all set so the minimum point is of equal distance for each size and is facing the same direction for each size; however, because the maximum points are not consistent in order to vary the stretch magnitude, there may be inconsistencies in the load on the motor throughout each rotation. By reversing the direction of every other cam, it may be possible to better balance the loads on the motor.

These results conclude Objective 1, and the next chapter discusses the methods and results of Objective 2 – analyzing the effects of dynamic culture (via the cyclic stretch bioreactor) on SMC rings.

Chapter 4: Analysis of Dynamically-Cultured SMC Rings

4.1 Introduction

This chapter describes the characterization of smooth-muscle cell rings that have been “mechanically conditioned” via dynamic culture in the stretch bioreactor. The overall goals of the following experiments were to quantify differences in dynamically-cultured rings compared statically-cultured rings, including changes in thickness, ultimate tensile strength, collagen synthesis, cellular alignment, and expression of smooth muscle cell contractile proteins. This chapter also includes the results of experiments that were conducted to analyze strain transmission (from the silicone tubing within the bioreactor) to the tissue rings to measure the actual dynamic distension of the rings during bioreactor operation.

4.2 Methods and Materials

4.2.1 Cell Culture and Ring Fabrication

All experiments utilized primary human coronary artery smooth muscle cells (hCaSMCs; lot no. 01272, passage 6; purchased from LifeLine Cell Technology). Cells were cultured in VasuLife Basal Medium (LifeLine, LM-0002) supplemented with L-Glutamine (10 mM), rh Insulin (5 µg/mL), rh FGF-b (5 µg/mL), Ascorbic Acid (50 µg/mL), rh EGF (5 ng/mL), and FBS (5%). Additional supplements included 250 µg/ml Amphotericin B (CORNING cellgro, 30-003-CF) and 10,000 IU/mL Penicillin – 10,000 µg/mL Streptomycin solution (CORNING cellgro, 30-002-CI). Medium was exchanged every other day and cells were routinely passaged at 85% confluency, as necessary.

Agarose molds were fabricated from 2% (w.v.) SeaKem[®] LE Agarose (Lonza, 50000) dissolved in 1X DMEM (Dulbecco’s Modification of Eagle’s Medium; CORNING cellgro, 10-013-CV). The agarose solution was autoclaved and immediately used to fill PDMS templates. The molds (agarose in PDMS template) were left to solidify for five minutes. Paddled forceps were used to gently remove the agarose mold from the PDMS template, taking care not to disrupt the 2 mm (diameter) agarose posts. Each agarose mold was then placed in a well of a six-well plate. Each well then received 5 mL of supplemented LifeLine media such that the agarose molds were

completely submerged. The plate was then incubated at 37°C and 5% CO₂ until use. Molds were fabricated 1-2 days before use.

To create rings, cells were trypsinized, resuspended at 8 million cells/mL, and seeded into agarose molds. The molds were removed from the incubator and the media surrounding each post on each mold was removed. Fifty microliters of cell suspension (400,000 cells) was then seeded in a circular pattern into around each post in the agarose molds (see Figure 19A and Figure 19C). The plate was then placed in the center of the incubator (37°C and 5% CO₂). At 24 hours, once the cells had aggregated around the posts (see Figure 19B and Figure 19D), 5 mL of fresh media was added to each well in the six-well plate; flooding the entire agarose mold. The media was changed every other day until the completion of the experiment.

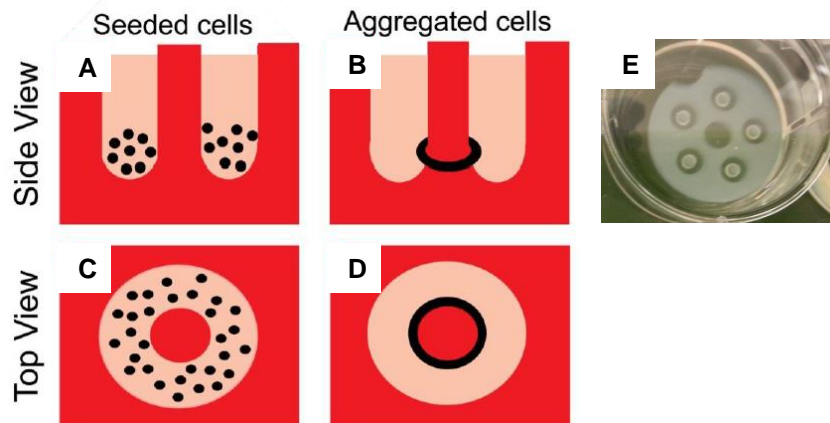


Figure 19 – Self-Assembly Ring Schematic.^[1] Cells are seeding into annular agarose molds with 2 mm central posts (A and C). The cells self-assemble into the ring shape and contract around the post (B and D). Self-assembled rings are cultured in the agarose molds in six-well plates (E) until use.

4.2.2 Analyzing Ring Distension using HDM

HDM was used to measure the strain values within the tissue rings during dynamic distension. The methods used for testing and data analysis were the same as described in 3.2.2.2: Dynamic Tubing Validation via HDM (page 33), with the addition of the following details. Six-day (culture time) SMC rings were loaded onto the tubing before connecting the tubing to the threaded luer fitting. The remaining samples remained incubated until testing. After the first sample was tested through each cam size, as previously described, the sample was discarded and the next sample was loaded onto the tubing. The ring and tubing were re-speckled, placed on the

bioreactor, and tested. This process was repeated for each sample and the same tubing assembly was used throughout.

HDM was also utilized to analyze ring distension as a function of tissue ring culture duration (2 days, 4 days, 6 days) to determine if younger (less culture time) rings are more susceptible to stretch. All samples were seeded into agarose wells on day 0, as previously described. Four samples were removed and tested at each time point (day 2, day 4, and day 6). The first ring was loaded on tubing, mounted in the bioreactor, speckled, and then tested through all four stretch magnitudes, beginning with 5% and ending with 15%. The ring was then removed from the tubing, and the next sample was loaded onto the same tubing assembly. This process was repeated for each ring sample at each time point.

4.2.3 Preparing and Setting up the Bioreactor for Experimentation

All materials used in the biosafety cabinet (tubing, diH₂O, chambers, lids, forceps, scalpel handle) were autoclaved according to general guidelines for packaged items (30 minutes at 121°C). The syringes and springs were ethylene oxide sterilized. The correct size cam(s) (5%, 7.5%, 10%, or 15%) were installed on the bioreactor before each experiment, as necessary. Immediately before loading the rings on the tubing, the bioreactor (minus the AC/DC converter and selector switch controller) was cleaned with 70% ethanol and UV-sterilized in the biosafety cabinet for fifteen minutes. After component sterilization, all materials were brought into the biosafety cabinet, except the bioreactor, which was placed in the incubator after UV-sterilization. The six-well plates with seeded agarose molds were removed from the incubator, wiped with 70% ethanol, and brought into the biosafety cabinet. Using a scalpel handle and size 10 blade, a section of the agarose mold was removed, and angled forceps were used to gently remove a ring from its agarose post. The ring (see Figure 20A) was placed in a small tissue culture plate filled with media and one of the silicone tubing assemblies was placed into the dish with the ring. Using a curved forceps in one hand and angled forceps in the other, the ring was gently pushed onto the tubing. This process was repeated until the tubing was loaded with 4-10 rings (see Figure 20B). The tubing was then placed in the tissue culture chamber and the luer fittings were connected. The pinch clamp was slipped on the end of the tubing (see Figure 20C). The syringe was then filled with sterile diH₂O, ensuring that no bubbles were present in the tubing. The

syringe was then connected to the threaded luer fitting and depressed to the 2.0 mL line, making sure that the tubing was completely filled. The pinch clamp was closed. The chamber was filled with 35 mL of pre-warmed LifeLine media (supplemented as previously described) and the lid was placed over the chamber. This process was repeated for all culture chambers. Static chambers were prepared according to the same protocol, with the exception of using single-use 1.0 mL disposable syringes (BD, 309628). The culture chambers were then loaded on the bioreactor in the incubator and the bioreactor was switched on. The static culture chambers were placed in the incubator adjacent to the bioreactor.

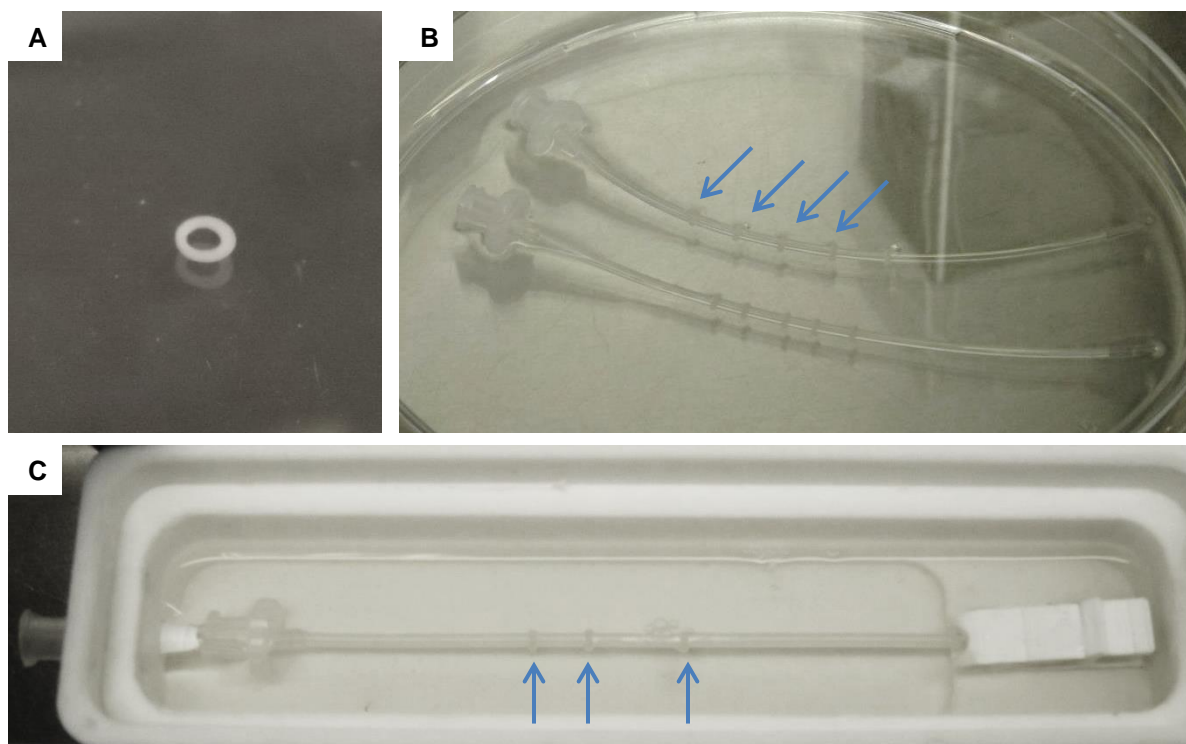


Figure 20 – Preparing SMC Rings for Dynamic Culture. (A) 2 mm SMC ring removed from the agarose mold and placed in culture medium; (B) SMC rings loaded onto the silicone tubing assemblies; (C) ring-loaded tubing assembly and pinch clamp positioned in the culture chamber. Blue arrows indicate tissue rings. All photographs were taken while tissues and components were in the biosafety cabinet.

4.2.4 Dynamic Culture Experiments

Rings were cultured in agarose molds for seven days and then loaded onto the bioreactor and cultured for an additional seven days of dynamic culture. Static control rings (“0% stretch”) were loaded onto tubing, but the chambers were not dynamically cultured. “Mold” control rings indicate that the rings were cultured in their molds for the entire length of the experiment (14

days) and never loaded onto silicone tubing. Rings dynamically cultured were fed once throughout the seven day period. Ten milliliters of media was removed from each chamber and ten milliliters of warmed, fresh media was added. Rings in molds were fed every other day, as previously described. Experimental variables included the type of control rings used (0% stretch or cultured in molds) and the stretch magnitudes (cam sizes) employed.

4.2.5 Calculating Ring Thickness

DVT[®] was used to measure the thickness of each ring at the conclusion of dynamic culture. Using a sample of tubing with a known diameter, a calibration image was captured. Then, each ring was removed from the agarose mold or silicone tubing assembly, placed in a tissue culture dish with 1X phosphate buffered saline (PBS), and positioned beneath the camera. The sensors were positioned with two sensors bounding the inner and outer boundary of the wall, and wall thickness (distance between sensors) was recorded. Four thickness values were recorded for each tissue ring sample (taken at approximately equal increments around the ring circumference). The four measurements were averaged to calculate the wall thickness of each individual ring.

4.2.6 Histological Analysis of ECM Composition

Tissue rings were placed in processing cassettes and fixed in 10% neutral buffered formalin for 60 minutes. The cassettes were then transferred to the automatic processor (Triangle Biomedical Sciences, Inc.) and subjected to a series of ethanols (70%, 80%, 15 minutes each; 95%, 20 minutes; 95%, 100%, 100%, 25 minutes each), xylenes (2 exchanges, 30 minutes each) and ultimately paraffin (2 exchanges, 30 minutes each). The samples were then embedded in paraffin and the blocks were allowed to cool. Before sectioning, the blocks were placed on ice for at least 30 minutes. The blocks were cut on a microtome in 5 μ m sections. The sections were placed on charged slides and baked for approximately 30 minutes at 60°C. The slides were then deparaffinized in two changes of xylene (3 minutes each) and rehydrated through two changes of 100% ethanol (3 minutes each), 95% ethanol (3 minutes), and 70% ethanol (3 minutes). Tissues were stained with picrosirius red/fast green (PR/FG) and Alcian blue per standard protocols. For PR/FG, Sirius red stains all collagen types red, and fast green is a counterstain that labels all non-collagenous proteins green. The Alcian blue stain identifies acidic polysaccharides, such as glycosaminoglycans, with a blue dye. All slides were coverslipped with Cytoseal 60 mounting

media (Thermo-Scientific) and imaged using brightfield with a Leica DMLB2 upright fluorescence microscope and DFC480 camera and the Leica Application Suite software (Leica Microscopes).

4.2.7 Immunohistochemical Analysis of Contractile Proteins and Proliferating Cells

Immunohistochemistry was performed to detect contractile proteins (α -SM actin and calponin) and proliferating cells (Ki67). Samples were fixed, processed, embedded, and sectioned as previously described. The slides were deparaffinized in the same manner and rinsed in running tap water (5 minutes) following the 70% ethanol incubation. For calponin and Ki67 staining, the slides were placed in a pressure cooker of boiling 1X Tris-EDTA buffer antigen retrieval solution, pH 9.0 (10X solution of 10 mM tris base, 1 mM EDTA solution, 0.05% Tween 20; diluted in diH₂O for a 1X working solution) to expose antigens and epitopes that may be masked by protein cross-linking during fixation. After 5 minutes of fully-pressurized cooking, the samples were retained in the pressure cooker and cold water was run around the pressure cooker to cool the equipment (2-5 minutes). The slides were then removed from the pressure cooker and washed three times in 1X PBS (5 minutes each). For Ki67 staining, each slide was then permeabilized with 100 μ L 0.25% Triton-X 100 in diH₂O for twenty minutes and blocked with 100 μ L of 5% normal goat serum (NGS) in 1X PBS for thirty minutes at room temperature. Samples were then incubated in 100 μ L of primary antibody (rabbit anti-Ki67 monoclonal antibody, Abcam, AB16667) diluted 1:100 in 3% NGS in PBS overnight at 4°C. Slides were then washed three times in PBS (5 minutes each); treated with 100 μ L of secondary antibody (Alexa Fluor 488 goat anti-rabbit IgG, Invitrogen, A110008) diluted 1:400 in 3% NGS in PBS, for one hour at room temperature and protected from light; and again washed three times in PBS (5 minutes each). Finally, samples were counterstained with 100 μ L of Hoechst dye (Hoechst 33342 trihydrochloride trihydrate, Life Technologies, H3570) diluted 1:6000 in diH₂O, for five minutes at room temperature to label cell nuclei; washed three times in PBS (5 minutes each); and coverslipped with ProLong Gold (Life Technologies). Samples were fluorescently imaged with a Leica DMLB2 upright fluorescence microscope and DFC480 camera and the Leica Application Suite software (Leica Microscopes).

For calponin staining, following the antigen retrieval final PBS wash, (non-permeabilized) sections were blocked with 100 μ L of 1.5% normal rabbit serum (NRS) in 1X PBS for 45 minutes at room temperature. Slides were then treated with 100 μ L of primary antibody (monoclonal mouse anti-human calponin, clone CALP, Dako M3556) diluted 1:100 in 1.5% NRS in PBS, for one hour at room temperature, followed by three more PBS washes (5 minutes each). The samples were treated with 100 μ L of secondary antibody (Alexa Flour 488 rabbit anti-mouse IgG, Invitrogen, A11059) diluted 1:400 in 1.5% NRS in PBS, for 45 minutes at room temperature and protected from light, followed by three more PBS washes (5 minutes each), followed by Hoechst counterstaining and coverslipping as described above.

Sections stained for α -SM actin were not treated with antigen retrieval nor permeabilized. Slides were moved from the running tap water, at the conclusion of deparaffinizing, into block solution. At this time, sections were stained according to the same protocol as calponin. Sections were blocked in 1.5% NRS in PBS, treated with primary (monoclonal mouse anti-human α -smooth muscle actin, clone 1A4, Dako, M851) and secondary (Alexa Flour 488 rabbit anti-mouse IgG, Invitrogen, A11059) antibody, counterstained with Hoechst, and coverslipped, as described for calponin staining. All immunohistochemistry staining was also completed on human tissue sections as a control (umbilical cord for α -SM actin and calponin; tonsil for Ki67).

4.2.8 Calculating Ring Cell Density

Two histological sections (10 μ m apart) were collected from a region approximately halfway through the tissue ring (more than 100 μ m) and used to calculate cell density. Sections were deparaffinized and stained with Hoechst, and images were acquired as previously described. Images of the tissue ring wall (0.04 mm² area) were captured and analyzed using ImageJ software (NIH). Each image included a tissue wall region that did not encompass any space outside of the tissue. The cell counter plugin (Kurt De Vos, University of Sheffield) was used to manually count each Hoechst-stained nucleus in the image (see Figure 21). This process was repeated an additional three times within each ring section such that a total of four images around the ring (top, bottom, left, right) were analyzed for each region in each ring sample. Approximately 70-80 nuclei, on average (for the first and second section, respectively), were counted per image (range of 35-135 per 0.04 mm² area), for a total of 280-320 nuclei, on average

(for the first and second section, respectively), counted per tissue ring sample. This process was repeated on human umbilical artery sections as a benchmark to native vessels.

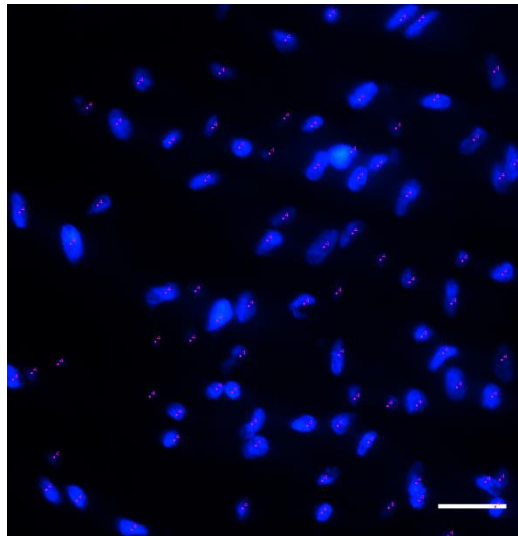


Figure 21 – Calculating Cell Density. ImageJ and the cell counter plugin were used to calculate cell density for each ring sample. A 0.04mm^2 region of the tissue was selected and each Hoechst-stained nucleus was manually counted (individual nuclei marked in pink); scale= $25\mu\text{m}$.

Cell density values calculated from eight images around the ring section and the two sections were averaged to produce an average cell density per ring sample. These densities were then averaged according to the test variable (eg. stretch magnitude) to calculate the final average cell density for each sample group (data are reported as mean \pm S.D.).

4.2.9 Calculating Nuclear Alignment

Nuclear alignment was calculated using ImageJ. The original, non-cropped, Hoechst-stained sections (RGB color) of the tissue samples described above were opened in ImageJ (see Figure 22A) and each image was split into the red, green, and blue channels. Only the blue channel (see Figure 22B) was used for the analysis. The threshold setting (threshold to 72) was applied on the blue channel image to convert the image to black and white and distinctly identify the nuclei (see Figure 22C). This setting was determined by adjusting the threshold value until as many nuclei were included, ensuring that each nuclei remained distinct from one another. This analysis is limited because some nuclei become excluded during the threshold process; however, the same threshold setting was utilized across all images. The watershed setting was then used on the image to automatically segment any large particle that remained into two or more particles

(individual nuclei). This process is at the discretion of the software and the algorithm for determining which particles require segmentation cannot be altered; however, each image was subjected to the watershed process to ensure consistent segmentation. Figure 22D shows the image after the watershed process. The blue arrow indicates that what was previously one particle has now been segmented into two particles by the software, as established by the white line.

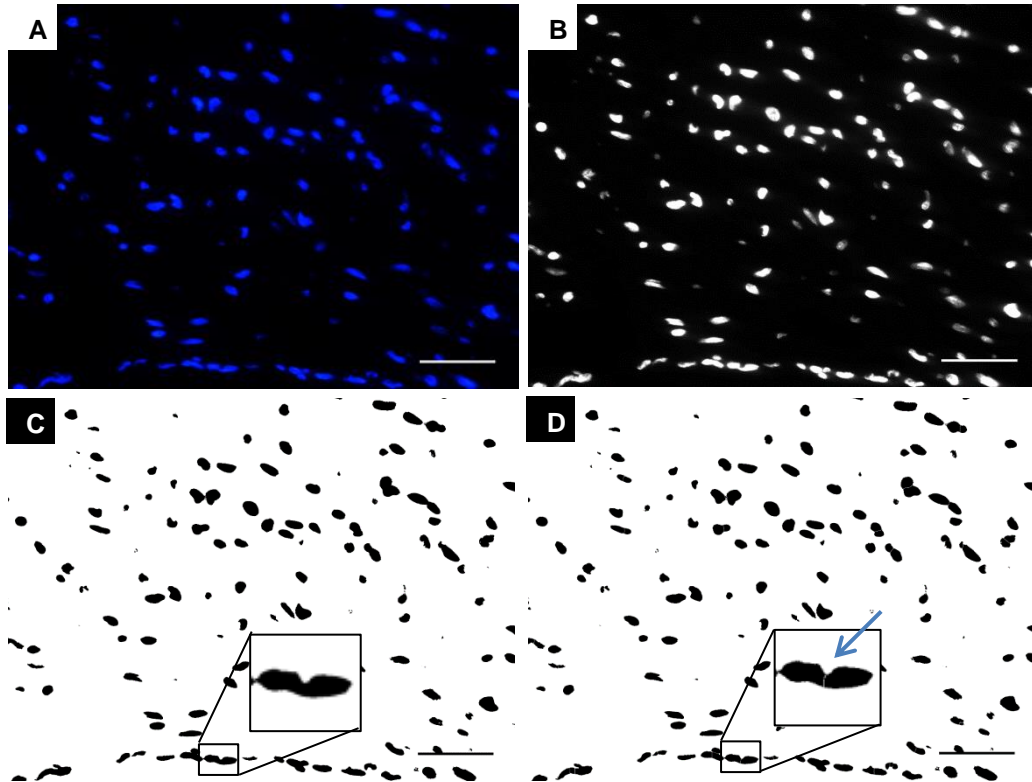


Figure 22 – Calculating Nuclear Alignment: Preparing the Image. (A) Original Hoechst image of SMC ring section; (B) blue channel image; (C) thresholded image; (D) thresholded image after watershed step. Blue arrow indicates that the cell has been split into two nuclei by the software; scale=50µm.

Once the image was fully prepared as described, a region (~0.4-0.5 mm² area) of the sample was selected for analysis (see Figure 23). Regions that extended through the width of the tissue were selected to include both the interior and exterior edges of the tissue. The particles were analyzed using the “Analyze Particles” feature in ImageJ (see Figure 23B). The size was set to 0.00001-infinity to exclude any small dots (inadequately defined nuclei) in the image. The circularity was set to the default (0.00-1.00) to include all particles, even perfectly round particles (circularity=1). The analysis was set to show ellipses, in which an ellipse was fit to each particle

(see Figure 23C). Once these parameters were set, the image was analyzed and the angle of each particle was measured. ImageJ determined the angular value by selecting the major and minor axis of each particle and calculating the angle relative to 0° . Next, the black and white image was used again and a line was drawn through the region previously selected (see Figure 23D). The line was drawn tangent to the lumen of the tissue ring region and reflects the 0° value if the cells were aligned to the shape of the tissue (eg. manually-drawn line is now parallel to anticipated direction of alignment). The inner and outer edge of the ring was used as a guideline to determine the direction of the tangent line. As discussed in Chapter Two, the cells were expected to align in a circumferential manner. The angle of this tangent line was then measured by ImageJ. Lastly, Excel was used to correlate the “original” (ImageJ) 0° and the “aligned” (manual) 0° . Because the angles determined by the software and the alignment angle manually drawn were not calculated using the same degree system (0 to 180 vs. 0 to -180), both the “original” 0° and “aligned” 0° were corrected to be within adjacent quadrants. The final angle of alignment (the number of degrees away from an aligned state) was then calculated by subtracting the two angles.

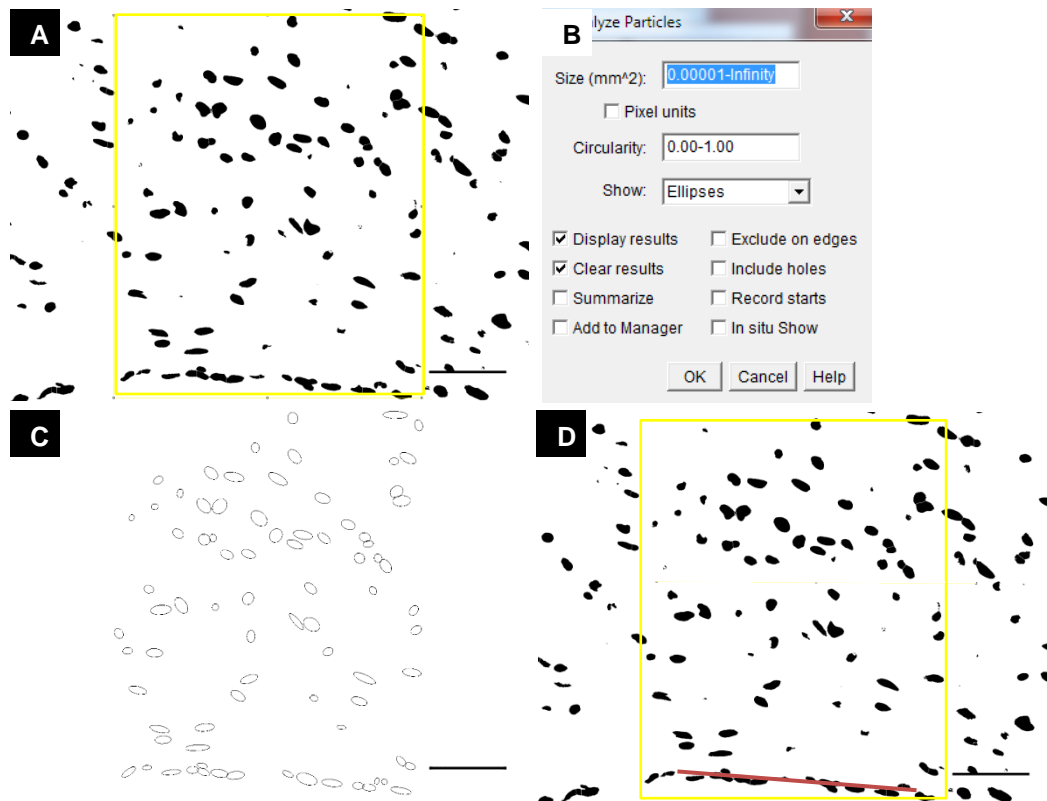


Figure 23 – Calculating Nuclear Alignment: Determining Angles. (A) Region of analysis is selected; (B) “Analyze Particles” feature in ImageJ; (C) ellipses fit over each particle (nucleus); (D) manually drawn line (red) indicating the direction of alignment for that section of tissue; scale=50µm.

Nuclear alignment values were calculated from two regions around the ring and averaged to produce an average angle of alignment per ring sample. In certain cases, the analyzed regions were not taken from the same tissue section in order to ensure that the regions of interest included both the interior of the tissue and the edge of the tissue. These angles were then averaged according to the test variable (eg. stretch magnitude) to calculate the final average angle of alignment for each sample group (data reported as mean \pm S.D.). Again, this process was also repeated on human umbilical artery sections as a benchmark to native vessels.

4.2.10 Uniaxial Tensile Testing

The mechanical properties of tissue ring samples (see Figure 24) were analyzed using uniaxial tensile testing with an Instron ElectroPuls E1000, 1 N load cell, and custom grips, as previously described in Gwyther, *et al.*^[1] Samples remained incubated until use and were hydrated in 1X PBS during testing. The area for each ring was calculated using the thickness values determined by DVT[®], as described in 4.2.5: Calculating Ring Thickness. Each sample was gently loaded

onto the custom grips using forceps. The tare load on the ring sample was adjusted to 5 mN and the distance between the grips was recorded using a caliper. The extension value on the BlueHill 2 software (Instron) was reset and the test was initiated. The sample was subjected to eight precycles (50 kPa tensile stress) and then pulled to failure at 10 mm/min. This process was repeated for each sample. All the data were then processed through a custom MATLAB program to compensate for the wire grips bending during the test.

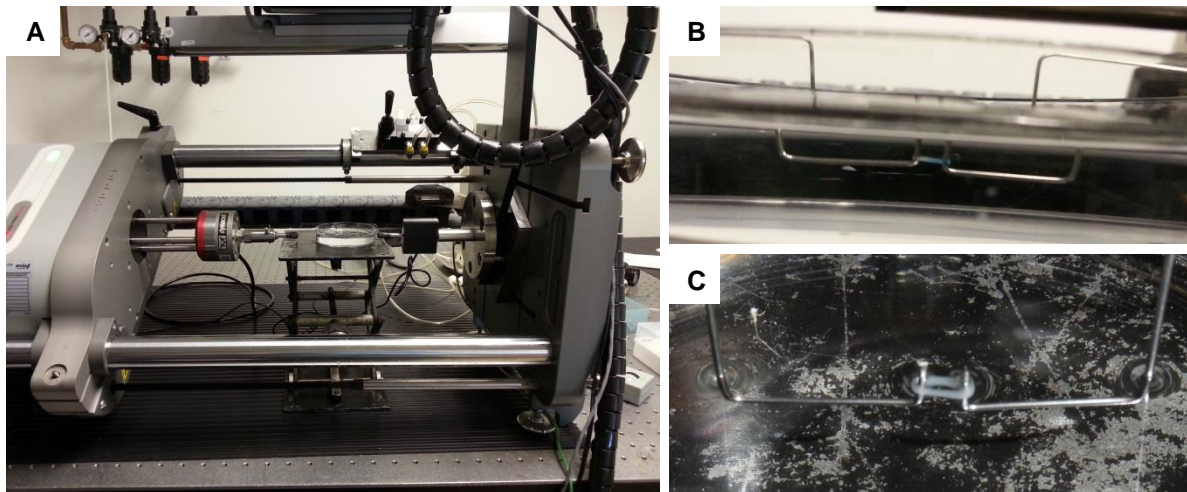


Figure 24 – Uniaxial Mechanical Testing Setup. (A) Instron ElectroPuls E1000 and 1 N load cell; side-view (B) and close-up (C) images of SMC ring in dish of PBS, loaded on the custom grips.

4.2.11 Determining Statistical Significance

Statistical analyses were performed using SigmaPlot 12.3 (Systat Software, Inc.). Data were tested using the Shapiro-Wilk normality test and the equal variance test. A one way analysis of variance (ANOVA) and post-hoc Tukey pairwise multiple comparison test (if applicable) were performed on all data. The one way ANOVA was used to compare the means of the samples and determine if a difference between the groups (eg. stretch magnitudes) existed. If the one way ANOVA detected that the means were not equal, the Tukey test was then performed to analyze any differences in the means of all possible two-way comparisons (eg. 5% vs. 7.5%, 5% vs. 10%, etc.). All tests utilized a p value of 0.05; a difference in means was considered statistically significant for any p value less than 0.05.

4.3 Results

4.3.1 Tissue Ring Distension during Dynamic Culture

High density mapping (HDM) was used to measure tissue ring distension during bioreactor operation and confirm that tissue ring distension values corresponded with tubing stretch magnitudes. Six day-old tissue rings were harvested from agarose molds and loaded onto the bioreactor for HDM analysis. An example of a tissue ring ROI selected for HDM analysis is shown in Figure 25A. Again, the green box refers to the small subimage that is tracked using the phase correlation algorithm. HDM analysis revealed that tissue ring distension was 31-56% less than the dynamic distension measurements in the tubing. Dynamic culture driven by cams designed to impart 5, 7.5, 10 or 15% circumferential stretch, resulted in mean tissue distension values of (\pm SEM, n=3) 2.5, 3.3, 3.6, and 7.9%, respectively (Figure 25B).

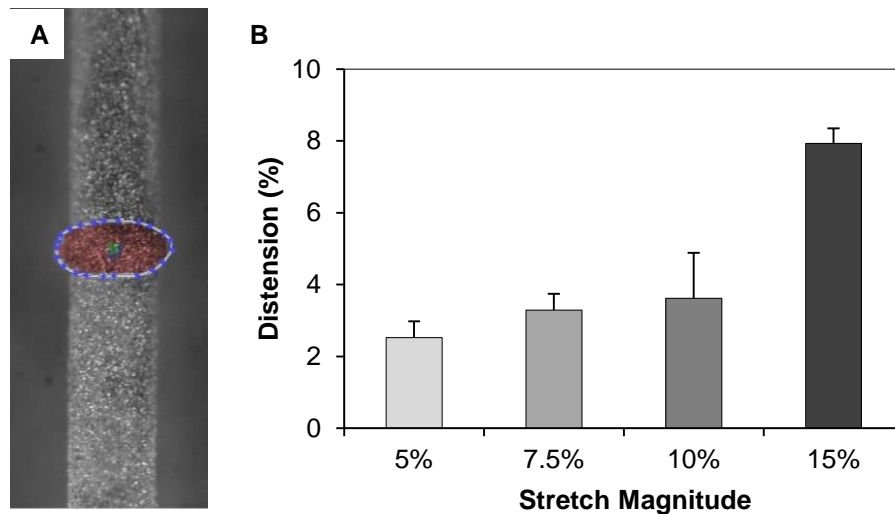


Figure 25 – SMC Ring Distension Analysis using HDM. (A) Example of speckled SMC ring on tubing. The tissue ROI for analysis is highlighted in red; (B) tissue distension at four stretch magnitudes. Data reported as mean \pm SEM, n=3.

To examine whether the observed reduction in tissue distension relative to tubing distension was due to tissue ring stiffness developed after six days of culture, “younger” tissue rings were cultured and analyzed by HDM. The effect of ring culture time on ring distension is shown in Figure 26. One of the 2 day rings (n=3) broke during harvest from the molds, indicating that the younger rings are less mechanically mature than the 4-day (n=4) and 6-day (n=4) rings. Consistent with the previously described 6-day old tissue ring studies, tubing distension values

increased with increasing cam size; however, the recorded tubing distension values varied considerably for each day testing was performed. However, the tissue ring distension values relative to tubing distension values suggest that tissue distension decreases with increased culture duration.

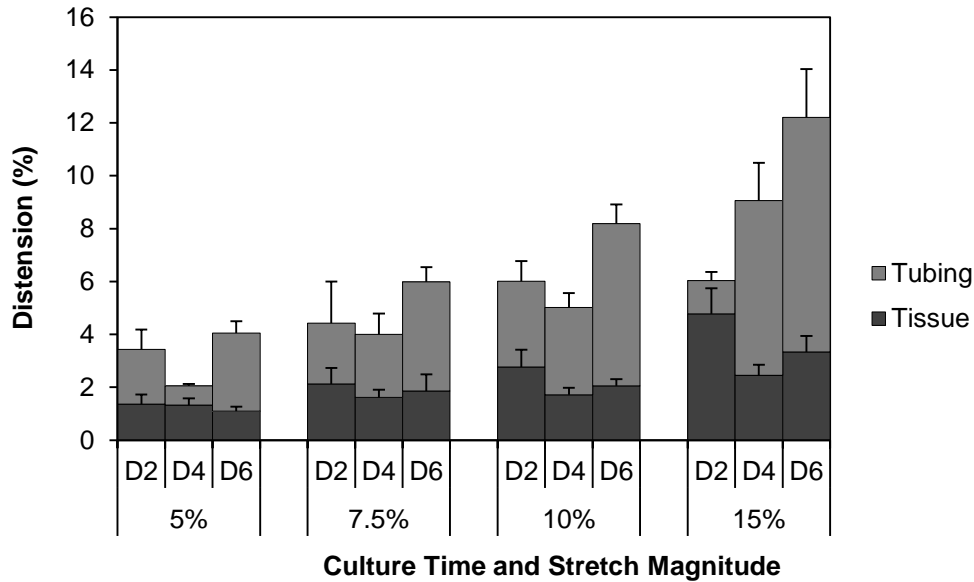


Figure 26 – SMC Ring Distension vs. Culture Time at Four Stretch Magnitudes. HDM was used to analyze the effect of tissue ring culture time on tissue ring distension. D2, D4, and D6 refer to the culture duration of 2, 4, or 6 days, respectively. Data reported as mean \pm SEM, n=3 (D2) or 4 (D4 and D6).

Table 2 documents the percentage that the ring stretched normalized to the percentage that the tubing stretched [(ring distension/tubing distension)*100]. These data indicate that at day 2, the ring is stretching approximately half as much as the tubing. By day 6, however, the ring is only stretching at approximately one third the magnitude of the tubing.

Table 2 – SMC Ring Stretch Normalized to Tubing Stretch. Values represent how much the ring is stretching divided by how much its corresponding tubing is stretching. Non-normalized distension data (effect of ring culture time on ring distension) are presented in Figure 26. Data reported as mean \pm SEM, n= 3 (D2) or 4 (D4 and D6).

	D2	D4	D6
5%	48.5 \pm 20.5%	63.9 \pm 11.4%	27.3 \pm 4.14%
7.5%	51.4 \pm 7.22%	51.1 \pm 19.0%	35.2 \pm 15.7%
10%	43.6 \pm 7.99%	34.4 \pm 4.52%	25.2 \pm 2.96%
15%	80.2 \pm 17.3%	33.4 \pm 14.8%	27.0 \pm 2.20%

A one way ANOVA was run (although the 5% and 10% group failed the equal variance test) on the day 2, 4, and 6 data for each of the stretch magnitudes (four separate tests). No significant differences were found between the mean distension values of the 2 day, 4 day, or 6 day samples for the 5% ($p=0.135$), 7.5% ($p=0.718$) or 10% ($p=0.121$) groups; however, the power of the test (0.050) for the 7.5% data were below the standard power (0.800) necessary to detect any significance, if it exists. An increase in sample would potentially increase the power (validity) of the data and enable detection of statistical significance. Differences in the mean values of the 2, 4, and 6 day rings for the 15% group were detected with a one way ANOVA ($p=0.031$) and statistical significance was detected by the Tukey test between the means for the day 2 and day 6 ($p=0.032$) rings.

4.3.2 Effect of Low Stretch on SMC Rings

To determine the effect of low-magnitude cyclic distension on SMC rings, 7 day old tissue rings were cultured dynamically with 5% and 7.5% cyclic stretch. A total of 30 rings were loaded onto tubing in the following groups: (10) 0% (control), (10) 5% rings, and (10) 7.5% rings. The total number of samples for each stretch magnitude group was divided between two chambers ($n=5$ rings/chamber).

Twelve samples were analyzed with histology (4 rings per group). Sections were stained with picrosirius red/fast green (PR/FG) for collagen and Alcian blue for GAGs. Picrosirius red (PR) staining revealed the presence of collagen in each of the sample groups (representative images shown in Figure 27). PR/FG staining indicates the presence of collagen in each of the groups, with no visually apparent differences between the stretch magnitudes or the control. Similarly, Alcian blue staining revealed that all samples synthesized GAGs, with no obvious indications that increased stretch is affecting GAG synthesis (images not shown).

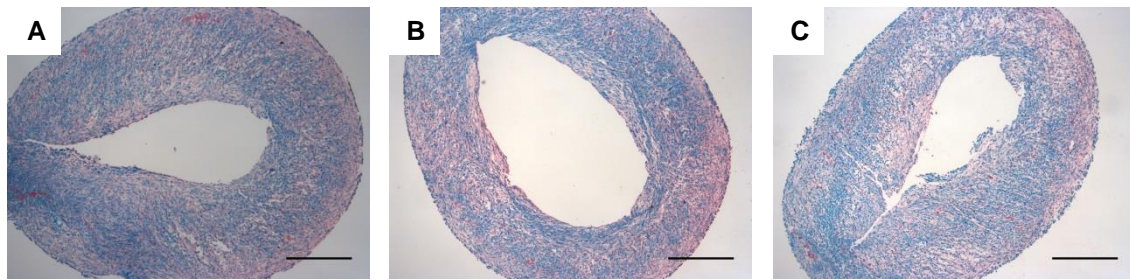


Figure 27 – Picrosirius Red/Fast Green Staining of SMC Rings Cultured at Low Stretch Magnitudes. Representative images of 14-day rings that were cyclically stretched at (A) 0%, (B) 5%, (C) or 7.5% for 7 days; scale=500 μ m.

Eighteen samples (six per group) were analyzed through mechanical testing. A representative image of a 0% stretch (control) ring is shown in Figure 28A. A one way ANOVA and post-hoc Tukey test (for pairwise comparison) were used to assess the data (although data failed the equal variance test). Mean thicknesses were 653, 729, and 745 μ m for the 0%, 5%, and 7.5% rings, respectively (Figure 28B), which suggests that ring thickness may increase with increasing stretch magnitude. There was a significant increase in both the 5% and 7.5% stretched rings over the control rings ($p=0.048$ and $p=0.014$, respectively). During mechanical testing, however, the majority of samples were too weak to successfully complete the testing protocol. Three of the control samples surpassed the pre-cycling phase (8 cycles at 50 kPa) and were pulled to failure; the remaining samples, however, failed during the pre-cycling phase.

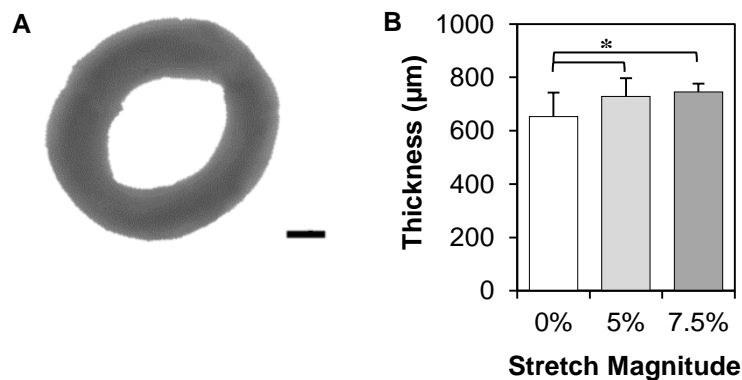


Figure 28 – DVT[®] Image and Average Thickness of SMC Rings Cultured at Low Stretch Magnitudes. (A) DVT[®] image of a 0% stretch ring; (B) thickness values were calculated using DVT[®] imaging analysis. Data reported as mean \pm S.D., $n=10$, * $p<0.05$ one way ANOVA; scale=500 μ m.

4.3.3 Effect of High Stretch on SMC Rings

The previous experiment was repeated using the higher stretch magnitudes (10 and 15%). Following seven days of static culture in molds, thirty-three rings were loaded onto tubing: (11) at 0%, (12) at 10% stretch, and (10) at 15% stretch. The total samples for each group were divided between two chambers. Seven rings served as agarose mold static culture controls (“molds”) and were never loaded onto tubing. After seven days of stretch, eleven rings were processed for histology (0%: n=3; 10% n=4; 15%: n=3; molds: n=1) and twenty-nine rings were imaged with DVT[®] and mechanically tested (0%: n=8; 10% n=8; 15%: n=7; molds: n=6).

Ring samples were stained with PR/FG and Alcian blue. Representative images of PR/FGstained rings are presented in Figure 29. Red staining indicates collagen deposition in all groups. The data suggest that the mold control ring (Figure 29A) synthesized and deposited more collagen than the rings loaded onto tubing (Figure 29B-D). There does not appear to be increased collagen deposition in the 10% and 15% stretched rings over the 0% stretched rings. However, biochemical analysis is required to quantify collagen in tissue ring samples.

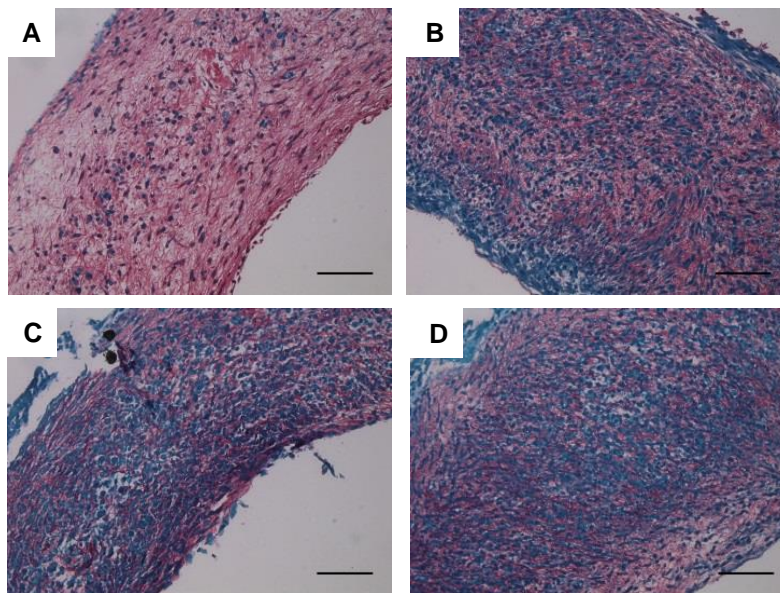


Figure 29 – Picrosirius Red/Fast Green Staining of SMC Rings Cultured at High Stretch Magnitudes. Representative images of 14-day (A) control rings in agarose molds and 14-day (B) rings stretched at 0%, (C) 10%, (D) or 15% for 7 days; scale=100 μ m.

Alcian blue staining highlights the presence of GAGs, which are uniformly distributed throughout the tissue (Figure 30) and suggests an increased density of GAGs in the matrix of the

rings loaded on tubing (Figure 30B-D) compared to the control rings cultured in agarose molds (Figure 30A). However, quantitative biochemical assays are required to confirm these observations.

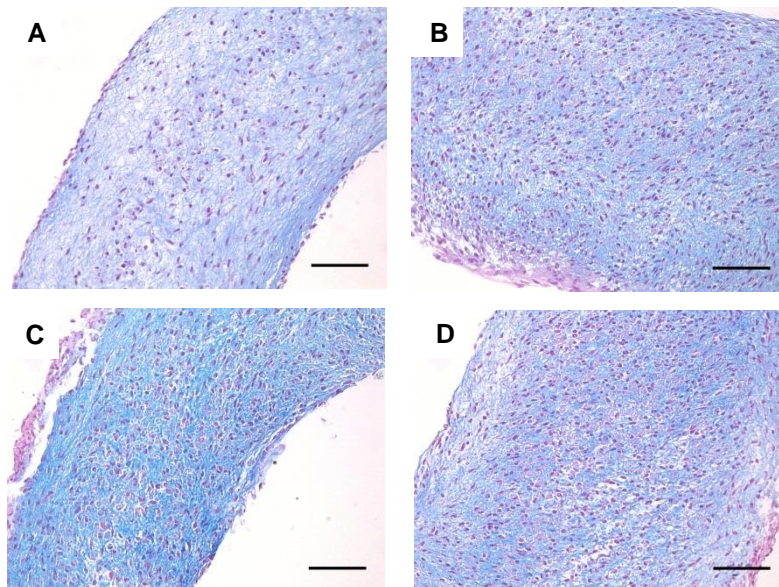


Figure 30 – Alcian Blue Staining of SMC Rings Cultured at High Stretch Magnitudes. Representative images of 14-day (A) control rings in agarose molds and 14-day (B) rings stretched at 0%, (C) 10%, (D) or 15% for 7 days; scale=100 μ m.

Eight control rings, eight 10% rings, seven 15% rings, and six mold control rings were analyzed with DVT[®] for thickness measurements and mechanically tested (Figure 31A and Figure 31B). Samples from both the 10% and 15% stretch groups exhibited a coiling “8” motion, as seen in Figure 31B. Rings coiled immediately upon ring removal from the tubing and the direction of coiling was indeterminate. The average ring thicknesses were 591, 523, 558, and 602 μ m for the 0%, 10%, 15%, and mold control rings, respectively (Figure 31C). The data were analyzed with a one way ANOVA and no significant difference was detected between the groups. A power test was conducted and the power (0.442) was below the standard (0.800), indicating that a difference may exist, but the data were not strong enough to detect it. This is presumably caused by the unbalanced sample number between the groups.

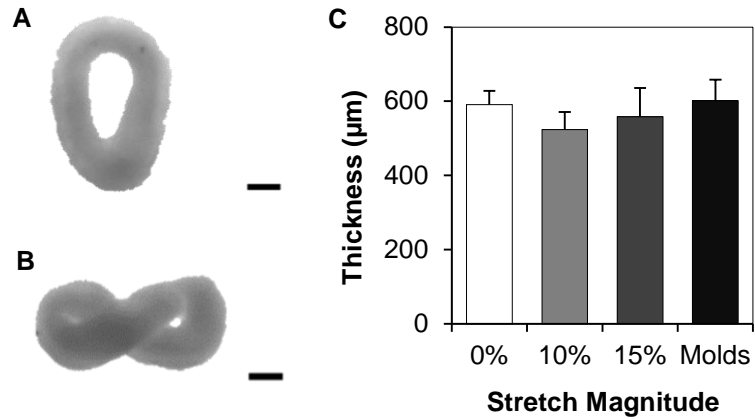


Figure 31 – DVT[®] Images and Average Thickness of SMC Rings Cultured at High Stretch Magnitudes. DVT[®] images of a (A) 0% stretched SMC ring and (B) coiled 10% stretched ring; (C) thickness values were calculated using DVT[®] imaging analysis. Data reported as mean \pm S.D., n=6 (molds), 7 (15%), 8 (0% and 10%); scale=500μm.

All mechanically-tested samples successfully completed pre-cycling and were pulled to failure. The ultimate tensile stress (UTS), maximum tangent modulus (MTM), maximum strain, and maximum load data are presented in Figure 32. A one way ANOVA and Tukey test were performed on the UTS data (Figure 32A), with average values at 224, 217, 162, and 293 kPa for the 0%, 10%, 15%, and mold control rings. The data suggest a possible negative trend in UTS with increasing stretch, and a significant difference was found between the mean UTS of the mold control and 15% stretched rings ($p=0.011$). The MTM data (Figure 32B) were analyzed with a one way ANOVA, and the means were not found to be unequal. However, the power of the test (0.347) was less than the desired power of 0.800 and an increase in same size may be necessary to detect statistical significance, if it exists; yet, no distinct trend in MTM with stretch was apparent. The mean MTMs were 0.244, 0.318, 0.252, and 0.284 MPa for the control, 10%, 15%, and mold control rings. In the same order, the average maximum strains (Figure 32C) were 1.05, 0.844, 0.869, and 1.27 mm/mm; the average maximum loads (Figure 32D) were 0.111, 0.0829, 0.0709, and 0.149 N. Maximum strain and maximum load data were also analyzed with a one way ANOVA and the Tukey test. The data suggest a decrease in maximum strain for rings loaded on tubing and a further decrease in the stretched rings. There is a significant difference between the molds and the 10% stretched rings ($p=0.001$) and the molds and the 15% stretched rings ($p=0.003$). The maximum load data demonstrate a similar (and stronger) negative trend with stretched rings. There is a statistically significant difference between the mold control rings

and the 0% ($p=0.0176$), 10% ($p<0.001$), and 15% ($p<0.001$) rings, as well as between the control rings and the 15% ($p=0.007$) rings.

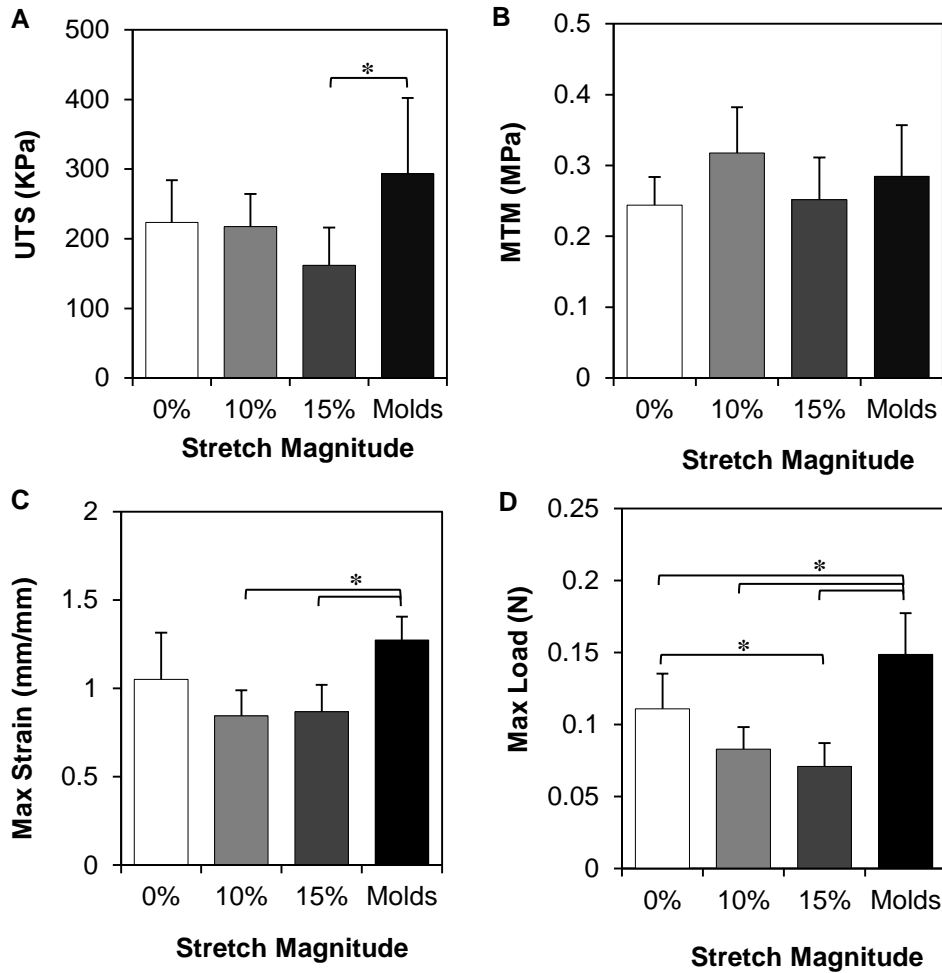


Figure 32 – Mechanical Testing Analysis of SMC Rings Cultured at High Stretch Magnitudes. (A) Ultimate tensile stress; (B) maximum tangent modulus; (C) maximum strain; (D) maximum load. Data reported as mean \pm S.D., $n=6$ (molds), 7 (15%), 8 (0% and 10%), * $p<0.05$ one way ANOVA.

4.3.4 Additional Analyses of SMC Rings Dynamically Cultured at 0-15% Stretch

Both low-stretch and high-stretch magnitudes were utilized in this experiment to provide a direct comparison of the effect of dynamic culture on the SMC rings. On day seven of static culture in agarose molds, the rings were loaded on tubing with the following sample distributions and treatment groups: ($n=10$) at 5% stretch, ($n=9$) at 7.5% stretch, ($n=10$) at 10% stretch, and ($n=10$) at 15% stretch. In addition, the control chamber (0% stretch) tubing was loaded with nine samples and there were nine control samples in agarose molds. Only one chamber was utilized

per group. Dynamically cultured rings were stretched at their respective magnitude for an additional seven days. Following the fourteen day (total) culture time, all samples were imaged with DVT[®] to measure thickness. Two (0%, 7.5%, and mold control groups) or three (5%, 10%, and 15% groups) samples from each treatment group were fixed and processed for histology and six (15% group) or seven (0%, 5%, 7.5%, 10%, and mold control groups) samples from each treatment group were mechanically tested. Analyses were conducted per previously described protocols.

Collagen was synthesized in tissue samples and representative images are displayed in Figure 33. The collagenous matrix of the 15% stretch sample (Figure 33E) appears less dense than the remaining samples; however, quantitative analysis is required to support this conclusion. Figure 34 indicates the substantial presence of glycosaminoglycans in all samples, but further assays are necessary to determine any significance in GAG content between the variables.

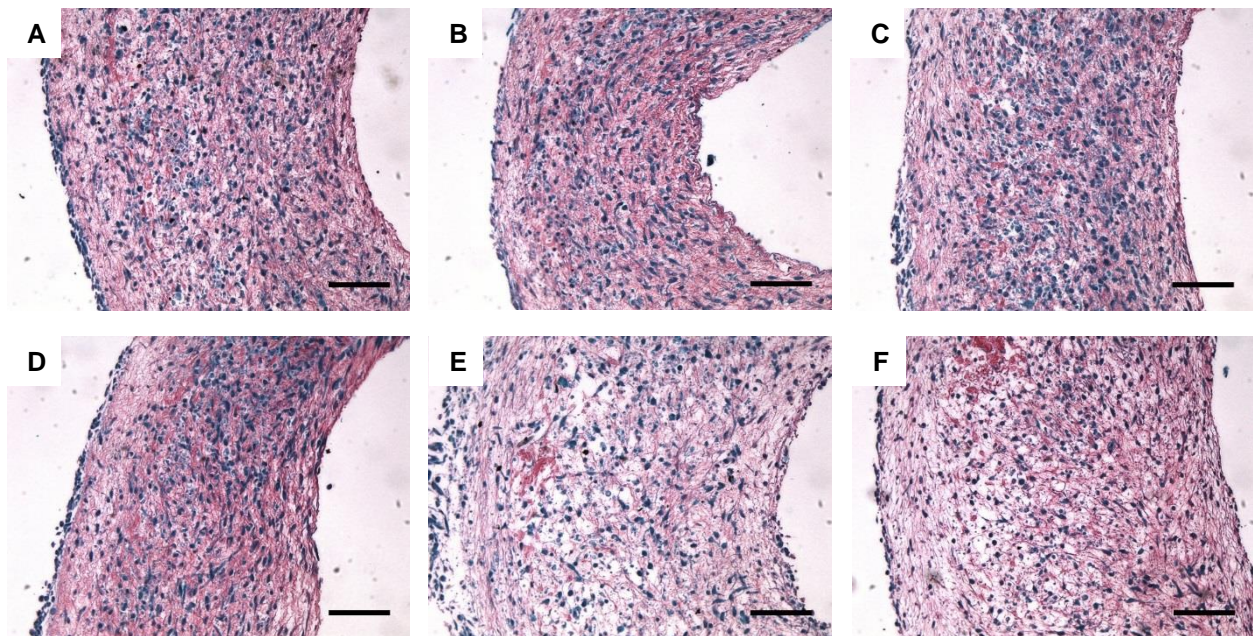


Figure 33 – Picrosirius Red/Fast Green Staining of Dynamically Cultured SMC Rings. Representative images of 14-day rings stretched at (A) 0%, (B) 5%, (C) 7.5%, (D) 10%, or (E) 15% for 7 days; (F) 14-day control rings in agarose wells; scale=100 μ m.

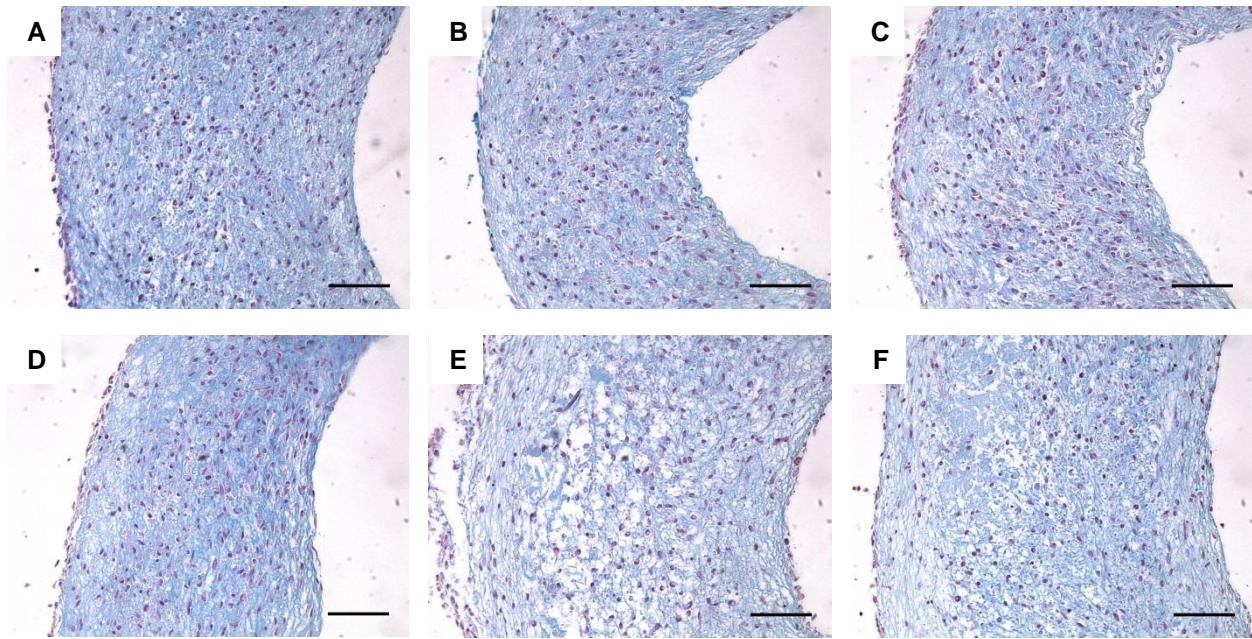


Figure 34 – Alcian Blue Staining of Dynamically Cultured SMC Rings. Representative images of 14-day rings stretched at (A) 0%, (B) 5%, (C) 7.5%, (D) 10%, or (E) 15% for 7 days; (F) 14-day control rings in agarose wells; scale=100µm.

Immunohistochemistry results (images not shown) indicate that while the ring constructs are synthesizing collagen, they are not synthesizing contractile proteins (α -SM actin and calponin), as observed by the lack of fluorescent antibody staining. Furthermore, at this stage (14 day total culture time), the cells within the constructs are no longer in a proliferative state, which would be identified by fluorescent green staining (Ki67) co-localized with fluorescent blue nuclei. No fluorescence was detected in the samples, but positive staining was observed in the positive control (human tonsil; image not shown).

Similar to the previous experiment, the 10% and 15% stretch rings spontaneously coiled upon removal from the tubing. Again, the coiling direction was unable to be determined. Figure 35 shows DVT[®] images of the 15% samples in the order that they were loaded onto the tubing.

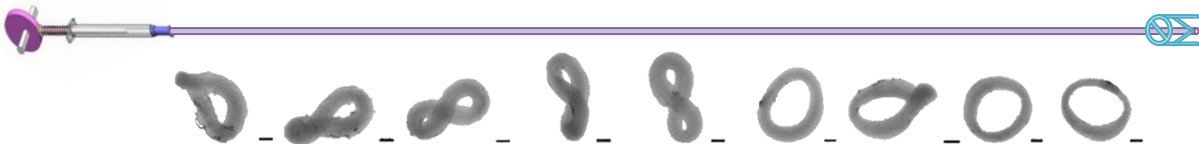


Figure 35 – Stretched SMC Ring Morphology as a Function of Tubing Position. DVT[®] images of 14-day-old SMC rings stretched at 15% for 7 days. SMC rings demonstrate a coiling effect upon removal from the tubing assembly. Effect may be dependent on ring location on tubing; scale=500µm.

Average thickness measurements for all rings (n=9: 0%, 7.5%, mold controls; n=10: 5%, 10%, 15%) are reported in Figure 36. Average thickness values for the 0%, 5%, 7.5%, 10%, and 15% stretch and the agarose mold controls are 441, 568, 519, 516, 549, and 547 μm . A one way ANOVA and Tukey pairwise comparison test were performed on the data using an alpha of 0.05. The 0% stretch rings were significantly thinner than the 5% stretch rings ($p=0.001$) and the 15% stretch rings ($p=0.007$). There was no significant difference in thickness between the stretch magnitudes.

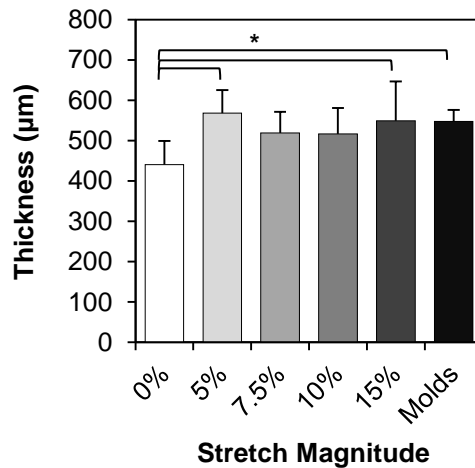


Figure 36 – Average Thickness of Dynamically Cultured SMC Rings. Thickness values were calculated using DVT[®] imaging analysis. Data reported as mean \pm S.D., n=9 (0%, 7.5%, and mold controls) or 10 (5%, 10%, and 15%), * $p<0.05$ one way ANOVA.

Average cell density of the rings is displayed in Figure 37. No nuclei were determined to be perfectly round and all data were analyzed. The 0% stretch samples had the highest number of cells per area and the 15% stretch samples had the lowest. In increasing order beginning with 0%, the results were 2511, 2090, 2217, 1905, and 1365 cells/ mm^2 . The results for the mold samples were 1611 cells/ mm^2 . A one way ANOVA and Tukey post-hoc test were run on the data. Statistical significance was detected between the 15% and the 0% ($p=0.006$), 5% ($p=0.044$), and 7.5% ($p=0.034$) groups. There was also a significant difference between the 0% and molds group ($p=0.041$).

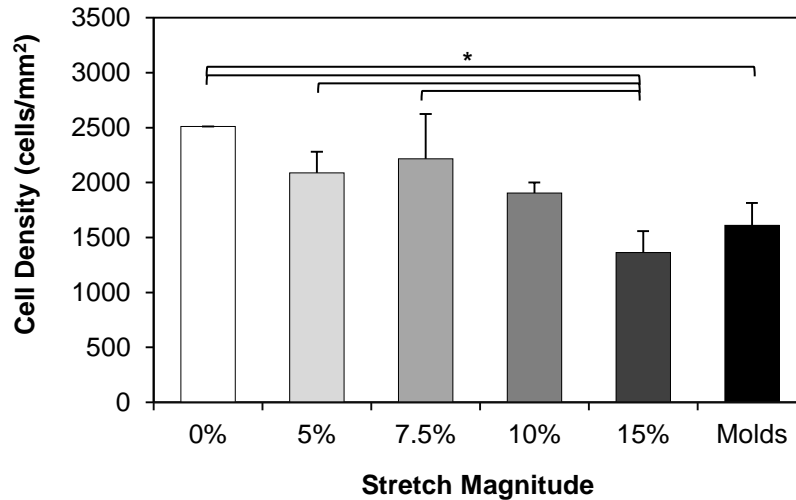


Figure 37 – Average Cell Density of Dynamically Cultured SMC Rings. Hoechst images were analyzed in ImageJ and cell nuclei were manually counted in a 0.04mm² section. Data reported as mean ± S.D., n=2 (0%, 7.5%, and mold controls) or 3 (5%, 10%, and 15%), *p<0.05 one way ANOVA.

Histograms of nuclear alignment for each stretch magnitude are presented in Figure 38. The alignment angle is the distance the cell is from being parallel to the determined aligned direction. Each histogram represents the data from all samples for each stretch magnitude (n=2: 0%, 7.5%, and mold controls; n=3: 5%, 10%, and 15%); any cell that is completely (circumferentially) aligned has an alignment angle of 0°. The analysis indicates that the mold control group was the most highly aligned, as observed by the right-skewed data (see Figure 38F). The highest frequency percentage was nuclei within 10° of aligned. The 15% and 5% groups were also right-skewed and had many aligned cells (within 10°); these histograms (see Figure 39B and Figure 39E) are very similar to the mold control group. The 10% group is also slightly right-skewed (see Figure 39D); however, the most frequent alignment angle for both the 10% and 5% groups was not 0-10°, as in the 15% and mold control groups. The most frequent alignment angle for the 7.5% group was 0-10°, but the rest of the data showed no trend or skewed distribution (see Figure 39C). The 0% group demonstrates a plateau distribution (see Figure 39A), indicating no preferential direction of alignment throughout the samples.

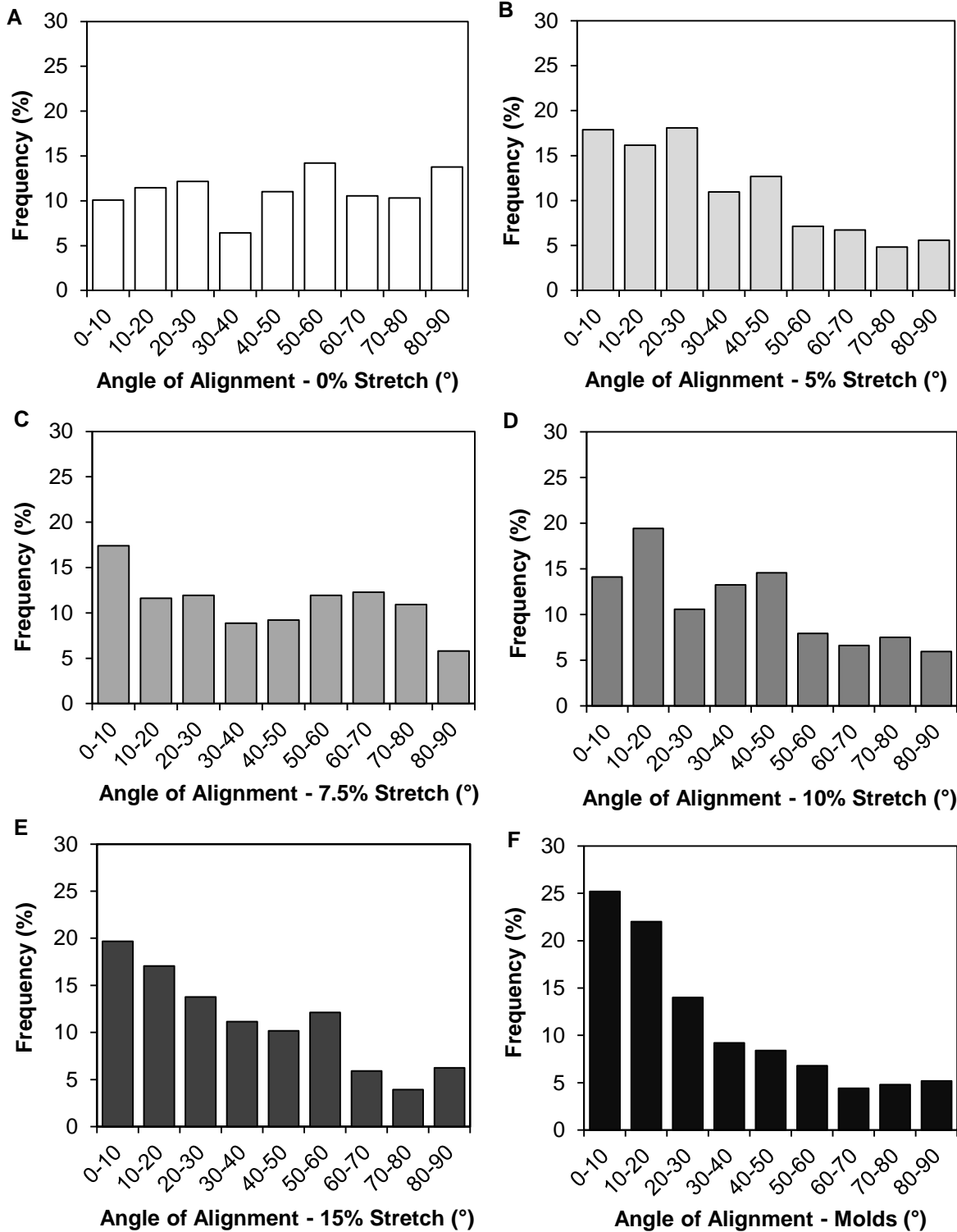


Figure 38 – Nuclear Alignment Analysis. ImageJ was used to analyze Hoechst images to quantify the alignment of cell nuclei in the SMC rings. The histograms are a compilation of samples, with rings stretched at (A) 0%, (B) 5%, (C) 7.5%, (D) 10%, and (E) 15%; (F) samples in molds controls. The “angle of alignment” is the number of degrees away the nucleus is positioned from the expected aligned direction for the selected region; n=2 (0%, 7.5%, and mold controls) or 3 (5%, 10%, and 15%).

These results are again presented in Figure 39 as a graph of average alignment angle according to stretch magnitude. These data support previous conclusions that nuclei in tissue rings cultured in agarose molds are most highly aligned circumferentially, with an average alignment angle of 29.4°. As described earlier, the 5% and 15% show similar alignment, with an average angle of alignment at 32° and 32.9°, respectively. The 7.5% and 10% groups showed less alignment (34.0° and 36.8°, respectively), and the 0% samples demonstrated no uniform directionality, with an average alignment angle of 45.3°. A one way ANOVA was run on the data and significance between the means was not detected ($p=0.387$); however, the power of the test was below 0.800 (0.076). An increase in sample size would increase the power and possibly detect a difference in the means.

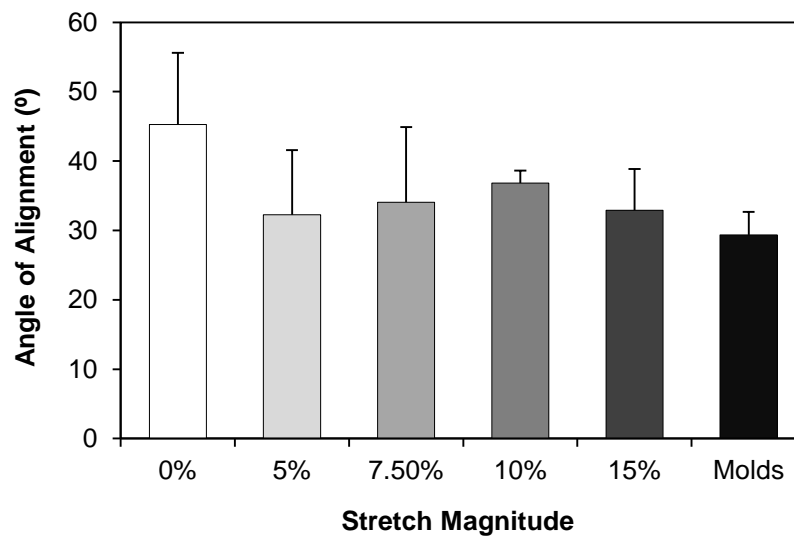


Figure 39 – Average Angle of Alignment per Stretch Magnitude. The average alignment angle for each stretch magnitude was calculated using ImageJ. Nuclei completely parallel to the expected alignment have an angle of 0°. Data reported as mean \pm S.D., $n=2$ (0%, 7.5%, and mold controls) or 3 (5%, 10%, and 15%).

Forty-nine samples ($n=7$ per group) were mechanically tested per the previously described protocol. One ring from the 15% group failed during pre-cycling; all other tissue rings were pulled to failure. Representative stress-strain curves are presented in Figure 40, and mechanical testing data are shown in Figure 41. Strain values represent engineering strain and are calculated as the total deformation divided by the initial dimension. Changes in decreasing ring thickness as strain was increased during the testing were not considered.

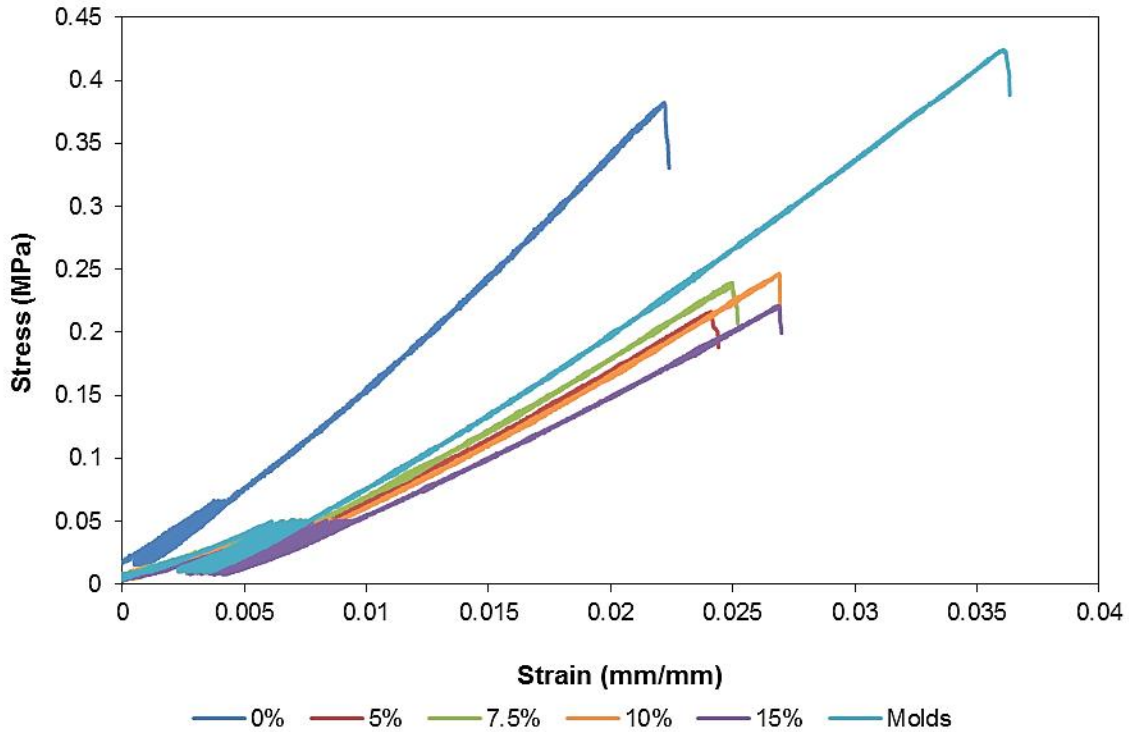


Figure 40 – Stress vs. Strain Curve of Dynamically Cultured SMC Rings. A representative sample from each group was selected. The samples were pre-cycled to 50kPa eight times and then pulled to failure at 10 mm/min.

A one way ANOVA and post-hoc Tukey test were performed on UTS, MTM, maximum strain, and maximum load data, although the MTM data failed the Shapiro-Wilk normality test. UTS values (Figure 41A) were 373, 224, 256, 290, 220, and 418 kPa for the 0-15% stretch and agarose molds, respectively. The average stiffness values (Figure 41B) (presented in the same order) were 0.685, 0.354, 0.430, 0.507, 0.410, and 0.471 MPa. Mean values for maximum strain (Figure 41C) were 0.672, 0.809, 0.756, 0.735, 0.702, and 1.13 mm/mm for the 0%, 5%, 7.5%, 10%, 15% stretch, and agarose mold controls, respectively. The maximum load averages (Figure 41D) (in the same order) were 0.0991, 0.111, 0.114, 0.108, 0.108, and 0.195 N.

The agarose mold controls achieved the highest UTS, maximum strain, and maximum load. These average UTS for these rings was significantly higher than the 5% ($p=0.005$), 7.5% ($p=0.028$), and 15% ($p=0.006$) stretch samples (see Figure 41A). The maximum strain of the mold control rings was significantly higher than all other variables ($p<0.001$ for 0, 5, 7.5, 10, and 15% stretch) (see Figure 41C). Similarly, the maximum load for the mold control rings was again significantly higher than all other samples ($p<0.001$ for 0, 5, 7.5, 10, and 15% stretch) (see

Figure 41D). The MTM data, however, revealed that the 0% stretched samples had the largest stiffness. These samples were significantly higher than both the 5% ($p<0.001$), 7.5% ($p=0.012$), and 15% ($p=0.009$) stretched samples (see Figure 41B). For all analyses, however, there was no significant difference in UTS, MTM, maximum strain, or maximum load between the 5%, 7.5%, 10%, or 15% stretch magnitudes.

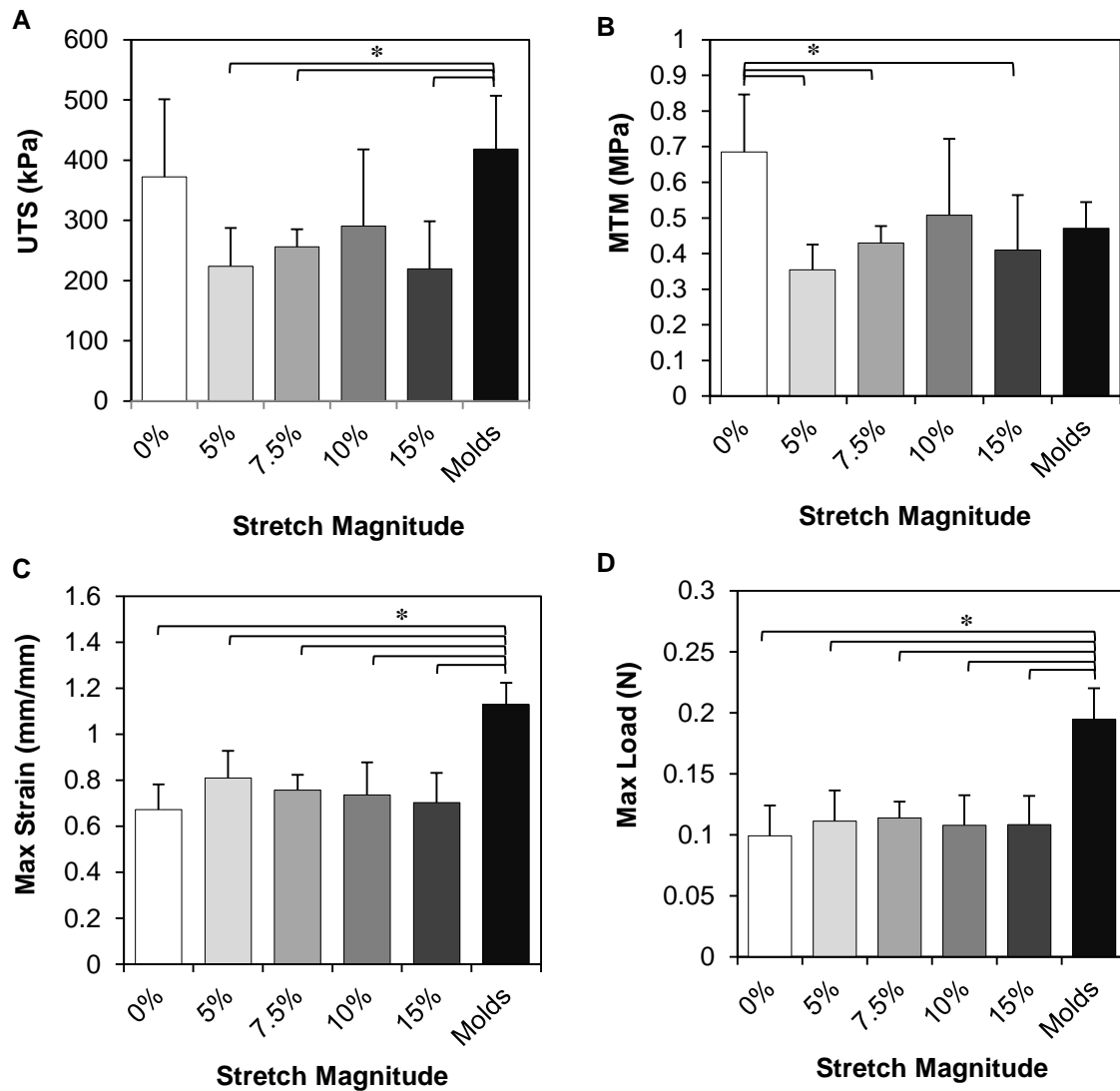


Figure 41 – Mechanical Testing Analysis of Dynamically Cultured SMC Rings. (A) Ultimate tensile stress; (B) maximum tangent modulus; (C) maximum strain; (D) maximum load. Data reported as mean \pm S.D., $n=6$ (15%) or 7 (0%, 5%, 7.5%, 10%, and mold controls), * $p<0.05$ one way ANOVA.

4.4 Summary and Discussion

The results presented in this chapter demonstrate that the cyclic stretch bioreactor mechanically stimulates human smooth muscle cell tissue rings and reports the effects of stretching on the tissue ring structure and strength. Initial high density mapping experiments verified that tissue ring distension increases with increasing stretch magnitudes for six-day-old SMC rings. The data also suggest that strain transmitted to the tissue rings is approximately half the magnitude measured in the tubing, with tissue strain values of 2.5-7.9%. This decrease in stretch may be partially explained by the increase in wall thickness of the ring compared to the tubing and that the distension values correspond to the circumferential stretch of the ring, which is less than luminal stretch. These results may also reflect how ring stiffness affects the tissue's response to stretch. Furthermore, this analysis is limited by the small area of the ring relative to the tubing. This reduces the size of the ROI and the area to be analyzed, potentially leading to an increase in error. Although coronary arteries experience strain values of 8-10%^[18, 19] *in vivo*, with the unique bioreactor system, new cams can be fabricated to compensate for the loss and potentially increase the distension values of the tissue rings to physiological values.

Additionally, because the rings were not distending the full amount, a second study was conducted to determine if we can influence how much the tissue distends by altering its culture duration. Rings were tested after 2, 4, or 6 days of culture, with the assumption that the structure and mechanical properties (eg. stiffness) of the rings would change with tissue culture duration. The first observation was that the day 6 rings were stretching only about one third as much as the tubing, unlike the previous experiment where 6-day rings distended at approximately half of the value recorded in the tubing. This result demonstrates the variability not only of the system, but batch-to-batch variability in the tissue ring samples. The 2-day rings, however, did stretch approximately half as much as the tubing. Overall, the data suggest a trend of decreasing tissue stretch with increasing culture time; however, there was only a significant difference between the 2-day and 6-day, 15% stretch samples. This indicates that younger (culture time) rings are more susceptible to stretch, possibly because the tissues are less stiff at this time. Modulus values for the 2, 4, and 6 day rings (measured by uniaxial tensile testing) would be necessary to confirm that the rings are stiffer at a later stage (longer culture duration). A caveat to these conclusions,

however, is that order of testing was not considered in the analysis. Because the rings were tested at 5%, then 7.5%, then 10%, then 15%, it is possible that the rings were preconditioned at the lower stretch magnitudes, thereby influencing the higher stretch magnitude data.

Histological analysis revealed the presence of collagen and glycosaminoglycans in all ring samples, including non-stretched controls. Using microscopy alone, there does not appear to be any visually noticeable difference in the amount or organization of collagen or GAGs between the 0%, 5%, 7.5%, and mold controls. The 10% group appears to have a denser matrix and the 15% samples, however, appear to a less dense matrix that is not observed in the other samples. Stretching at 15% may be beyond the limit of beneficial conditioning for our self-assembled rings. Others have reported that there is a minimum threshold of stretch before which point (<5%) the conditioning has no effect,^[56] yet there is little report about a maximum threshold. Additional analysis is necessary to quantify the amount of collagen present in the samples in order to further conclude the effect of stretch on protein synthesis.

Immunohistochemistry did not indicate the presence of the contractile proteins α -smooth muscle actin and calponin. Although the synthesis of these proteins was an expected outcome of this research, it is possible that the chemical culture conditions were not sufficient to initiate the production of these proteins. All culture experiments were conducted in “growth” medium, which contains growth factors and additional supplements to support cell proliferation. It is known, however, that vascular smooth muscle cells are influenced by their culture medium, and that low-serum or serum-free “quiescence” media is often used to differentiate the cells into the contractile smooth muscle cell phenotype.^[70, 71] The contractile phenotype, determined by the presence of α -SM actin, has been observed with mechanical stimulation and similar, non-quiescent medium, but these studies did not include radial stretch of cell-derived tissues. The data presented were the results of stretch on 2D culture of VSMCs,^[61] 3D culture of VSMCs on PLCL scaffolds,^[62] and 3D culture of rat aortic SMCs in a collagen gel.^[59]

A negative trend in cell density with respect to an increase in stretch was observed, with 2511 cells/mm² for the 0% stretch samples and dropping to 1365 cells/mm² for the 15% stretch samples. The cell densities measured in the 15% samples were significantly lower than the 0%, 5%, and 7.5% samples, and the mold control samples were significantly lower than the 0%

stretch samples. The 0% data most closely resembled native cell density (2725 cells/mm²), but as stretch was applied, the cell density was reduced such that the 15% group and the mold control group were similar in value. These results demonstrate a significant, and interesting, difference in cell density between the two static control groups (0% stretch and molds). By moving the rings from static culture in agarose molds (in six-well plates) to static culture on silicone tubing (in a large culture chamber), there is an increase in cell density. However, by imparting mechanical stimulation, this effect was reversed and the cell density decreased with increasing stretch magnitude. It is possible that the rings statically cultured on tubing (0% stretch) were more proliferative than the mold control rings, but the increase in mechanical stimulation reduced the proliferative capacity of the rings. Others have indicated, however, both an increase in cell number,^[60, 62] as well as no change in cell number,^[19] with mechanical conditioning. Further analysis is required to quantify total cell number per ring, but immunohistochemistry did not reveal any proliferating cells at 14 days.

Similar trends were observed in the nuclear alignment data. The mold control samples demonstrated the most circumferential alignment, with frequency percentages and a distribution highly similar to native controls (see Figure 42).

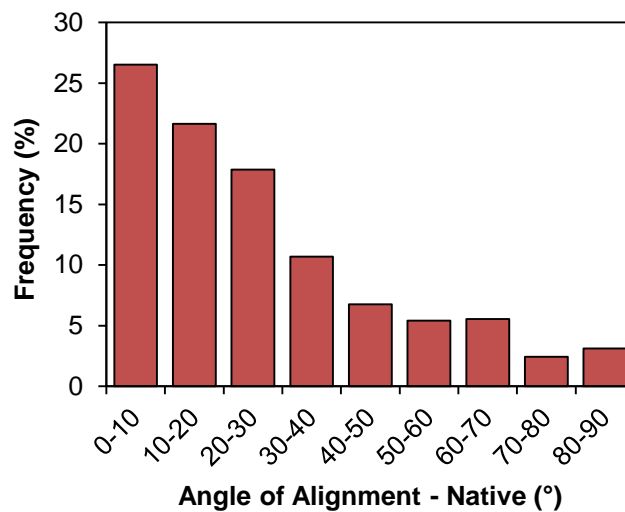


Figure 42 – Alignment Analysis of Native Vessel Control. ImageJ was used as previously described to determine circumferential nuclear alignment of human umbilical artery as a benchmark for native vessels.

However, rings statically cultured on tubing (0% stretch group) demonstrated no preferential direction of alignment, again suggesting the effect of the culture environment. By removing the

rings from the less stiff agarose molds (reported as ~14 kPa for 2% gel using indentation testing^[72]) in a six-well plate to a much stiffer silicone tubing (reported as 1.94 MPa at 200% elongation^[73]) in a large culture chamber, there is a profound effect on the cells that influences them to lose their pre-established alignment. Yet, as the tissues were subject to mechanical stimulation, the nuclei began to reorient and partial alignment was observed.

At this time, it is unknown as to why the rings coiled after being removed from the tubing. It is possible that the stretching mechanism is creating areas of higher tension in certain regions of the ring, and once the ring is removed, residual stresses on the wall are pulling the tissue together, creating this twisting shape. However, this phenomenon is not exhibited in all samples. A possible hypothesis for this relates to the stretch magnitudes and the regional tubing distension analysis described in Chapter Three. In the latest experiment, the majority of the 15% stretch rings that twisted were located on one end of the tubing, closer to the cam. As already discussed, the region on the tubing furthest from the cam (5.5-7 cm) showed decreased tubing distension, although this result was not statistically significant. The data suggest that the coiling may be dependent on higher stretch magnitudes, which was observed by coiling in the 10% and 15% samples, but not the low-magnitude stretched samples (5% and 7.5%), nor the 0% stretch controls. This conclusion may be further supported by the presence of coiling in rings closer to the cam, which again, are subjected to higher strains than the rings positioned in the last region of the tubing, distal to the cam. This suggests that the rings subjected to higher stretch are developing more residual stresses, influencing the tissues to contort upon removal from the tubing. Additionally, it is possible that not only the rings closest to the cams, but also the edges closest to the cam were strained more, which would influence the direction of the coiling. A similar result was observed using rat aortic SMCs seeded in a collagen gel.^[19] The constructs were cyclically distended via pneumatic stretching for a total of five weeks, and upon removal from the mandrel, the constructs exhibited a coiling affect over a one-hour period, whereas the static controls exhibited no shape change. However, no discussion regarding why the shape change occurred was presented.

Overall, the mechanical testing analyses indicate that the bioreactor is not improving the strength of the tissue rings, but instead is significantly weakening them. Thickness values for all rings (14 days culture time) for all studies ranged from 440 μm to 745 μm . In the final experiment, the

static mold control samples had a significantly higher UTS, maximum strain, and maximum load than stretched samples and the 0% stretch control had a significantly higher MTM than stretched samples. There was no significant difference between the mean values (UTS, MTM, max strain, or max load) of the different stretch magnitudes. These data are re-presented in Figure 43 and are compared to mechanical testing results of the previous experiments. In the first experiment utilizing low stretch magnitudes (5% and 7.5%), the samples were too weak to complete the uniaxial tensile testing protocol. The results (mean) from the second experiment at higher stretch magnitudes (10% and 15%) are indicated on the graph by the blue lines. There are some differences in the means between the experiments, as expected due to batch-to-batch variation of the rings. The averages for the UTS, MTM, and max load for the second experiment were lower than the averages for the final (third) experiment, although there appears to be some overlap between the means of experiment two and the standard deviations of experiment three, indicating consistent results between the experiments.

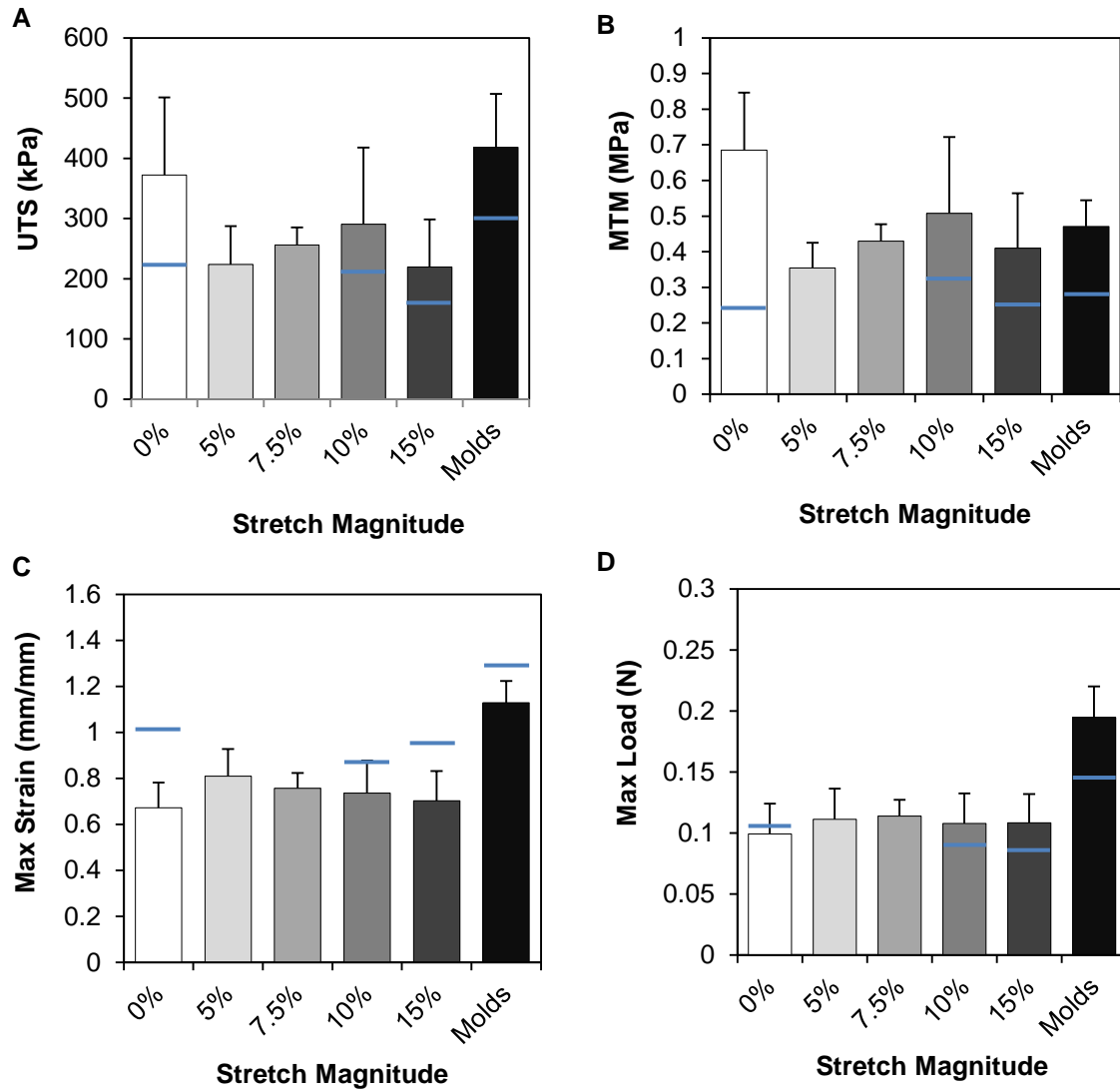


Figure 43 – Comparing Mechanical Testing Results between Experiments. (A) Ultimate tensile stress; (B) maximum tangent modulus; (C) maximum strain; (D) maximum load. Data presented (reported as mean \pm S.D., $n=6$ (15%) or 7 (0%, 5%, 7.5%, 10%, and mold controls)) are for the final experiment utilizing all stretch magnitudes. The blue lines refer to the mean for the high-stretch ($n=6$: molds; $n=7$: 15%; $n=8$: 0% and 10%) magnitude experiment. Data are not available for the low-stretch magnitude experiment.

In comparison, reported UTS values of native arteries is ~ 2 MPa,^[4-6] which is ~ 10 -fold higher than the stretched samples. However, these results are comparable to data reported by other groups utilizing cyclic stretch on vascular grafts. Isenberg and Tranquillo observed UTS values of ~ 200 kPa (controls) and ~ 150 kPa (5% strain, 0.5 Hz, and 12.5% duty) after two weeks of cyclic distension and ~ 240 kPa (controls) and ~ 385 kPa (5% strain, 0.5 Hz, and 12.5% duty) after five weeks of cyclic distension for rat SMC-seeded collagen gel “media equivalents.”^[19]

The data presented in this work achieved higher UTS and stiffness values reported by Seliktar *et*

al. for human SMC-seeded collagen gels.^[45] After four days of 10% radial strain, the UTS values were 4.5 kPa (control) and 22 kPa (strained), and the modulus values were 16 kPa (control) and 48 kPa (strained). These values were further reduced after eight days of conditioning (UTS: 3.3 kPa (control), 4.9 kPa (strained); modulus: 11 kPa (control), 14 kPa (strained)).^[45] Syedain *et al.*,^[56] however, has reported higher UTS and modulus values than those presented in this work using porcine valve interstitial cells in fibrin gels. Slices of the construct were used for tensile testing and the maximum UTS value ($2,500 \pm 261$ kPa) was achieved using two incremental stages of stretch (5% \rightarrow 10% \rightarrow 15%) over a period of three weeks. In comparison, the lowest UTS value reported was 673 ± 103 kPa (5% stretch), which is 255 kPa higher than the largest UTS value presented in this work (418 kPa, mold controls). Additionally, stiffness values reported in Syedain *et al.*^[56] were 10-20 times larger than those reported here.

In regard to mechanical properties, there is no impact on the 14-day tissue when subject to 7 days of stretch at 5% vs. 7.5% vs. 10% vs. 15%. However, because there is a substantial impact of stretching vs. not-stretching, it is possible that presence of the tubing (eg. stiffness of tubing vs. stiffness of agarose mold: 1.94 MPa^[73] vs. ~ 14 kPa^[72]) or the culture environment (eg. volume of media in chamber vs. volume of media in agarose mold: 35 mL vs. 5 mL) have a more prominent role on ECM structure and composition than the dynamic culture (stretching). A second explanation for these results is that the continuous stretching at 1 Hz for seven days is an overly aggressive conditioning protocol and is potentially damaging to the cells. For comparison, this system is currently running at 1 cycle/second (1 Hz frequency) and a 100% duty cycle [(time signal is active/total time)*100]. Others have published data on stretching cell-seeded fibrin gels (3D) operating at 0.5 Hz (1 cycle/2 seconds) with a 12.5% duty cycle (0.25 seconds of stretch in a 2 second cycle period)^[56] and stretching cells on Flexcell[®] strain units (2D) at 0.5 Hz with a 25% duty cycle (0.5 seconds of stretch in a 2 second cycle period).^[60] Additionally, it has been shown that longer stretch times (0.375 seconds to 0.5 seconds) result in small increases in UTS and stiffness, whereas lower stretch times (0.125 seconds to 0.25 seconds) promotes increased UTS values.^[19] As such, an altered duty cycle may be required to introduce a rest period into the protocol, such that the tissues are stimulated for a specified duration, and then the system is shut off for a specified duration to allow the cells to respond to the stimulation. The data presented here and in other work^[19] suggest that smooth muscle cells are negatively affected when

subjected to continuous mechanical loads. The constant stimulation may be damaging the matrix, as demonstrated in the picosirius red staining of the 15% stretch samples, and preventing the cells from adapting into a mature, contractile vascular smooth muscle cell.

This concludes the results and discussion for Chapter Four – analyzing the effects of cyclic stretch on SMC rings. The following chapter briefly concludes the accomplishments of this thesis research and future studies to complete the goals of this project.

Chapter 5: Conclusions and Future Work

In this present work, a device to mechanically stimulate engineered vascular tissue rings was designed, manufactured, and tested; the final outcome was a cyclic stretch bioreactor. The bioreactor utilized the principal stretching mechanism from a prototype design, in which distension is driven by a tubing-syringe-cam system. The tubing and syringe are filled with fluid and the system is closed. Fluid from the syringe is forced into the tubing with each cam rotation, causing the tubing to distend. As the cam continues to rotate, the syringe plunger is pulled to its initial position by a spring and the fluid returns to the syringe, causing the tubing to relax to its baseline position. Bioreactor components were designed, new features were installed, all non-commercial parts were manufactured, and the entire system was assembled. Key changes over the prototype design include: a switch from five motors to support five chambers to a single (working) motor operating four chambers; an enclosure to protect the motor from the humid incubator environment; a support bracket to stabilize the syringes; sealed chamber lids to protect sterility; glass syringes that can support continuous movement for more than seven days; and four different cam sizes corresponding to four stretch magnitudes (5%, 7.5%, 10%, and 15%).

The bioreactor was validated using digital imaging analysis and high density mapping. Static testing was conducted with DVT[®] SmartImage Sensor technology and dynamic testing was conducted using high density mapping, a procedure that (1) uses a high speed camera to record video of an item coated in “speckle” (silicon carbide particles and retroreflective beads) and (2) analyzes the video by tracking the speckle to calculate strain values. Static and dynamic measurements of tubing distension were within 0.3% and 1-2%, respectively, of the desired values (5, 7.5, 10, or 15%). Distension along the length of the tubing during bioreactor operation was not consistent, and an increase in sample size may detect statistical significance between the regions of the tubing. There appears to be a slightly negative trend such that the tubing distends less as the distance from the cam increases. This result may attribute to the twisting feature of the SMC rings demonstrated at the higher stretch magnitudes (10% and 15%). Immediately upon removal from the tubing, several, but not all, samples coiled into an “8” shape, which may be caused by residual stresses at increased stretch. The samples that did not change shape, however, were predominately located on the region of tubing furthest from the cam. If the tubing is not

stretching uniformly and is decreasing in stretch along the length of the tube, it is possible that these results support each other. Also, the coiling direction may be influenced by higher strains observed in certain regions of the tissue. These conclusions may be tested in future studies by marking a region of the ring to determine the direction the ring twists and analyzing the strain values (with HDM) in opposite sections of the ring to determine any changes in regional tissue strain.

Dynamic distension testing of the SMC rings concluded a 31-56% reduction in tissue stretch compared to tubing stretch. This result was further analyzed by testing younger culture time rings to determine if, at a younger age (culture time), the rings are more susceptible to stretching. Rings were tested at all four stretch magnitudes at 2, 4, and 6 days (culture time) and the percentage of the tubing that the ring stretched was calculated. The data indicated a decrease in this normalized stretch with an increase in culture time, and a significant difference was detected between the 2 and 6 day samples for the 15% stretch. Based on this data, seven days in static culture before dynamic culture may not be maximizing the benefits of the bioreactor. An additional experiment would be to load 2, 4, and 6 (or 7) day rings onto the bioreactor (using one stretch magnitude) to analyze the effects of long term conditioning of various-aged rings. If the younger rings are more susceptible to stretch, it is possible that there would be an improvement in the mechanical properties over the older (culture time) rings.

Histological analysis was unable to provide quantitative conclusions about the ECM composition of the SMC rings, but we can conclude that both stretch and non-stretched rings synthesized collagen and GAGs. The rings did not, however, synthesize the contractile proteins α -smooth muscle actin and calponin, as observed by the lack of bright antibody staining during immunohistochemical analysis. It is possible that these results are a reflection of the culture media used during testing. The rings were cultured in a growth media, which does not provide the necessary chemical cues for the smooth muscle cells to differentiate to mature, contractile smooth muscle cells. Future testing should repeat previous experiments, using only one cam size to control the scale of the experiment, and treating the media as the variable. It is recommended that future studies incorporate quiescence media, which consists of DMEM/F12, 1% FBS, 1% glutamine, 1% ITS, 1% pen/strep, and 50 μ g/mL ascorbate (modified from Lavender, *et al.*^[74]).

The rings also did not stain for Ki67, a proliferating cell marker, which may be expected with 14-day rings.

Additional analysis indicated a statistically significant negative trend in cell density with increased stretch and a significant decrease in cell density of the mold control samples compared to the 0% stretch control samples. The mold controls and 0% stretch controls also differed in alignment angle. Rings cultured in the agarose molds for the entirety of the experiment were the most highly aligned, whereas the rings cultured on the tubing at 0% stretch demonstrated no alignment of nuclei (eg. nuclei had no directional preference). Furthermore, rings that were placed on tubing and cultured at 5-15% stretch regained cellular alignment, but to a lesser extent than the mold controls.

Mechanical testing concluded that there is no significance in UTS, MTM, max strain, or max load between the stretch magnitudes; there is, however, a significance in these values between stretched and non-stretched samples. The 5%, 7.5%, and 15% stretched samples were significantly weaker (UTS) than the mold control samples, and both the max strain and max load for the 0%, 5%, 7.5%, 10%, and 15% were significantly lower than the mold control. The 0% stretch samples however, had a significantly higher MTM than the 5% and 15% stretch samples. Overall, the stretching does have a negative impact on the mechanical properties of the SMC rings, but as previously described, this effect may be attributed to an excessive and potentially damaging conditioning protocol of seven days of continuous stretch at 1 Hz. Fortunately, it is possible to address this limitation. The motor enclosure is capable of supporting a different motor (of the same body style), so a new motor with a lower frequency can be (easily) installed. Additionally, as mentioned in Chapter Three, the cams have an eccentric profile. New cams with a pear (or egg-shaped) profile can be fabricated to reduce the stretch period per each cycle (see Figure 44).

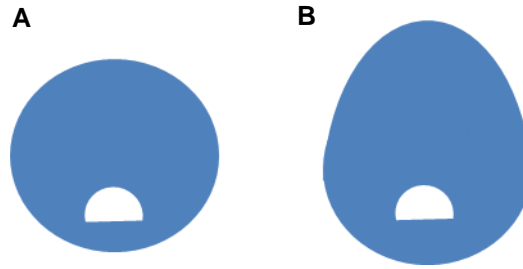


Figure 44 – Cam Profiles. (A) Current design: eccentric (circular) profile with an offset axis of rotation provides smooth, continuous motion; (B) future design: pear profile provides dwelling time within in each cycle.

Unlike eccentric cams which have no dwell time, pear cams have a dwell time that is half the period of the cycle. This means that for half the cycle, the follower (plunger, in this design) is not moving. This would introduce the necessary rest period into the cycle and reduce the continuous load on the tissues. Furthermore, it is also possible to only operate the bioreactor for several minutes or hours, and then shut the system off for a period of time. Again, this would provide a period for the cells to gradually adjust to the conditioning.

An additional variable in the system to consider is the effect of multiple rings positioned on the tubing. It is possible that the rings create constrictions in the tubing throughout the length of the tubing. Further validation testing using HDM should be considered to determine dynamic stretch of the tubing and tissue rings when greater than 6 rings are loaded on each tubing sample. The HDM studies presented in this work utilized one ring on the tubing at a time.

In summary, we have developed a cyclic circumferential stretch bioreactor to mechanically condition smooth muscle cell rings. The bioreactor has been characterized and validated and it functions as designed. Benefits of the conditioning, as expected from literature, included increased synthesis of ECM components, improved tensile strength, cellular alignment, and a shift to the contractile phenotype. Although these goals were not fully met and further analysis and testing is required to achieve all these goals, this bioreactor has the ability to create strong, aligned rings that can be used to create functional blood vessels.

References

- [1] T. Gwyther, J. Hu, A. Christakis, J. Skorinko, S. Shaw, K. Billiar, *et al.*, "Engineered Vascular Tissue Fabricated from Aggregated Smooth Muscle Cells," *Cells Tissues Organs*, vol. 194, pp. 13-24, 2011.
- [2] K. Adams, K. Bishop, and E. Casey, "Design of a Bioreactor to Cyclically Strain Tissue Engineered Blood Vessels," Bachelor's of Science, Biomedical Engineering, Worcester Polytechnic Institute, Worcester, MA, 2011.
- [3] D. J. Kelly, E. U. Azeloglu, P. V. Kochupura, G. S. Sharma, and G. R. Gaudette, "Accuracy and Reproducibility of a Subpixel Extended Phase Correlation Method to Determine Micron Level Displacements in the Heart," *Medical Engineering & Physics*, vol. 29, pp. 154-162, 2007.
- [4] M. Adham, J. P. Gournier, J. P. Favre, E. De La Roche, C. Ducerf, J. Baulieux, *et al.*, "Mechanical characteristics of fresh and frozen human descending thoracic aorta," *Journal of Surgical Research*, vol. 64, pp. 32-34, 1996.
- [5] C. M. Garcia-Herrera, J. M. Atienza, F. J. Rojo, E. Claes, G. V. Guinea, D. J. Celentano, *et al.*, "Mechanical behavior and rupture of normal and pathological human ascending aortic wall," *Medical & Biological Engineering & Computing*, vol. 50, pp. 559-566, 2012.
- [6] Z. Teng, D. Tang, J. Zheng, P. K. Woodard, and A. H. Hoffman, "An experimental study on the ultimate strength of the adventitia and media of human atherosclerotic carotid arteries in circumferential and axial directions," *Journal of Biomechanics*, vol. 42, pp. 2535-2539, 2009.
- [7] American Heart Association, "Heart Disease and Stroke Statistics - 2013 Update: A Report from the American Heart Association," *Circulation*, vol. 127, pp. e6-e245, 2013.
- [8] American Heart Association. (2013, May 28). *Atherosclerosis*.
- [9] U.S. Department of Health and Human Services. (2011, Aug 31). *What is Atherosclerosis?* Available: <http://www.nhlbi.nih.gov/health/health-topics/topics/atherosclerosis/>
- [10] A.D.A.M. Health Solutions. (2012, December 12). *Hardening of the Arteries*. Available: <http://www.ncbi.nlm.nih.gov/pubmedhealth/PMH0001224/>
- [11] U.S. Department of Health and Human Services. (2011, Aug 31). *How is Atherosclerosis Treated?* Available: <http://www.nhlbi.nih.gov/health/health-topics/topics/atherosclerosis/treatment.html>
- [12] Centers for Disease Control and Prevention. (2012, August 30). *Leading Causes of Death*. Available: <http://www.cdc.gov/nchs/fastats/lcod.htm/>
- [13] U.S. Department of Health and Human Services. (2012, Aug 31). *What is Coronary Artery Bypass Grafting?* Available: <http://www.nhlbi.nih.gov/health/health-topics/topics/cabg/>
- [14] A. C. Burton, "Relation of Structure to Function of the Tissues of the Wall of Blood Vessels," *Physiological Reviews*, vol. 34, pp. 619-642, 1954.
- [15] R. M. Nerem and D. Seliktar, "Vascular Tissue Engineering," *Annual Review of Biomedical Engineering*, vol. 3, pp. 225-243, 2001.
- [16] M. Hoenig, G. Campbell, B. Rolfe, and J. Campbell, "Tissue-Engineered Blood Vessels: Alternative to Autologous Grafts?," *Arteriosclerosis, Thrombosis, and Vascular Biology*, vol. 25, pp. 1128-1134, 2005.
- [17] J. K.-J. Li, *Dynamics of the Vascular System* vol. 1. New Jersey: World Scientific Publishing Co. Pte. Ltd., 2004.
- [18] P. B. Dobrin, "Mechanical Properties of Arteries," *Physiological Reviews*, vol. 58, pp. 397-460, 1978.

- [19] B. C. Isenberg and R. T. Tranquillo, "Long-term cyclic distension enhances the mechanical properties of collagen-based media-equivalents," *Annals of Biomedical Engineering*, vol. 31, pp. 937-949, 2003.
- [20] J. E. Wagenseil and R. P. Mecham, "Vascular Extracellular Matrix and Arterial Mechanics," *Physiological Reviews*, vol. 89, pp. 957-989, 2009.
- [21] R. C. Henrikson, G. I. Kaye, and J. E. Mazurkiewicz, *Histology* vol. 518. Maryland: Lippincott Williams & Wilkins, 1997.
- [22] D. E. Mohrman and L. J. Heller, *Cardiovascular Physiology*, 5th ed. New York: Lange Medical Books/McGraw-Hill, 2003.
- [23] N. F. Worth, B. E. Rolfe, J. Song, and G. R. Campbell, "Vascular Smooth Muscle Cell Phenotypic Modulation in Culture is Associated with Reorganisation of Contractile and Cytoskeletal Proteins," *Cell Motility and the Cytoskeleton*, vol. 40, pp. 130-145, 2001.
- [24] A. T. Halka, N. J. Turner, A. Carter, J. Ghosh, M. O. Murphy, J. P. Kirton, *et al.*, "The effects of stretch on vascular smooth muscle cell phenotype in vitro," *Cardiovascular Pathology*, vol. 17, pp. 98-102, 2008.
- [25] M. S. Baguneid, A. M. Seifalian, H. J. Salacinski, D. Murray, G. Hamilton, and M. G. Walker, "Review: Tissue Engineering of Blood Vessels," *British Journal of Surgery*, vol. 93, pp. 282-290, 2006.
- [26] X. Wang, P. Lin, Q. Yao, and C. Chen, "Development of Small-Diameter Vascular Grafts," *World Journal of Surgery*, vol. 31, pp. 682-689, 2007.
- [27] L. Niklason and R. Langer, "Advances in Tissue Engineering of Blood Vessels and Other Tissues," *Transplant Immunology*, vol. 5, pp. 303-306, 1997.
- [28] P. Zilla, R. Fasol, P. Preiss, M. Kadletz, M. Deutsch, H. Schima, *et al.*, "Use of Fibrin Glue as a Substrate for in vitro Endothelialization of PTFE Vascular Grafts," *Surgery*, vol. 105, pp. 515-522, 1989.
- [29] J. Meinhart, M. Deutsch, and P. Zilla, "Eight Years of Clinical Endothelial Cell Transplantation: Closing the Gap Between Prosthetic Grafts and Vein Grafts," *ASAIO Journal*, vol. 43, pp. M515-M521, 1997.
- [30] B. C. Isenberg, C. Williams, and R. T. Tranquillo, "Small-Diameter Artificial Arteries Engineered In Vitro," *Circulation Research*, vol. 98, pp. 25-35, 2006.
- [31] M. Peck, D. Gebhart, N. Dusserre, T. N. McAllister, and N. L'Heureux, "The Evolution of Vascular Tissue Engineering and Current State of the Art," *Cells Tissues Organs*, vol. 195, pp. 144-158, 2012.
- [32] D. Shum-Tim, U. Stock, J. Hrkach, T. Shinoka, J. Lien, M. A. Moses, *et al.*, "Tissue Engineering of Autologous Aorta Using a New Biodegradable Polymer," *Then Annals of Thoracic Surgery*, vol. 68, pp. 2298-2304, 1999.
- [33] T. Shin'oka, G. Matsumura, N. Hibino, Y. Naito, M. Watanabe, T. Konuma, *et al.*, "Midterm Clinical Result of Tissue-Engineered Vascular Autografts Seeded with Autologous Bone Marrow Cells," *The Journal of Thoracic and Cardiovascular Surgery*, vol. 129, pp. 1330-1338, 2005.
- [34] R.-J. M.C., P. E. Swanson, D. C. Johnson, R. B. Schuessler, and J. L. Cox, "An Experimental Model of Small Intestinal Submucosa as a Growing Vascular Graft," *Journal of Thoracic Cardiovascular Surgery*, vol. 116, pp. 805-811, 1998.
- [35] C. B. Weinberg and E. Bell, "A Blood Vessel Model Constructed from Collagen and Cultured Vascular Cells," *Science*, vol. 231, pp. 397-400, 1986.
- [36] E. D. Grassl, T. R. Oegema, and R. T. Tranquillo, "A Fibrin-Based Arterial Media Equivalent," *Journal of Biomedical Materials Research Part A*, vol. 66, pp. 550-561, 2003.
- [37] N. L'Heureux, S. Paquet, R. Labbe, L. Germain, and F. Auger, "A Completely Biological Tissue-engineered Human Blood Vessel," *FASEB Journal*, vol. 12, pp. 47-56, 1998.

- [38] R. Gauvin, T. Ahsan, D. Larouche, P. Levesque, J. Dube, F. A. Auger, *et al.*, "A Novel Single-Step Self-Assembly Approach for the Fabrication of Tissue-Engineered Vascular Constructs," *Tissue Engineering: Part A*, vol. 16, pp. 1737-1747, 2010.
- [39] M. T. Zaucha, R. Gauvin, F. A. Auger, L. Germain, and R. L. Gleason, "Biaxial Biomechanical Properties of Self-Assembly Tissue-Engineered Blood Vessels," *Journal of the Royal Society Interface*, vol. 8, pp. 244-256, 2011.
- [40] N. L'Heureux, N. Dusserre, G. Konig, B. Victor, P. Keire, T. N. Wight, *et al.*, "Human Tissue-Engineered Blood Vessel for Adult Arterial Revascularization," *Nature Medicine*, vol. 12, pp. 361-365, 2006.
- [41] M. T.N., M. Maruszewski, S. A. Garrido, W. Wystrychowski, N. Dusserre, A. Marini, *et al.*, "Effectiveness of Haemodialysis Access with an Autologous Tissue-Engineered Vascular Graft: A Multicentre Cohort Study," *Lancet*, vol. 373, pp. 1440-1446, 2009.
- [42] H.-C. Chen and Y.-C. Hu, "Bioreactors for Tissue Engineering," *Biotechnology Letter*, vol. 28, pp. 1415-1423, 2006.
- [43] I. Martin, D. Wendt, and M. Heberer, "The Role of Bioreactors in Tissue Engineering," *TRENDS in Biotechnology*, vol. 22, pp. 80-86, 2004.
- [44] B. Liu, M. Qu, K. Qin, H. Li, Z. Li, B. Shen, *et al.*, "Role of Cyclic Strain Frequency in Regulating the Alignment of Vascular Smooth Muscle Cells In Vitro," *Biophysical Journal*, vol. 94, pp. 1497-1507, Feb 15 2008.
- [45] D. Seliktar, R. M. Nerem, and Z. S. Galis, "Mechanical Strain-Stimulated Remodeling of Tissue-Engineered Blood Vessel Constructs," *Tissue Engineering*, vol. 9, pp. 657-666, 2003.
- [46] K. Kanda, T. Matsuda, and T. Oka, "Two-dimensional orientational response of smooth muscle cells to cyclic stretching," *ASAIO Journal*, vol. 38, pp. M382-M285, 1992.
- [47] P. R. Standley, A. Camaratta, B. P. Nolan, C. T. Purgason, and M. A. Stanley, "Cyclic Stretch Induces Vascular Smooth Muscle Cell Alignment via NO Signaling," *American Journal of Physiology - Heart and Circulatory Physiology*, vol. 283, pp. H1907-H1914, 2002.
- [48] C. Neidlinger-Wilke, E. Grood, J.-C. Wang, R. Brand, and L. Claes, "Cell alignment is induced by cyclic changes in cell length: studies of cells grown in cyclically stretched substrates," *Journal of Orthopaedic Research*, vol. 19, pp. 286-293, 2001.
- [49] R. Buck, "Reorientation response of cells to repeated stretch and recoil of the substratum," *Experimental Cell Research*, vol. 127, pp. 470-474, 1980.
- [50] D. Seliktar, R. A. Black, R. P. Vito, and R. M. Nerem, "Dynamic Mechanical Conditioning of Collagen-Gel Blood Vessel Constructs Induces Remodeling In Vitro," *Annals of Biomedical Engineering*, vol. 28, pp. 351-362, 2000.
- [51] K. Kanda and T. Matsuda, "Behavior of arterial wall cells cultured on periodically stretched substrates," *Cell Transplantation*, vol. 2, pp. 475-484, 1993.
- [52] P. R. Standley, A. Camaratta, B. P. Nolan, C. T. Purgason, and M. A. Stanley, "Cyclic Stretch Induces Vascular Smooth Muscle Cell Alignment via NO Signaling," *American Journal of Physiology Heart and Circulatory Physiology*, vol. 283, pp. H1907-H1914, 2002.
- [53] J.-H. Zhu, C.-L. Chen, S. Flavahan, J. Harr, B. Su, and N. A. Flavahan, "Cyclic Stretch Stimulates Vascular Smooth Muscle Cell Alignment by Redox-dependent Activation of Notch3," *American Journal of Physiology - Heart and Circulatory Physiology*, vol. 300, pp. H1770-H1780, 2011.
- [54] D. Leung, S. Glagov, and M. Mathews, "Cyclic Stretching Stimulates Synthesis of Matrix Components by Arterial Smooth Muscle Cells in Vitro," *Science*, vol. 191, pp. 475-477, Feb 6 1976.

- [55] B.-S. Kim, J. Nikolovski, J. Bonadio, and D. J. Mooney, "Cyclic Mechanical Strain Regulates the Development of Engineered Smooth Muscle Tissue," *Nature Biotechnology*, vol. 17, pp. 979-983, 1999.
- [56] Z. H. Syedain, J. S. Weinberg, and R. T. Tranquillo, "Cyclic distension of fibrin-based tissue constructs: Evidence of adaptation during growth of engineered connective tissue," *Proceedings of the National Academy of Sciences*, vol. 105, pp. 6537-6542, 2008.
- [57] D. Seliktar, R. M. Nerem, and Z. S. Galis, "The Role of Matrix Metalloproteinase-2 in the Remodeling of Cell-Seeded Vascular Constructs Subjected to Cyclic Strain," *Annals of Biomedical Engineering*, vol. 29, pp. 923-934, 2001.
- [58] J. P. Stegeman, H. Hong, and R. M. Nerem, "Mechanical, biochemical, and extracellular matrix effects on vascular smooth muscle cell phenotype," *Journal of Applied Physiology*, vol. 98, pp. 2321-2327, 2005.
- [59] J. P. Stegeman and R. M. Nerem, "Phenotype Modulation in Vascular Tissue Engineering Using Biochemical and Mechanical Stimulation," *Annals of Biomedical Engineering*, vol. 31, pp. 391-402, 2003.
- [60] K. Birukov, V. Shirinsky, O. Stepanova, V. Tkachuk, A. Hahn, T. Resink, *et al.*, "Stretch Affects Phenotype and Proliferation of Vascular Smooth Muscle Cells," *Molecular and Cellular Biochemistry*, vol. 144, pp. 131-139, Mar 23 1995.
- [61] M.-J. Qu, B. Liu, H.-Q. Wang, Z.-Q. Yan, B.-R. Shen, and Z.-L. Jiang, "Frequency-Dependent Phenotype Modulation of vascular Smooth Muscle Cells under Cyclic Mechanical Strain," *Journal of Vascular Research*, vol. 44, pp. 345-353, 2007.
- [62] S. I. Jeong, J. H. Kwon, J. I. Lim, S.-W. Cho, Y. Jung, W. J. Sung, *et al.*, "Mechanoactive tissue engineering of vascular smooth muscle using pulsatile perfusion bioreactors and elastic PLCL scaffolds," *Biomaterials*, vol. 26, pp. 1405-1411, 2005.
- [63] Y. Narita, K.-I. Hata, H. Kagami, A. Usui, M. Ueda, and Y. Ueda, "Novel Pulse Duplicating Bioreactor System for Tissue-Engineered Vascular Construct," *Tissue Engineering*, vol. 10, pp. 1224-1233, 2004.
- [64] C. Williams and T. M. Wick, "Perfusion Bioreactor for Small Diameter Tissue-Engineered Arteries," *Tissue Engineering*, vol. 10, pp. 930-941, 2004.
- [65] J. W. Bjork and R. T. Tranquillo, "Transmural Flow Bioreactor for Vascular Tissue Engineering," *Biotechnology and Bioengineering*, vol. 104, pp. 1197-1206, 2009.
- [66] M. S. Hahn, M. K. McHale, E. Wang, R. H. Schmedlen, and J. L. West, "Physiological Pulsatile Flow Bioreactor Conditioning of Poly(ethylene glycol)-based Tissue Engineered Vascular Grafts," *Annals of Biomedical Engineering*, vol. 35, pp. 190-200, 2007.
- [67] R. Gauvin, R. Parenteau-Bareil, D. Larouche, H. Marcoux, F. Bisson, A. Bonnet, *et al.*, "Dynamic mechanical stimulations induce anisotropy and improve the tensile properties of engineered tissues produced without exogenous scaffolding," *Acta Biomaterialia*, vol. 7, pp. 3294-3301, 2011.
- [68] P. Engbers-Buijtenhuijs, L. Buttafoco, A. A. Poot, P. J. Dijkstra, R. A.I. de Vos, L. M. T. Sterk, *et al.*, "Biological characterisation of vascular grafts cultured in a bioreactor," *Biomaterials*, vol. 27, pp. 2390-2397, 2006.
- [69] L. Niklason, J. Gao, W. Abbott, K. Hirschi, S. Houser, R. Marini, *et al.*, "Functional Arteries Grown in Vitro," *Science*, vol. 284, pp. 489-493, 1999.
- [70] P. Libby and K. V. O'Brien, "Culture of quiescent arterial smooth muscle cells in a defined serum-free medium," *Journal of Cellular Physiology*, vol. 115, pp. 217-223, 1983.
- [71] S. Li, S. Sims, Y. Jiao, L. H. Chow, and J. G. Pickering, "Evidence from a novel human cell clone that adult vascular smooth muscle cells can convert reversibly between

- noncontractile and contractile phenotypes," *Circulation Research*, vol. 85, pp. 338-348, 1999.
- [72] P. Scandiucci de Freitas, D. Wirz, M. Stolz, B. Gopfert, N.-F. Friederick, and A. U. Daneils, "Pulsatile dynamic stiffness of cartilage-like materials and use of agarose gels to validate mechanical methods and models," *Journal of Biomedical Materials Research Part B: Applied Biomaterials*, vol. 78, pp. 347-357, 2006.
- [73] Dow Corning, "Product Information: Class VI Elastomers," 2003.
- [74] M. D. Lavendar, Z. Pang, C. S. Wallace, L. E. Niklason, and G. A. Truskey, "A system for the direct co-culture of endothelium on smooth muscle cells," *Biomaterials*, vol. 26, pp. 4642-4653, 2005.

Appendix A: Bill of Materials

Component	Item	Description	Part No.	Company
Base	Material	Impact-Resistant UHMW Polyethylene Sheet Black, 1/2" Thick, 12" X 24"	4296A46	McMaster-Carr
	Feet	Leveling Mount, Easy Adjust, 3/8"-16 X 1-1/2" L Thread, 1-3/8" Base Diameter, Packs of 4	23015T65	McMaster-Carr
Tray	Material	Impact-Resistant UHMW Polyethylene Sheet Black, 1/2" Thick, 12" X 24"	4296A46	McMaster-Carr
	Handles	Cable clamps: nyl natural	CCL009A	Alliance Express
Motor Mount	Material	Impact-Resistant UHMW Polyethylene Rectangle Bar, 2-1/2" Thick, 2-1/2" Width, Black	8702K633	McMaster-Carr
	Lid material	LEXAN 10 in. x 8 in. Polycarbonate Sheet (GE, 31-GE-XL-1)	987295	Home Depot
	Gasket	PDMS		
	Stopper	Tapered plug: EPDM black	STP05307 9B	Alliance Express
	Brackets	Aluminum 5052-H32 sheet, 0.249", cut to 12"x12"		OnlineMetals.com
	Ball bearing	440C Stainless Steel/ABEC 3 Ball Bearing Lubricated with Oil (MIL-L-6085A)	A 7Y55-FSS3725	Stock Drive Products
Motor	Motor	6-12V, 60RPM 70:1 Spur Gear Motor	RB-Sct-183	RobotShop, Inc.
	Moisture seal wrap	Moisture-Seal Polyolefin Heat-Shrink Tubing 1-1/2" ID Before, 3/4" ID After, 6" L, Black	74965K58	McMaster-Carr
	Wiring	Red/white/black 12V electrical wire		Turn 4 Hobbies
	Selector switch	PB ENC 22mm 1-HOLE GRY 51mm DEEP, plastic	SA100SL	AutomationDirect.com
	AC/DC converter	100-240W AC Input to 12V DC Output	HF25W-SL-12	Hengfu
Chambers	Material	High Temperature UHMW Polyethylene Sheet 1-1/2" Thick, 12" X 12"	8270K81	McMaster-Carr
	Lid material-plastic	LEXAN 10 in. x 8 in. Polycarbonate Sheet (GE, 31-GE-XL-1)	987295	Home Depot
	Lid material-aluminum	Aluminum 5052-H32 sheet, 0.249", cut to 12"x12"		OnlineMetals.com
	Lid screws	18-8 Stainless Steel Button Head Socket Cap Screw, 4-40 Thread, 3/16" Length	92949A105	McMaster-Carr
	Threaded luer fitting	Female Luer Thread Style Panel Mount to Male Luer, Use with FSLLR Lock Ring, Animal-Free Natural Polypropylene	FTLLBMLR L-6005	Value Plastics, Inc.

	Dowel pins	Corrosion Resistant Dowel Pin, Type 316 Stainless Steel, 1/8" Diameter, 3/8" Length	97395A435	McMaster-Carr
Tubing	Material	TUBE .058" X .077" 50 D CL	76P058-210-077	Specialty Manufacturing, Inc.
	Luer fitting to barb	Female Luer Lug Style to Classic Series Barb, 1/16" (1.6 mm) ID Tubing, Animal-Free Natural Polypropylene	FTL10-6005	Value Plastics, Inc.
	Pinch clamp	Ergonomic pinch clamp	EOPC-0.110-PP-W-minature	Z-man Corp.
	Heat shrink wrap	Heat Shrink Tubing and Sleeves 1/8in ID SHRNK TUBN 4ft STICK CLEAR	602-FIT3501/8-25	Mouser Electronics
Cams	Material	1/4" Cast Acrylic Sheets (8"x5")		PlastiCare
	Shaft collars	Aluminum Set Screw Shaft Collar 1/4" Bore, 1/2" Outside Diameter, 5/16" Width	9946K11	McMaster-Carr
Shaft	Material	1/4" Aluminum Rod, milled to D-profile shape		Home Depot
	Shaft support	0.25 in. Bore, Pillow Block-Mount with Stainless Steel Pressbearing	A 7Z29-XS250	Stock Drive Products
	Coupling	One-piece Rigid Shaft Coupling, 1/4" bore, Stainless Steel	CL X-4-4-SS	Ruland
Shaft extender	Material	1/4" Aluminum Rod		Home Depot
	Double-wide shaft collar	Double Wide Shaft Collar, 6mm bore, Aluminum	M WCL-6-A	Ruland
Syringe support	Material	Impact-Resistant UHMW Polyethylene Sheet Black, 1/2" Thick, 12" X 24"	96A46 ⁴²	McMaster-Carr
Syringes		Model 1001 TLL Syringe, 1mL	60 375-497	VWR
Springs		(1/4" x 1-3/8" x 0.020) Springs	608 ^{C-}	Century Spring Corp.

Appendix B: CAD Drawings

